

Electronic Theses and Dissertations, 2004-2019

2019

Development of a Functional Testing Platform for the Sensory Segment of the Neuromuscular Reflex Arc

Alisha Colon
University of Central Florida

 Part of the [Animal Experimentation and Research Commons](#), and the [Medical Neurobiology Commons](#)

Find similar works at: <https://stars.library.ucf.edu/etd>
University of Central Florida Libraries <http://library.ucf.edu>

This Doctoral Dissertation (Open Access) is brought to you for free and open access by STARS. It has been accepted for inclusion in Electronic Theses and Dissertations, 2004-2019 by an authorized administrator of STARS. For more information, please contact STARS@ucf.edu.

STARS Citation

Colon, Alisha, "Development of a Functional Testing Platform for the Sensory Segment of the Neuromuscular Reflex Arc" (2019). *Electronic Theses and Dissertations, 2004-2019*. 6821.
<https://stars.library.ucf.edu/etd/6821>

DEVELOPMENT OF A FUNCTIONAL TESTING PLATFORM FOR THE SENSORY
SEGMENT OF THE NEUROMUSCULAR RELFEX ARC

by

ALISHA MARIE COLÓN
B.S. University of Central Florida, 2012
M.S. University of Central Florida, 2015

A dissertation submitted in partial fulfillment of the requirements
for the degree of Doctor of Philosophy
in the Burnett School of Biomedical Sciences
in the College of Medicine
at the University of Central Florida
Orlando, Florida

Summer Term
2019

Major Professor: James J. Hickman

© 2019 Alisha Marie Colón

ABSTRACT

Investigations of human biology and disease have been hindered by the use of animal models. The information obtained from such studies often results in clinically irrelevant results and drug trial failures. Additionally, several governing bodies have been formulating legislation to move away from animal models and toward more ethical and efficient testing platforms for drug discovery and cosmetic research. As an answer to these issues, “body-on-a-chip” systems have been a rapidly developing field which easily recapitulates *in vivo* functionality, providing a more relevant, repeatable, and ethical testing platform to better predict biology. These systems can be used as human-based testing platforms to evaluate human physiology, disease progression, and drug responsiveness for specific cell types and multi-organ systems. Diseases such as amyotrophic lateral sclerosis (ALS) and spinal muscular atrophy (SMA) have significant research challenges, specifically with translating research findings into treatment plans. The complexity of the neuromuscular reflex arc, the biological system affected by these diseases, is difficult to study with traditional molecular techniques, namely because the many components of this disease system interact with each other using complex pathways. This work pushes the existing platform to a more complete human model of neuromuscular disease with the incorporation of gamma motoneurons, development of the first human induced pluripotent cell (iPSC) derived intrafusal fibers, and proposals to incorporate nociceptive neurons all on a functionally interrogative platform. The incorporation of these components will allow for a more complete, clinically relevant model to study neuromuscular disorders and for preclinical drug discovery.

I dedicate this work to my parents, my husband, and my siblings. This work is not forged by my hands, but by your love and encouragement.

ACKNOWLEDGEMENTS

I would like to thank my committee chair, James Hickman and committee members, Stephen Lambert, Annette Khaled, and William Self, for their dedication to my success. I would like to thank Xiufang “Nadine” Guo, Christopher McAleer, Christopher Long, John Rumsey, and Frank Sommerhage for their detailed guidance, training, and astonishing patience during my development into a proficient scientist. I would also like to thank all of my past and present lab mates for making work seem a lot less like “work.”

TABLE OF CONTENTS

LIST OF FIGURES	ix
LIST OF TABLES	xv
CHAPTER ONE: INTRODUCTION.....	1
CHAPTER TWO: TISSUE ENGINEERING THE MECHANOSENSORY CURCUIT OF THE STRETCH REFLEX ARC WITH HUMAN STEM CELLS: SENSORY NEURON INNERVATION OF INTRAFUSAL FIBERS	3
Introduction	3
Results	6
Development of a defined system for the induction of intrafusal fibers, utilizing a serum-free medium	6
Phase contrast evaluation of the induction of intrafusal fibers.....	6
Immunocytochemical evaluation of intrafusal fiber induction.....	9
Immunocytochemical evaluation of sensory nerve endings on intrafusal fibers.....	11
Electrophysiological properties of intrafusal fibers in the co-culture	14
Immunocytochemical analysis indicates innervation of intrafusal fibers by human sensory neurons.....	16
Discussion	18
Materials and Methods	21
Induction of intrafusal fibers from human satellite cells.....	21
Co-culture of human sensory neurons with human intrafusal fibers.....	24
Immunocytochemistry and microscopy.....	25
Electrophysiological recording.....	26
Quantification	27
CHAPTER THREE: FUNCTIONAL ANALYSIS OF HUMAN INTRAFUSAL FIBER INNERVATION BY HUMAN Γ -MOTONEURONS.....	28
Introduction	28
Results	32
Morphological analysis.....	32
Immunocytochemical analysis	35
RNA expression analysis.....	41
Electrophysiological analysis	42
Discussion	44

Materials and Methods	47
Surface modification.....	47
Cell culture	47
Immunocytochemistry	49
Quantitative polymerase chain reaction	50
Electrophysiology	51
Statistical analysis.....	52
CHAPTER FOUR: DIFFERENTIATION OF HUMAN INTRAFUSAL FIBERS FROM INDUCED PLURIPOTENT STEM CELLS	53
Introduction	53
Results	57
Morphological analysis and quantification of bag fibers	57
Immunocytochemical analysis	63
Discussion	66
Materials and Methods	68
Surface modification.....	68
Satellite cell culture	69
iPSC extrafusal cell culture	69
iPSC intrafusal cell culture	70
Immunocytochemistry-pErbB2 and phalloidin	71
Immunocytochemistry-S46 and phalloidin	71
Image analysis	72
CHAPTER FIVE: INVESTIGATION OF NOCICEPTIVE MUSCLE SPINDLE ACTIVITY	73
Introduction	73
Results	75
Immunocytochemical analysis of hNP1-derived sensory neurons.....	75
Functional evaluation of hNP1-derived neurons	76
Immunocytochemical evaluation of intrafusal fibers	77
Discussion	78
Materials and Methods	79
Surface preparation.....	79
Human neural progenitor cell expansion and differentiation	80
Electrophysiological Evaluation of hNP1 cells	81

Human Intrafusal fiber differentiation.....	82
Immunocytochemical analysis	82
CHAPTER SIX: PIEZOELECTRIC BIOMEMS CANTILEVER FOR MEASUREMENT OF MUSCLE CONTRACTION AND FOR ACTUATION OF MECHANOSENSITIVE CELLS .	84
Introduction	84
Experimental Details	86
Design and fabrication of piezoelectric cantilevers.....	86
Surface modification of piezoelectric cantilevers	89
Cell culture on the piezoelectric cantilevers and housing system assembly	89
Contractile force measurement with piezoelectric cantilevers	90
Immunocytochemical imaging of cardiomyocytes on piezoelectric cantilevers.....	91
Detection system for actuation of piezoelectric cantilevers	92
Results and Discussion.....	95
Piezoelectric sensing for cardiomyocyte force measurements	95
Actuation of piezoelectric cantilevers	96
Conclusion.....	98
CHAPTER SEVEN: GENERAL DISCUSSION	99
LIST OF REFERENCES	103

LIST OF FIGURES

Figure 1: Phase contrast micrographs. A) A bag fiber in an induced culture after 16 days of differentiation. Note the equatorial distribution of multiple nuclei in the bag-shaped myofiber. Scale bar: 20 μm . B) A chain fiber in an induced culture after 16 days of differentiation. Note the linear assembly of the nuclei inside the myotube. Scale bar: 20 μm . C) A low magnification image of an induced culture after 17 days of differentiation. Scale bar: 80 μm . D) Graph comparison of the percentage of bag fibers when NRG/LMN/FN was added to the culture at different times during differentiation (* means $P < 0.05$). 8

Figure 2: A&B) Immunocytochemistry of induced intrafusal muscle cultures stained with the bag fiber-specific antibody S46 (green), and co-stained with Phalloidin (red) which is a general marker for all myofibers. A) A representative bag fiber is highlighted with a yellow arrow and a blue arrow indicates a myofiber that was partially stained by S46 but did not present apparent bag morphology, suggests the possibility of chain fiber or an emerging bag fiber formation. B) An image of a bag-fiber at higher magnification. C) A bag fiber immunostained with the BA-G5 antibody..... 10

Figure 3: Activation of Neuregulin signaling pathway demonstrated by immunocytochemistry. A) Co-immunostaining of Phalloidin and erbB2- p . To visualize the erbB2- p clusters on the cell membrane, two regions of the low magnification image were enlarged. Image a' and b' are the higher magnifications of regions a and b respectively. Abundant erbB2- p signals (indicated by arrows) were observed only on multi-nuclei bag fibers (b and b'), and rarely observed on the others (a and a'). B) Immunostaining of Egr3 co-stained with S46. Egr3-positivity was only observed in S46-positive myofibers, confirming its specificity. C) A bag fiber under higher magnification. 11

Figure 4: Immunocytochemical analysis of the co-culture of human sensory neurons and intrafusal fibers indicates connectivity. A) Phase image of a Day 10 co-culture. Note the pseudounipolar sensory neuron (orange arrow) and bipolar sensory neuron (red arrow) in the vicinity of a bag-shaped myofiber. B&C) Co-immunostaining of Peripherin and BA-G5 revealed two typical sensory terminal structures around intrafusal fibers: annulospiral wrappings (B) and flower spray endings (C), as indicated by the arrows in both images 13

Figure 5: Optical section of a sensory terminal structure indicating annulospiral wrappings on intrafusal fibers immunostained with Peripherin and BA-G5. A) Projected image of an intrafusal fiber with sensory axons. B) Series of optical sections of the intrafusal fiber demonstrated in A). 14

Figure 6: Patch clamp recording from intrafusal fibers in the co-culture system. A) Phase micrograph of the recorded cell. B) Current clamp recording indicating repetitive firing of APs. C) An example trace of active Na⁺ and K⁺ currents from a voltage clamp recording. D) An example trace of an Action Potential (AP) elicited when the cell received a saturated stimulus (2 msec 200pA inward current)..... 15

Figure 7: Immunocytochemical analysis of the connection of human sensory neurons and intrafusal fibers from a day 5 co-culture by co-immunostaining with PICK1 and Neurofilament antibodies. Co-localization of PICK1 expression on the myofiber at the neural terminal ending site is indicated by the arrow 17

Figure 8: Schematic diagram of the culture protocol and timeline..... 25

Figure 9: The cell culture scheme for the differentiation of the human intrafusal fibers derived from satellite cells. MNs added on day 10 of the culture were subjected to 2–10 DIV differentiation. 33

Figure 10: Phase contrast analysis of the human skeletal muscle and motoneurons. **(A)** Human muscle at 4 DIV. **(B)** Human MNs at 4 DIV. **(C and D)** Human muscle cultured without **(C)** and with **(D)** MNs at 17 DIV. **(E and F)** Morphological confirmation of intrafusal fibers in both muscle only **(E)** and muscle and MNs co-cultures **(F)**. **(G)** An enlarged view of image F to demonstrate the contacts of axon terminals with intrafusal fibers. Intrafusal fibers are indicated with **arrows** and MNs are indicated with black arrowheads. Neuromuscular contacts are indicated with white arrowheads. Black scale bars are 500 μ M. White scale bars are 50 μ M. 34

Figure 11: Immunocytochemical analysis of intrafusal fibers and γ -MNs. **(A and B)** Intrafusal fibers were identified with the antibodies against EGR3 **(A)** and pErbB2 **(B)**. Myotubes were visualized with the antibody against All Myosin Heavy Chains, and nuclei were identified by DAPI **(A and B)**. A sample image of a chain fiber is shown in panel A and bag fiber in panel B. **(C)** Motoneuron cultures were stained with Neurofilament and γ -MNs were additionally stained with an antibody against ERR γ . Scale bars are 50 μ M. 37

Figure 12: Immunocytochemical analysis of motoneuron only cultures. Markers for Wnt7a (Abcam ab100792) **(A)** NeuN (Millipore MAB377) **(B)** and ERRGamma **(C)** immunocytochemistry in motoneuron only controls. Scale bars are 50 μ M. 39

Figure 13: Immunocytochemical analysis of intrafusal fibers and motoneurons co-cultures. **(A)** Co-cultures were stained with Bungarotoxin (BTX), Neurofilament, and ERR γ . **(B)** High definition image for the boxed area in **(B)** indicates a close apposition of an axonal terminal from a γ -MN with BTX-488 patches (white arrow). Scale bars are 50 μ M. 40

Figure 14: Quantitative PCR: Quantification of ERR γ in the motoneuron culture compared to that in their undifferentiated precursors, human SCSCs 41

Figure 15: Patch-clamp analysis of intrafusal fibers. (A,B) Representative bright field microscopy of patched intrafusal cells in motoneuron-muscle co-cultures (A) and muscle only controls (B). (C,D) Gap-free recordings from patched intrafusal fibers in motoneuron–muscle co-cultures (C) and muscle only controls (D). Addition of glutamate (marked with green arrows) in the co-culture elicited increased activity and addition of curare (marked with red arrow) terminated activity (C) but no activity change was induced by either of them in intrafusal fibers in the muscle culture alone (D). 43

Figure 16: Statistical analysis. Percentages of glutamate responding and glutamate nonresponding intrafusal fibers in muscle-motoneuron co-culture conditions and muscle only conditions. P value = 2.17e-9. 44

Figure 17: Cell culture protocol. Cells were differentiated into myoblasts from a previous protocol and frozen into stocks. Cells were then expanded and treated with either intrafusal fiber differentiation or extrafusal fiber differentiation. 61

Figure 18: Phase Contrast Analysis. Morphological comparison between Intrafusal fibers derived from satellite cells and iPSC myoblasts treated with different differentiation protocols. A) and D) Cultures of satellite cells treated with an intrafusal induction protocol. B) and E) Cultures of iPSC myoblasts treated with an extrafusal-centered differentiation protocol C) and F) Cultures of iPSC myoblasts treated with an intrafusal induction protocol. White arrowheads show cells with intrafusal morphology. G) Quantification of morphologically assessed bag fibers. (Error bars=SEM, p=0.002). All scale bars are 100 microns. 62

Figure 19: Immunocytochemical Analysis of the myotubes induced under different conditions. Molecular comparison between ErbB2 phosphorylation in Intrafusal fibers derived from satellite cells and iPS cells treated with different differentiation protocols. A-E) Cultures of satellite cells

treated with an intrafusal induction protocol. F-J) Cultures of iPS cells treated with an extrafusal-centered differentiation protocol K-O) Cultures of iPS cells treated with an intrafusal induction protocol. P) Quantification of pERBb2 clustering within iPSC cultures. (Error bars are SEM, ***p=0.00054). All scale bars are 100 microns..... 64

Figure 20: Immunocytochemical Analysis of the myotubes induced under different conditions. Molecular comparison between s46 expression in Intrafusal fibers derived from iPS cells treated with different differentiation protocols. (Error bars are SEM, *p=0.03) All scale bars are 100 microns..... 65

Figure 21: Immunocytochemical analysis of hNP1-derived neurons. Evaluation of TRPV1 and TRKA expression in hNP1-derived neurons. All scale bars are 100 microns..... 76

Figure 22: Raster plot demonstrating the electrophysiological response of hNP1-derived neurons to capsaicin..... 77

Figure 23: Immunocytochemical analysis of human skeletal muscle. Cultures were evaluated for TRPV1 and S46. All scale bars are 100 microns..... 78

Figure 24: Fabrication of piezoelectric cantilevers. (a) Ti/Pt bottom electrodes and contact pads were deposited on an SOI wafer with insulation layers on the front and backside and patterned via liftoff. (b) Piezoelectric AlN was reactively sputtered and patterned via liftoff. (c) Top metal electrodes and contact pads were deposited and patterned via liftoff. (d) Top insulation layer (ONO) was deposited via PECVD. (e) The insulation layer was patterned by RIE. (f) The front and backside were etched via DRIE to define and release the cantilevers, followed by an HF dip to remove the buried oxide layer..... 88

Figure 25: Piezoelectric cantilever chip layout (a) Piezoelectric cantilever chip design showing location of cantilevers, wires, and contact pads. (b) SEM image of piezoelectric cantilevers

showing top surface of platinum and SiO₂ insulation. Because the cantilever chip was not coated with a separate conductive layer, the piezoelectric element and platinum wires appear darker, as the adjacent insulation layers charge slightly under the electron beam..... 89

Figure 26: Sensing of muscle contraction using piezoelectric cantilevers. (a) Confocal image of skeletal muscle on a piezoelectric cantilever, with myosin heavy chain shown in red and DAPI in blue. (b) Schematic of recording setup for cardiomyocyte force measurements using piezoelectric cantilevers. (c) Measurement of cardiomyocytes on piezoelectric cantilevers showing control (top) and after treatment with addition of 3 μm epinephrine (bottom)..... 91

Figure 27: Actuation of piezoelectric cantilevers. (a) Schematic of optical deflection system. (b) Piezoelectric cantilever actuation under a 5V monophasic 150 ms stimulation pulse. (c) Piezoelectric cantilever actuation under a ±5V biphasic (total duration 300 ms) stimulation pulse. Slight offset observed at end of actuation in (a) and (b) due to baseline drift in raw data (Figure 28). 94

Figure 28: Raw data from actuation of piezoelectric cantilevers. (a) Piezoelectric cantilever actuation under a 5V monophasic 150 ms stimulation pulse. (b) Piezoelectric cantilever actuation under a ±5V biphasic (total duration 300 ms) stimulation pulse. 94

LIST OF TABLES

Table 1: Electrophysiological properties of induced intrafusal bag fibers in the co-culture with human sensory neurons.....	16
Table 2: Composition of Enriched Co-culture Media (Medium 2)	23
Table 3: Listing of primary antibodies used to characterize γ -motoneurons, intrafusal fibers and the co-cultures.	36
Table 4: Medium formulations used to differentiate intrafusal fibers from induced pluripotent stem cells.....	58
Table 5: Medium formulations used to differentiate extrafusal fibers from induced pluripotent stem cell derived myoblasts	60

CHAPTER ONE: INTRODUCTION

Investigations of human disease is an enormous motivator for the progression of scientific inquiry. The utilization of animal models has provided a way to investigate drugs and other products used by humans for efficacy and potential hazards. Unfortunately, animal modeling has several pitfalls which are influencing the outcome of research pertaining to clinical trials and disease modeling(1). Also, several governing bodies have chosen to move toward more ethical and high-throughput methods of human-based biological inquiry. As an answer to these concerns more *in vitro* testing platforms have become a large area of interest in the scientific community. More specifically, “body-on-a-chip” technology can integrate modern micro-scale engineering along with human-based investigational platforms to provide an ethical way of predicting clinical trials and testing the effects of drugs and cosmetics (1). This technology has already been used to model several single and multi-organ systems (1-10), providing a platform of *in vitro* investigation for human pathology and drug discovery. Further development of these systems will allow for a more comprehensive array of high-throughput platforms for human biology investigation

While several platforms have been developed for interrogating human organ systems, the neuromuscular reflex arc is a complex system that needs further development to be more representative of *in vitro* biology. This system is very complex and has multiple interacting cell types, each of which can mediate disease states and drug efficacy (11, 12). The neuromuscular reflex arc has two basic cell types (neurons and muscle) each of which has their own further subcategories of cell types. Motoneurons are an efferent neurons that sends signals from the central nervous system (CNS) to the periphery (13). Motoneurons typically innervate extrafusal fibers, the contractile component of muscle tissue. Upon stimulation from the motoneurons,

these fibers can contract and relax, controlling limb position, dexterity, and strength. Conversely, there is an afferent component to this system. Embedded within the extrafusal fibers are muscle spindles. These are encapsulations of specialized muscle fibers called intrafusal fibers. These act as the sensory organ of muscle tissue (14). They are innervated by sensory neurons and relay information regarding muscle tension, speed of contraction or relaxation, and proprioception up through afferent sensory neurons and up to the CNS (15). Additionally, there are specialized motoneurons (γ -motoneurons) which innervate these intrafusal fibers of the muscle spindle (16). They send the intrafusal fibers signals to contract or relax in response to muscle length in order to maintain an efficient feedback loop. There has also been evidence of nociceptive nerve endings within the muscle spindle (17). These neurons are responsible for conveying sensations of pain up to the CNS. Collectively, these cell types interact with many intrinsic feedback systems which do not accurately depict human physiology or disease states. Therefore, it is integral to the progression of neuromuscular research to find an alternative model for investigating neuromuscular diseases and potential drug treatments with more clinically relevant, human-based results.

To further the clinical relevance of this technology, investigating the integration of induced pluripotent stem cells (iPSCs) have become a relevant inquiry (11). These cells are obtained from simple procedures, namely biopsies, and are treated to reverse the differentiation process. These cells can then be differentiated into a wide variety of cell types, allowing for the investigation of disease with complex genetic and posttranslational onsets as well as a more personalized approach for specific diseases or biological variants within a range. Integration of this technology with “body-on-a-chip” platforms advance the potential for having personalized medicine and a testing platform that can relate functional *in vitro* data to clinical outcomes.

CHAPTER TWO: TISSUE ENGINEERING THE MECHANOSENSORY CIRCUIT OF THE STRETCH REFLEX ARC WITH HUMAN STEM CELLS: SENSORY NEURON INNERVATION OF INTRAFUSAL FIBERS

The work in this chapter was published as listed below and, as per the publication agreement, does not require permission for use in this thesis.

Guo, X., Colon, A., Akanda, N., Spradling, S., Stancescu, M., Martin, C., & Hickman, J. J. (2017). Tissue engineering the mechanosensory circuit of the stretch reflex arc with human stem cells: Sensory neuron innervation of intrafusal muscle fibers. *Biomaterials*, *122*, 179–187.

doi:10.1016/j.biomaterials.2017.01.005

Introduction

Proprioception is the sensation of axial body position and the awareness of limb and body movement through space. Muscle spindle fibers, or muscle mechanoreceptors, are small encapsulated sensory organs that lie in parallel with skeletal (extrafusal or contractile) muscle fibers. While extrafusal muscle fibers generate force via muscle contraction to initiate skeletal movement, intrafusal fibers serve as musculoskeletal sensory organs to detect the amount and rate of change of muscle length and monitor muscle position (proprioceptors). This mechanical information is converted to electrical action potentials which are then sent to the central nervous system (CNS) through its connection with proprioceptive type Ia and type II sensory neurons (18, 19). Reciprocally, after integrating the inputs from sensory neurons and those from the motor cortex through corticospinal tract, the CNS can regulate motor activity through motoneurons (MNs): α MNs for extrafusal fibers to induce muscle contraction and γ MNs for intrafusal fibers to modulate the sensitivity of the proprioceptors. Despite their lower number in human muscle compared to extrafusal fibers(20), intrafusal fibers are indispensable for

proprioception and coordination of movement. Impairment of this sensory circuit can cause motor deficits, especially in fine or coordinated motor activity (21, 22). This proprioceptive system has been extensively investigated with animal models (23, 24), but research to address function in human systems has been gaining increased attention. A representative clinical problem is human deafferentation, in which a patient loses their afferent sensory input due to a number of causes, including neuropathy (25). In the absence of proprioceptive feedback, these patients suffer difficulties in motor control. They cannot control the magnitude and speed of the motion of their limbs leading to problems in balance and gait (26). Basic life skills such as mastication, swallowing, even walking can become difficult unless the patient exerts increased levels of mental concentration and visual monitoring (27, 28). In addition, impairment of proprioceptive sensory feedback has been found in a wide range of diseases such as autism, ADHD (29), Parkinson's disease (30), Huntington's disease, dystonia (31), neuropathy (27) and multiple sclerosis (32). However, deficits in proprioception and motor control may only be a side effect of the disease and therefore not a primary focus in the investigation of these diseases. However, these side effects do cause significant impact to their clinical symptoms and quality of a patient's life(28, 30). Pathology of the proprioceptive function could be caused by deficits in central integration of sensory and motor systems such as in neurodegenerative/development diseases like Parkinson's and autism (30, 33), or by direct damage to the intrafusal sensory system such as in deafferentation due to neuropathy which can be induced by immune system attack, viral infection, drug toxicity or other pathological conditions (25, 28, 32). Developing an in vitro model of this circuit would not only provide a valuable platform for the investigation of developmental, physiology as well as function of the somatosensory-motor system, but also for the construction of relevant disease models. Due to difficulties in translating the findings from

animal models to clinical applications, human-based in vitro systems are becoming increasingly utilized for etiological studies and for drug development. The rapid expansion of the availability of stem cells in recent years has provided an avenue for the unlimited supply of human cells for tissues, and a straightforward way to generate desired cell types. In addition, induced pluripotent stem cells (iPSC) technology provides the flexibility to investigate patient genetic diversity in these in vitro models. Our goal was to develop a human-based, in vitro muscle-sensory neuron circuit utilizing human stem cells as the source of the intrafusal fibers and sensory neurons, and to establish and characterize the resultant intrafusal innervations. Intrafusal muscle fibers have been induced in vitro from rat embryonic muscle cells (34), and the establishment of connections with rat sensory neurons from primary DRG neurons in a defined in vitro system has previously been demonstrated (14). In vitro induction of intrafusal fibers from human myoblasts had also been reported but by utilizing a serum-containing system and with a focus on molecular mechanism of signal transduction (35). We have successfully differentiated functional myotubes (extrafusal fibers) from human satellite cells (36), then co-cultured them in a serum-free defined medium with motoneurons (MNs) to form NMJs (37). We have also differentiated functional proprioceptive sensory neurons from human neural progenitors (38). The identity of these sensory neurons has been confirmed by the expression of sensory neuron markers Brn3a and peripherin, and their proprioceptive identity has been further confirmed by the markers of parvalbumin and vGluT1 (38). In this study, we generated intrafusal fibers from human satellite cells and established innervation by the stem cell-derived human proprioceptive sensory neurons and established functional connections. Surprisingly, the intrafusal fibers were capable of repetitively firing upon stimulation, which hadn't previously been observed in any extrafusal myofibers (36, 39) or rat intrafusal myofibers (34). This human-based, in vitro mechanosensory

model could find important applications in the etiological study of relevant diseases such as deafferentiation, neuropathies and possibly neuropathic pain. It could also provide a plausible phenotypic model for the drug screening and potential therapy development for these diseases

Results

Development of a defined system for the induction of intrafusal fibers, utilizing a serum-free medium

Considering the common origin, environment and multiple needs shared by both intrafusal and extrafusal fibers during development, the protocol for generating functional extrafusal fibers (14, 34) developed in our laboratory was used as a starting point for designing protocols for intrafusal fiber induction. As previously reported, neuregulin 1- β -1 (NRG) is necessary for the specification of nuclear bag fibers and for spindle development (35, 40). Additionally, the basal laminar molecules, laminin and agrin, are especially important for NRG signaling for intrafusal induction by activating a dystroglycan receptor on the myotube membrane which then potentiates the NRG-Egr3 signaling pathway (41). Therefore, these three factors, NRG, laminin and agrin, were included in the differentiation process. The composition of medium 2 is as described in Table 2.

Phase contrast evaluation of the induction of intrafusal fibers

The human satellite cells were plated, expanded and differentiated as described in the Methods. Myocyte fusion was initiated after switching to medium 1, which defines the start of the differentiation process, and multinuclear myocytes were evident after 3~4 days in vitro. The cultures are then switched to medium 2 and multinuclear myotubes continued to mature as

indicated by more individualized myotubes with better defined morphology under phase microscopy. Starting approximately at day 7, myofibers with morphology consistent with bag fibers could be identified and were increasingly evident and numerous as the culture matured. Some demonstrated equatorial nucleation which is typical for bag fibers (18, 42) (Figure 1 A, C). Myofibers with a chain of nuclei were also observed frequently and identified as chain fibers (Figure 1 B). During development, nuclear bag morphology is thought to be the earliest reliable feature for identifying young intrafusal fiber bundles in human muscle (42), however, the identification of chain fibers under phase microscopy is not as well defined. Thus, the number of induced muscle bag fibers was used to optimize the induction protocol. To determine whether the generation of bag fibers was NRG-dependent as postulated from in vivo studies(43), the percentage of bag fibers over the total number of myofibers was compared with control cultures in which the three factors were omitted (NRG, laminin and agrin). Also, to determine the optimal timing of factor addition, the percentage of bag fibers was analyzed from factors inclusive from day 0, 4 & 7 of differentiation in medium 1. As displayed in Figure 1 D, inclusion of the three factors caused a significant increase of the percentage of bag fibers from 3.02 +/- 3.95% to at least 15.80 +/- 6.62% ($P < 0.05$) But there is no significant difference when added at different time points during differentiation in medium 1. Later analysis indicated that switching to medium 2 on day 4 generated more consistent results in intrafusal induction than on day 7. Therefore, cells were induced for 4 days in medium 1 before switching to medium 2 in all subsequent experiments.

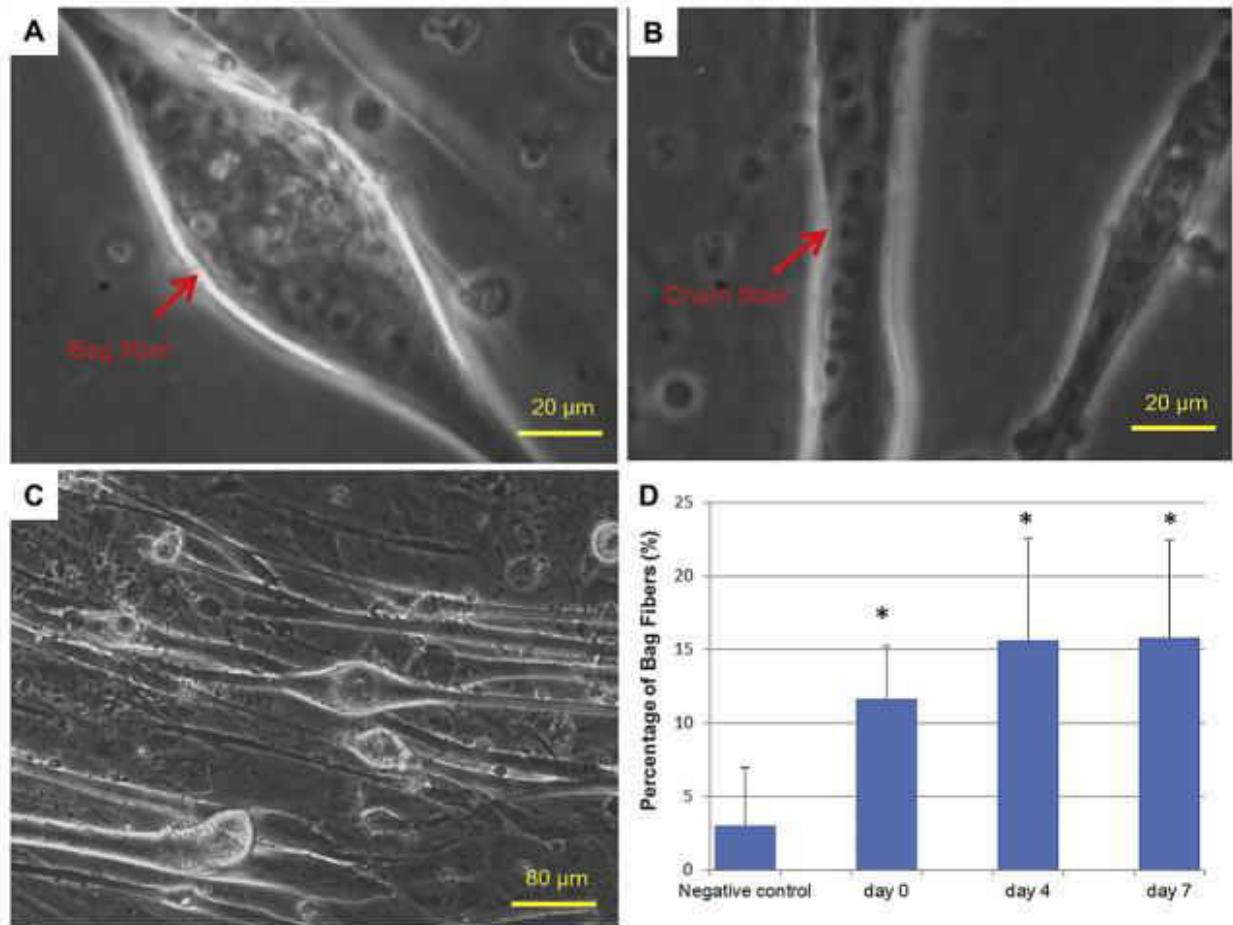


Figure 1: Phase contrast micrographs. A) A bag fiber in an induced culture after 16 days of differentiation. Note the equatorial distribution of multiple nuclei in the bag-shaped myofiber. Scale bar: 20 μm . B) A chain fiber in an induced culture after 16 days of differentiation. Note the linear assembly of the nuclei inside the myotube. Scale bar: 20 μm . C) A low magnification image of an induced culture after 17 days of differentiation. Scale bar: 80 μm . D) Graph comparison of the percentage of bag fibers when NRG/LMN/FN was added to the culture at different times during differentiation (* means $P < 0.05$).

Immunocytochemical evaluation of intrafusal fiber induction

Immunostaining was used to confirm the identity of the induced bag fibers. The hSKM culture treated with NRG/LMN/Agrin as described above, was evaluated for the expression of the bag fiber-specific myosin heavy chain (MHC) with the S46 antibody (44, 45). As indicated in Figure 2 A, a sub-population of myofibers expressed the slow tonic MHC and were identified as S46-positive myotubes. In addition, these bag fibers expressed α cardiac-like MHC which was indicated by immunocytochemical staining with the BA-G5 antibody (Figure 2 C) (44, 46). In vivo, NRG induction functions through the ErbB2 receptor (47). Its activation through phosphorylation can then increase the expression of the transcription factor Egr3 (43), which triggers downstream genes that then delineate intrafusal fiber differentiation. Therefore, the induced cultures were analyzed for the expression and distribution of phosphorylated ErbB2 (ErbB2- P) and Egr3 (Figure 3). ErbB2- P was specific for a subset of myofibers and was found in all S46- positive myotubes (Figure 3 A). The induced cultures were then analyzed for the expression of Egr3, the intrafusal fiber-specific transcription factor. As in Figure 3 B&C, Egr3 was found to be expressed in bag fibers which were also identified by staining for the S46-antibody. Both the expression of ErbB2- P and Egr3 in the induced intrafusal fibers suggest the activation of the ErbB2 receptor-mediated signaling pathway by NRG treatment, similar to what occurs during in vivo development.

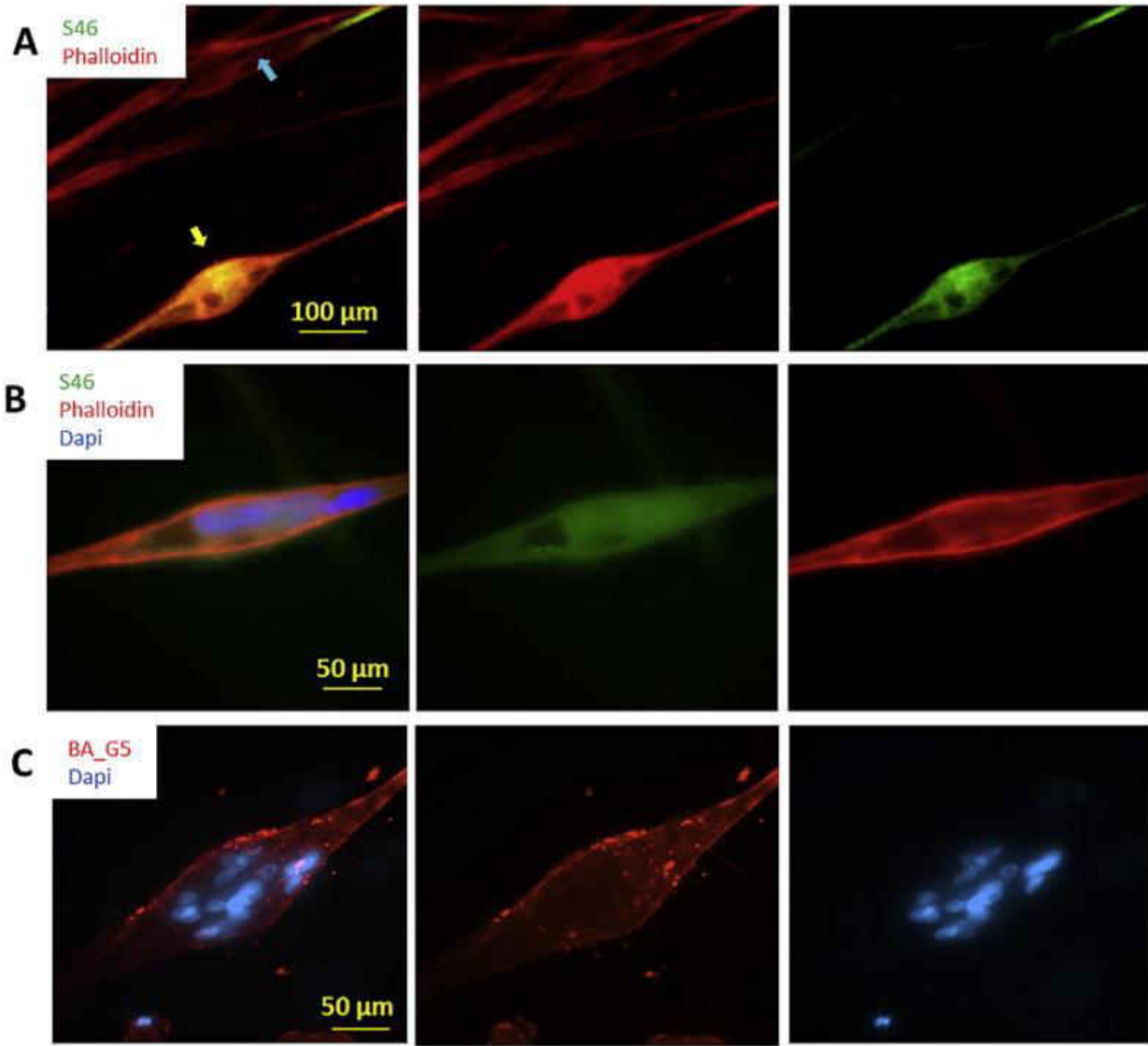


Figure 2: A&B) Immunocytochemistry of induced intrafusal muscle cultures stained with the bag fiber-specific antibody S46 (green), and co-stained with Phalloidin (red) which is a general marker for all myofibers. A) A representative bag fiber is highlighted with a yellow arrow and a blue arrow indicates a myofiber that was partially stained by S46 but did not present apparent bag morphology, suggests the possibility of chain fiber or an emerging bag fiber formation. B) An image of a bag-fiber at higher magnification. C) A bag fiber immunostained with the BA-G5 antibody.

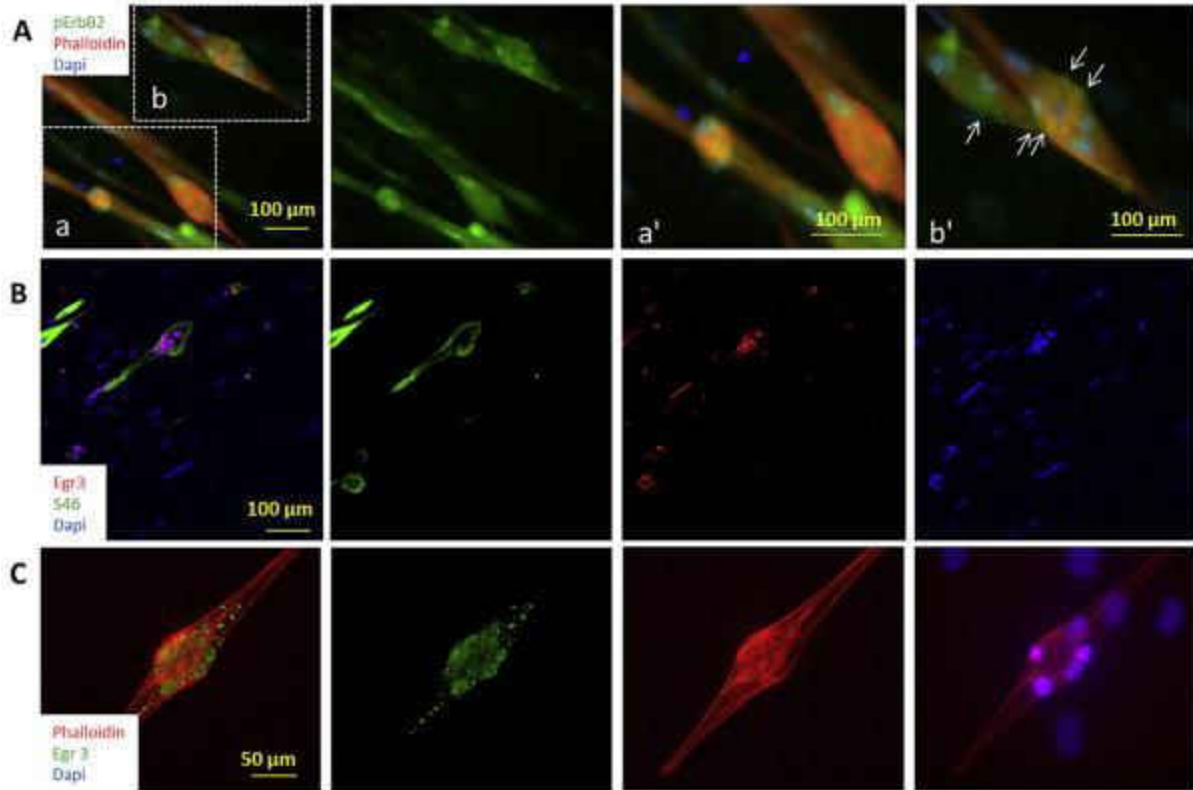


Figure 3: Activation of Neuregulin signaling pathway demonstrated by immunocytochemistry.

A) Co-immunostaining of Phalloidin and erbB2- p . To visualize the erbB2- p clusters on the cell membrane, two regions of the low magnification image were enlarged. Image a' and b' are the higher magnifications of regions a and b respectively. Abundant erbB2- p signals (indicated by arrows) were observed only on multi-nuclei bag fibers (b and b'), and rarely observed on the others (a and a'). B) Immunostaining of Egr3 co-stained with S46. Egr3-positivity was only observed in S46-positive myofibers, confirming its specificity. C) A bag fiber under higher magnification.

Immunocytochemical evaluation of sensory nerve endings on intrafusal fibers

The induced intrafusal fibers were co-cultured with human stem cell-derived sensory neurons (38) and evaluated for innervation characteristic of this mechanosensory system. The differentiated sensory neurons were added to the partially differentiated muscle culture (after

step 1 differentiation) and co-cultured for approximately 10 days (Figure 8). Both sensory neurons and intrafusal fibers survived well in the co-culture system as indicated by the phase images (Figure 4 A). In order to evaluate the synaptic connections the co-cultures were immunostained with the sensory neuron marker peripherin and the intrafusal marker BA-G5. In vivo sensory nerve endings on intrafusal fibers normally demonstrate two distinct morphological structures: annulospiral wrappings (ASWs) and flower spray endings (FSEs) (18). As shown in Figure 5 B-C, both terminal structures were observed in the developed co-culture system. An example of the annulospiral association between sensory terminals and the intrafusal fibers is demonstrated in the detailed optical series depicted in Figure 5.

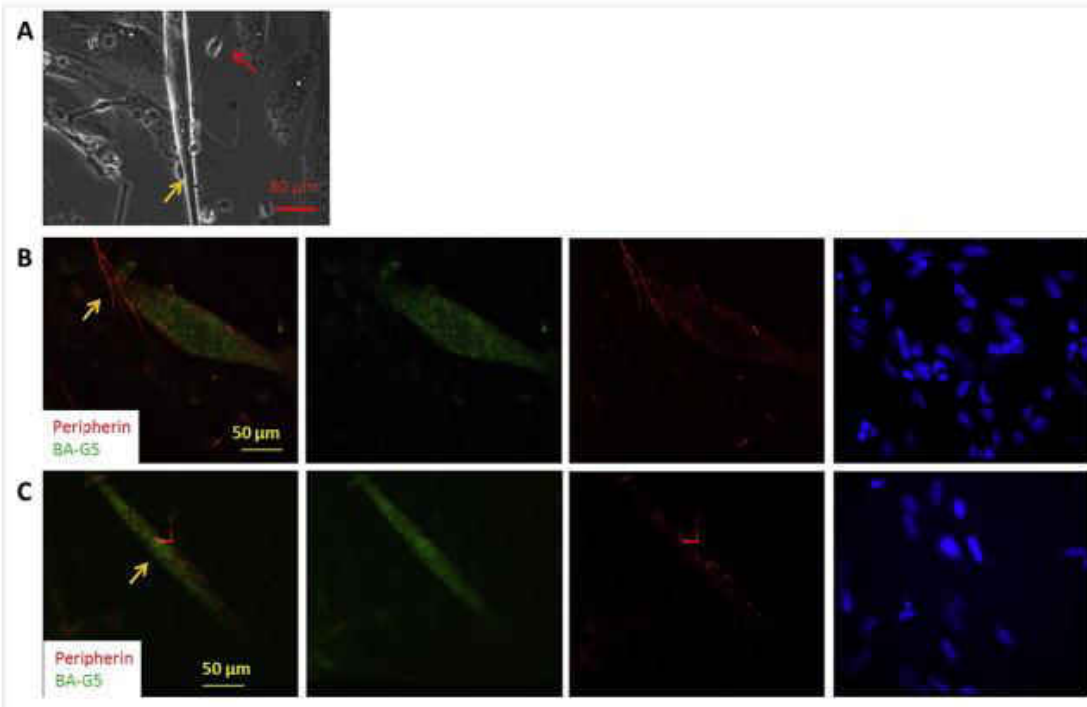


Figure 4: Immunocytochemical analysis of the co-culture of human sensory neurons and intrafusal fibers indicates connectivity. A) Phase image of a Day 10 co-culture. Note the pseudounipolar sensory neuron (orange arrow) and bipolar sensory neuron (red arrow) in the vicinity of a bag-shaped myofiber. B&C) Co-immunostaining of Peripherin and BA-G5 revealed two typical sensory terminal structures around intrafusal fibers: annulospiral wrappings (B) and flower spray endings (C), as indicated by the arrows in both images

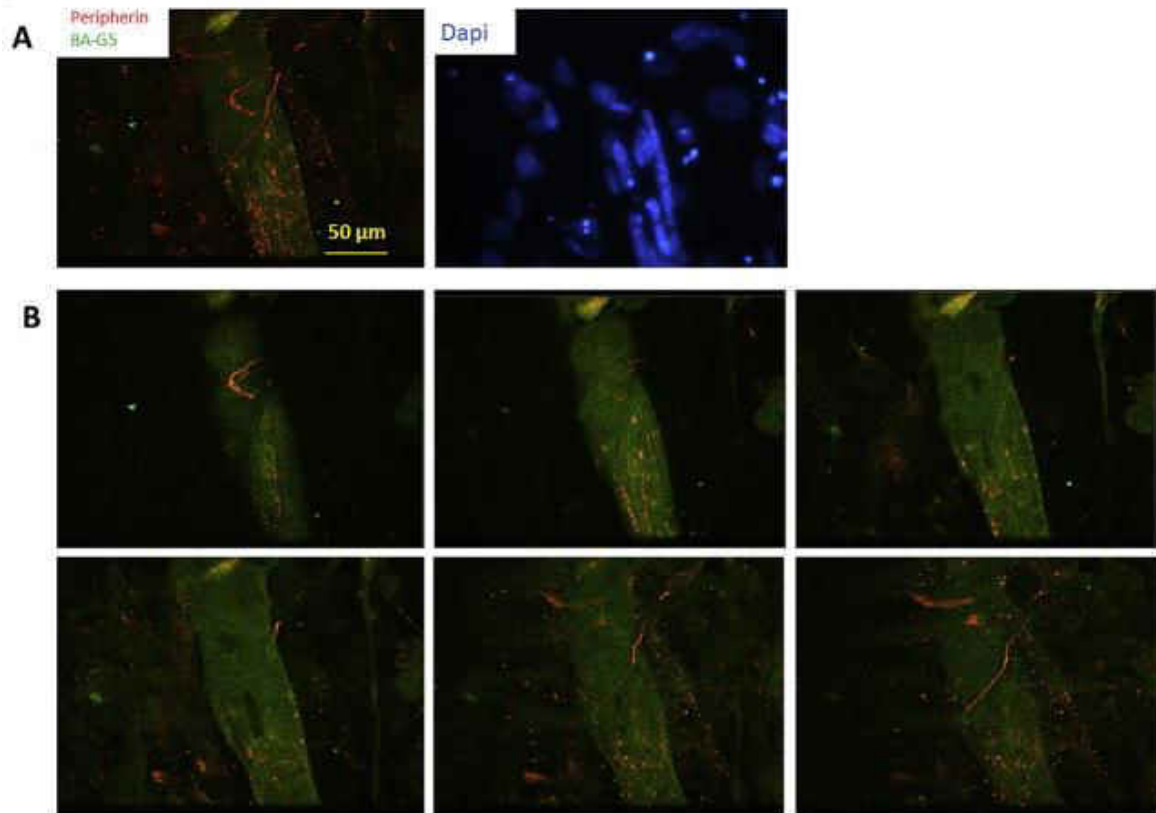


Figure 5: Optical section of a sensory terminal structure indicating annulospiral wrappings on intrafusal fibers immunostained with Peripherin and BA-G5. A) Projected image of an intrafusal fiber with sensory axons. B) Series of optical sections of the intrafusal fiber demonstrated in A).

Electrophysiological properties of intrafusal fibers in the co-culture

The electrophysiological properties of the intrafusal fibers in the co-culture were evaluated using voltage and current clamp recordings. Representative voltage-clamp and current-clamp recordings for intrafusal fibers are shown in Figure 6. Similar to extrafusal fibers (7, 36), intrafusal fibers demonstrated prominent sodium and potassium currents and generated action potentials. Most interestingly repetitive firing was observed in 10 out of 19 bag fibers recorded in the system (Figure 6 B). The electrophysiological properties of intrafusal fibers are listed in Table 1.

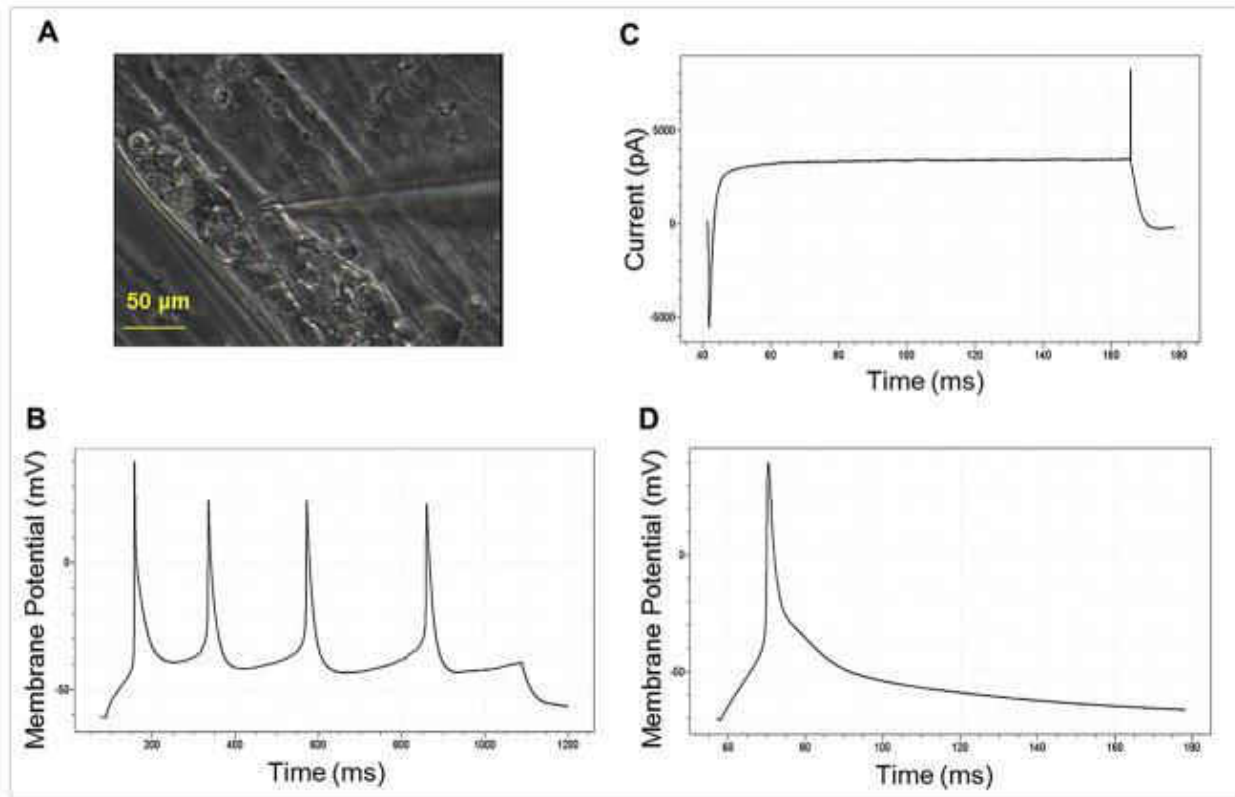


Figure 6: Patch clamp recording from intrafusal fibers in the co-culture system. A) Phase micrograph of the recorded cell. B) Current clamp recording indicating repetitive firing of APs. C) An example trace of active Na⁺ and K⁺ currents from a voltage clamp recording. D) An example trace of an Action Potential (AP) elicited when the cell received a saturated stimulus (2 msec 200pA inward current).

Table 1: Electrophysiological properties of induced intrafusal bag fibers in the co-culture with human sensory neurons

	Resting Membrane Potential (mV)	Membrane Resistance (MΩ)	Membrane Capacitance (pF)	No. of Aps (s)	Inward Current (pA)	Outward Current (pA)	AP Amplitude (mv)
Average +/- STDEV	-53.0 +/- 9.6	365.2 +/- 235.9	207.9 +/- 65.0	3.1 +/- 2.5	5043.6 +/- 1888.8	1932.3 +/- 1311.9	95.9 +/- 11.5

Immunocytochemical analysis indicates innervation of intrafusal fibers by human sensory neurons

To examine in detail the connections between the sensory neuron terminals and intrafusal fibers, the co-culture was analyzed by immunostaining with PICK1 (PRKCA-binding protein) and peripherin. PICK1 contains a PDZ domain and functions as an adaptor protein that organizes a variety of membrane proteins including the stretch sensitive sodium channel BNaC1 on the membrane of intrafusal fibers. Co-localization of PICK1 with nerve terminals was observed. Figure 7 demonstrates an example of a flower spray endings associated with a myofiber and its co-localization with PICK1, suggesting a functional connection between intrafusal fibers with the axonal terminals of sensory neurons, which is a key connection for mechanosensory function.



Figure 7: Immunocytochemical analysis of the connection of human sensory neurons and intrafusal fibers from a day 5 co-culture by co-immunostaining with PICK1 and Neurofilament antibodies. Co-localization of PICK1 expression on the myofiber at the neural terminal ending site is indicated by the arrow

Discussion

This study reports the de novo induction of human intrafusal skeletal muscle fibers from satellite cells and their synaptic connection with human stem cell-derived sensory neurons in a defined in vitro system. The induction of intrafusal fibers was characterized by morphology and fiber-type specific transcription factor expression using phase microscopy and immunocytochemistry. The connections between sensory neurons and the intrafusal fibers were observed morphologically type-specific innervation patterns using phase microscopy and immunocytochemistry. The functional maturity of the induced intrafusal fibers was confirmed by patch-clamp electrophysiological analysis. During development, induction of muscle spindles depends on trophic factors released by sensory neurons. Neuregulin (NRG), specifically the Ig-Nrg1 isoform, is a proteoglycan released by type Ia proprioceptive sensory neurons and is sufficient to induce muscle spindle differentiation in vivo (43). The NRG-ErbB2-Egr3 signaling pathway has been proposed to be the central pathway for this effect (19). Mice with a conditional knockout of ErbB2 have progressive defects in proprioception due to the loss of muscle spindles (21). Egr3 has an essential role for the phenotypic differentiation of spindles (48) and mice deficient in Egr3 have gait ataxia and lack muscle spindles (49). Therefore, it is hypothesized that NRG released by sensory axons, through the activation of ErbB2 receptors on the myotube membrane, can turn on the transcription factors Egr3/Pea3/Erm, which then initiates downstream genes and delineates the differentiation of intrafusal fibers and muscle spindles (19, 21, 35, 40, 48, 49). In addition to this major pathway, the basal laminar molecules, laminin and agrin, are especially important for NRG signaling and intrafusal induction by activating a dystroglycan receptor on the myotube membrane which then potentiates the NRG-Egr3 signaling pathway (41). In this study, both pathways were employed for the in vitro induction of intrafusal myofibers as

evidenced by the increased expression of ErbB2-⁺ and Egr3 in BA-G5-positive myotubes. The electrical function of the induced intrafusal fibers was confirmed by patch-clamp electrophysiological analysis. However, these results differed from previous experiments with human extrafusal fibers, which only fire a single action potential during depolarization (36), in that the majority (53%) of the intrafusal fibers examined exhibited repetitive firing. The rest fired single action potentials probably due to maturation issues. This repetitive firing phenomenon has not been observed in the electrophysiology of rat intrafusal fibers (34). This is the first electrophysiological analysis of human intrafusal fibers and the first report concerning the unique electrophysiological property of these myotubes. This unique electrophysiological result for a human muscle fiber may actually be intrinsic to its function as a mechano-electrical transducer. Sensory receptors of multiple modalities utilize firing frequency to encode stimulus intensity such as the sensing of temperature, pain and touch (50-54). Thus, repetitive firing may be important for the normal function of these sensory transducers, endowing them the potential to code stimulus intensity with firing frequency. This result is in agreement with numerous previous studies from human microneurography, an in vivo approach to monitor the impulses in sensory nerves while applying the stimulus, such as touch or movement (54, 55). All the dynamic responses of human muscle intrafusal sensory afferents from these studies displayed multiple discharges at various frequencies depending on the stimulation protocols (54, 56-58). Overall, these results establish that there are important electrophysiological differences between intrafusal and extrafusal fibers, and also between human intrafusal and rat intrafusal fibers, which could have new implications for understanding muscle physiology. In vitro systems composed of the main component of the specialized stretch receptors could allow studies of perception and coordination of limb movement in a defined, controlled system. Mice lacking spindle fibers

within skeletal muscle present with profound gait ataxia and other motor deficits (49). Impairment of proprioception has been well represented in deafferentation cases in which proprioceptive sensory nerves are damaged due to neuropathy (25, 59), and can also be associated with many diseases including multiple sclerosis (60), spinal cord injury (61), diabetes mellitus (62) and other degenerative diseases (30). Humans with proprioception dysfunction typically have deficits in motor planning, motor control, grading movement and postural stability. While previous publications covering motor control/learning as well as rehabilitation have been obtained from deafferentated patients (63-65), a human-based in vitro system would constitute a valuable phenotypic model for this sensorimotor circuit. The in vitro system reported in this study using a well-defined serum-free medium provides a platform for the dissection of the physiological/molecular/developmental mechanism and regulation of this mechanosensory system. The human nature of this biological system makes it more relevant and amenable to the study of neurological and/or muscular disease modeling, drug discovery and regenerative medicine.

Materials and Methods

DETA Surface Modification Glass coverslips (6661F52, 22x22 mm No. 1; Thomas Scientific, Swedesboro, NJ, USA) were cleaned using HCl/methanol (1:1) for a minimum of 2 hours, rinsed with water, soaked in concentrated H₂SO₄ for at least 2 hours and rinsed with water. The coverslips were then boiled in nanopure water and oven dried. The trimethoxysilylpropyldiethylenetri-amine (DETA, T2910KG; United Chemical Technologies Inc., Bristol, PA, USA) film was formed by the reaction of the cleaned surfaces with a 0.1% (v/v) mixture of the organosilane in freshly distilled toluene (T2904; Fisher, Suwanne, GA, USA). The DETA coated coverslips were heated to ~80°C, cooled to room temperature (RT), rinsed with toluene, reheated to approximately 80°C, and then cured for at least 2 hours at 110°C. Surfaces were characterized by contact angle and X-ray photoelectron spectroscopy as previously described (39, 66, 67).

Induction of intrafusal fibers from human satellite cells

Human skeletal muscle stem cells (hSKM SCs)/progenitors were isolated, proliferated and differentiated as described in Thorrez et al. (68). Briefly, the primary human skeletal muscle cells (hSKMs) were isolated by needle biopsy (69) and expanded in the myoblast growth medium (MGM; SkGM (Cambrex Bio Science, Walkersville, MD) plus 15% (v/v) fetal bovine serum. Biopsies were performed on adult volunteers according to procedures approved by the Institutional Clinical Review Board of the Miriam Hospital. Cell preparations averaged 70% myogenic content based on desmin-positive staining (70).

To induce intrafusal fibers from these hSKM SCs, a unique protocol was developed in this study. For each culture, hSKM SCs/progenitors with about 20 doubling times were plated on DETA

coverslips at a density of 100 cells/mm² in hSKM Growth Medium (Lonza, CC-3160) and fed every 2 days by changing the entire medium until confluency. Myoblast fusion was then induced by switching to the differentiation medium 1(36) (high-glucose DMEM (Invitrogen, Carlsbad, CA) supplemented with Insulin (10 µg/ml), bovine serum albumin (BSA) (50 µg/ml), Epidermal Growth Factor (10 ng/ml) and Gentamicin (50 µg/ml)). For intrafusal fiber induction, Neuregulin (10 ng/ml), Laminin (10 ng/ml) and Agrin (10 ng/ml) were added to the differentiation medium on day 0, day 4 or day 7 after the initiation of differentiation. The cells were fed every 2 days by changing half of the medium. Four days after differentiation initiation, the medium was switched to the co-culture medium or medium 2 (Table 2). The cells were fed once using the same medium 2 days later by changing half of the medium. Thereafter, the cultures were fed every 2 days using NBactive4 (Brain Bits, Nb4-500) by replacing half of the medium.

Table 2: Composition of Enriched Co-culture Media (Medium 2)

Component	Full Name	Concentration	Company	Catalog Number
Neurobasal /Neurobasal A			Invitrogen	10888/21103
B27 (50X)		1X	Invitrogen	17504-044
Glutamax (100X)		1X	Invitrogen	35050
rhNRG	Neregulin 1- β 1 EGF domain	100 ng/ml	R&D	396-GF/CF
RH β -NGF	Nerve Growth Factor	100 ng/ml	R&D	256-GF/CF
GDNF	Glial-derived growth factor	10 ng/ml	Cell Sciences	CRG400B
BDNF	Brain-derived growth factor	20 ng/ml	Cell Sciences	CRB600B
Shh	Sonic Hedgehog, N-terminal peptide	50 ng/ml	R&D	1845-SH-025
RA	Retinoic Acid	0.1 μ M	Sigma	R2625
IGF-1	Insulin-like Growth Factor	10 ng/ml	PeptoTech	100-11
cAMP	Adenosine 3',5'-cyclic Monophosphate	1 μ M	Sigma	A9501
CNTF	Ciliary Neurotrophic Factor	5 ng/ml	Invitrogen	CRC400A
NT-3	Neurotrophin-3	20 ng/ml	Invitrogen	CRN500B
NT-4	Neurotrophin-4	20 ng/ml	Cell Sciences	CRN501B
Vitronectin		100 ng/ml	Sigma	V8379
Laminin	Mouse Laminin	4 μ g/ml	Invitrogen	23017-015
G5 (100X)		1X	Invitrogen	17503-012
Agrin		100 ng/ml	R&D	550-AG-100

Co-culture of human sensory neurons with human intrafusal fibers

Co-cultures were established according to the procedures depicted in Figure 8. Human sensory neurons (hSNs) were differentiated from human neural progenitor cells, STEMEZTMhNP1 (Neuromics, Edina, Minnesota) as described in Guo et al. (37). Neuromics' product information states that their cells can be expanded through 10 passages before any genotypic monitoring is necessary (<http://www.neuromics.com/>). In this study, passage 9 or 10 cells were used. Briefly, hNP1 cells in the growth phase were manually dissociated and replated onto glass coverslips pre-coated with DETA, followed by Polyornathine/Laminin/Fibronectin (71), at a density of 400 cells/mm². The cells were expanded in the proliferation medium for 2 to 3 days to achieve ~90% confluence before induction. To initiate sensory neuron differentiation, the medium was replaced with KSR medium which contained 10 μ M SB43152 (Tocris, Cat 1614) and 500 ng/ml Noggin (R&D, Cat 6057-NG-025). To feed the cells during differentiation, the medium was replaced and gradually switched from KSR medium (ThermoFisher, Cat 10828028) to N2B medium (NeuralStem Inc) according to the following schedule: day 0 (100%KSR, 0% NB), day 2 (75% KSR, 25% N2B), day 4 (50% KSR, 50% N2B), day 6 (25% KSR, 75% N2B), days 8 & 10 (0% KSR, 100% N2B). However, the content of SB43152 and Noggin (10 μ M and 500 ng/ml, respectively) remained constant throughout the procedure. Starting with day 12, the cells were fed with a differentiation medium by changing 1/3 of the medium every 2 days. After 14 days of differentiation, SNs were harvested by trypsinization and added to the muscle culture at a density of 75 cells/mm², timed so the muscle culture was on day 4 of differentiation and right after it had been switched to co-culture medium.

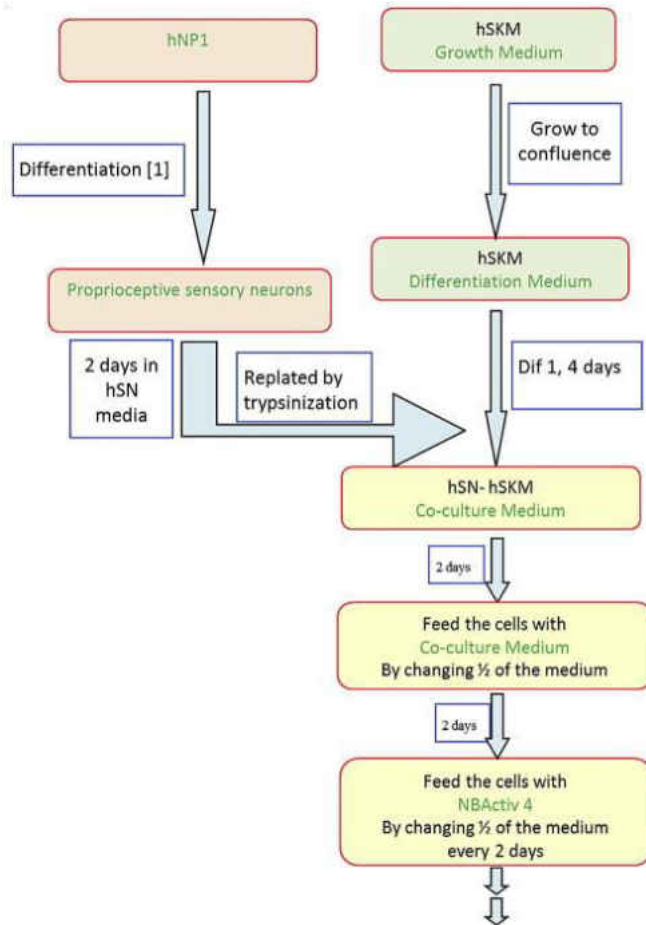


Figure 8: Schematic diagram of the culture protocol and timeline.

Immunocytochemistry and microscopy

Cultures were analyzed with immunocytochemistry and microscopy as described before (37, 38). Cells on the DETA coverslips were fixed utilizing freshly prepared 4% paraformaldehyde in PBS for 15 min. Cells were then washed twice in Phosphate Buffered Saline (PBS) (pH 7.2, w/o Mg²⁺, Ca²⁺) for 10 min at room temperature and then permeabilized with 0.1% triton X-100/PBS for 15 min. Non-specific binding sites were blocked using Blocking Buffer (5% Donkey serum plus 0.5% BSA in PBS) for 45 min at room temperature. Cells were then incubated with primary antibodies overnight at 4 °C. After being washed with PBS 3x10 min, the

cells were then incubated with secondary antibodies for 2.5 hours at room temperature. The cells were again washed with PBS 3x for 10 min and mounted utilizing Vectashield with 4'-6-Diamidino-2-Phenylindole (DAPI) (Vector laboratories, Inc.). Primary antibodies used in this study included: Goat-anti-Peripherin (Santa Cruz Biotech, 1:25), Rabbit-anti-MHC H-300 (Santa Cruz, 1:200), Goat-anti-PICK1 (Santa Cruz, 1:200), Mouse-anti-Neurofilament (Sigma, 1:1000), Rabbit-anti-Egr3 (Santa Cruz, 1:100), erbB2-[®]-Alexa488 (Millipore, 1:250). The monoclonal antibody against slow tonic muscle heavy chain (S46, 1:10) was obtained from the Developmental Studies Hybridoma Bank which is under the auspices of the NICHD and maintained by the University of Iowa. Phalloidin-568 (Life Technologies, 1:40) was included during the secondary antibody incubation. The monoclonal antibody against cardiac muscle heavy chain BA-G5 was produced as described in Rumsey et al.(34). Secondary antibodies include: Donkey-anti-Mouse-568 (Invitrogen, 1:250), Donkey-anti-Rabbit-488 (Invitrogen, 1:250), and Donkey-anti-Rabbit-568 (Invitrogen, 1:250) Donkey-anti-Gt-488 (Invitrogen, 1:250). All antibodies were diluted in Blocking Buffer.

Electrophysiological recording

Electrophysiological properties of human intrafusal fibers were investigated after ~10 days of co-culture with human sensory neurons utilizing whole-cell patch-clamp recording techniques (67). The recordings were performed in a recording chamber located on the stage of a Zeiss Axioscope 2FS Plus upright microscope (72). Intrafusal fibers were identified visually under an infrared DIC-video microscope by their typical bag fiber morphology. Patch pipettes, with a resistance of 6-10 M Ω , were made from borosilicate glass (BF 150-86-10; Sutter, Novato, CA) with a Sutter P97 pipette puller (Sutter Instrument Company). Current-clamp and voltage-clamp recordings were made utilizing a Multiclamp 700A amplifier (Axon, Union City, CA).

According to the standard protocol that has been used routinely (67, 73, 74), the pipette (intracellular) solution contained (in mM) Kgluconate 140, MgCl₂ 2, Na₂ATP 2, Phosphocreatine 5, Phosphocreatine kinase 2.4 mg and Hepes 10; pH 7.2. After the formation of a giga ohm seal and membrane puncture, the cell capacitance was compensated. The series resistance was typically <23 M Ω , and it was compensated 60% using the amplifier circuitry. Signals were filtered at 3 kHz and sampled at 20 k Hz using a Digidata 1322A interface (Axon instrument). Data recording and analysis were performed with pClamp8 software (Axon instrument). Membrane potentials were corrected by the subtraction of a 15 mV tip potential, which is the liquid junction potential between intracellular solution and extracellular solution, was calculated using Axon's pClamp8 program, and it is within the normal range of junction potential for patch clamp (10~20 mV) (75). Membrane resistance and capacitance were calculated using 50 ms voltage steps from -85 to -95 mV without any whole-cell or series resistance compensation. The resting membrane potential and depolarization-evoked action potentials were recorded in current-clamp mode. Depolarization-evoked inward and outward currents were examined in voltage-clamp mode. Single APs were elicited by a brief saturated depolarization current.

Quantification

For the quantification of bag fiber induction under phase microscopy, a minimum of 10 random fields were imaged under phase microscopy. The number of bag fibers out of the total number of myotubes was quantified for each experimental condition and compared to the control. At least 3 independent cultures were analyzed for each condition. Statistical analysis by T-Test (one tail, two samples with unequal variance) was performed to compare differences between samples and P<0.05 was considered significantly different.

CHAPTER THREE: FUNCTIONAL ANALYSIS OF HUMAN INTRAFUSAL FIBER INNERVATION BY HUMAN Γ -MOTONEURONS

The work in this chapter was published as listed below under a Creative Commons license and therefore does not require copyright permission.

Colón A, Guo X, Akanda N, Cai Y, Hickman JJ. Functional analysis of human intrafusal fiber innervation by human γ -motoneurons. *Sci Rep.* 2017 Dec 8;7(1):17202.

A.C. performed preparations of all muscle and some motoneuron cultures, all immunocytochemistry, some experimental design and most data analysis. X.G. performed experimental design, data analysis, set data interpretation guidelines and helped with manuscript revision. N.A. performed all electrophysiology recordings. Y.C. performed most of the motoneuron culture. J.J.H. designed the experiments and directed the work as well as edited the manuscript until it was in its final form.

Introduction

There has been a recent emphasis on the development of *in vitro* “human-on-a-chip” systems for use in drug discovery studies as well as basic cell biology investigations. While animal models have been the standard for disease and drug evaluation, many of the effects seen in these models are incongruent with the effects seen in humans. Furthermore, various organizations have restricted the use of animal models for ethical considerations. To avoid these difficulties, *in vitro* systems that integrate human cell culture with bio-microelectromechanical systems (BioMEMS) devices are being investigated for their ability to recapitulate functional human organ systems(1, 8, 9, 76-80). The high content analysis

capabilities, reproducibility, ethical considerations, and biological flexibility with relevant cell types have increased the demand for realistic functional *in vitro* systems. The neuromuscular reflex arc is a highly complex biological circuit, where the actuation segment has been successfully evaluated using *in vitro* systems(13, 14, 37, 81-83). We have previously shown functional neuromuscular junction formation *in vitro* for both animal and human cells on a non-biological substrate(13, 37). We have also demonstrated the fundamental sensory portion of the arc by animal and human sensory neuron innervation of intrafusal fibers (14, 15). Further elaboration of this system, by incorporating additional sensory components, allows for a more accurate recapitulation of *in vivo* functionality and serves as a better representative platform for investigating prosthetic design, neuromuscular diseases and understanding the mechanism of action for relevant drugs and their targets(84, 85).

The stretch reflex arc is the physiological system that regulates skeletal muscle movement and tension. This arc can be broken down into two primary components: the efferent and afferent domains. The efferent domain regulates mechanical actuation, muscle tension and relaxation through extrafusal fibers(86). The regulatory control of tension and contraction is mediated by innervating α -motoneurons. Embedded within the extrafusal fiber tissue are muscle spindles, the sensory organ for afferent (sensory) signals to regulate muscle function(86). The spindles are composed of intrafusal fibers encapsulated in collagen and innervated by both sensory and gamma-motoneurons (γ -MNs)(86-88). The primary role of intrafusal fibers is the detection of the magnitude and speed of stretch or flexion of the muscle and the position of the limbs, or proprioception(86, 87). Upon a change in muscle tension, the muscle spindles send signals through afferent sensory neurons which are relayed to neurons within the spinal cord.

Motoneurons receiving afferent information can then signal to intrafusal or extrafusal fibers to

relax or contract in response to sensory input(86). With the afferent sensory feedback, the reflex arc acts as an automated closed loop so that voluntary movement can be achieved accurately and properly.

Several types of neurons innervate both the extrafusal and intrafusal fibers of the muscle tissue. The extrafusal fibers are primarily innervated by α motoneurons while intrafusal fibers are innervated by both sensory neurons and γ -MNs(86). The Type Ia sensory neurons innervate the intrafusal fibers with annulospiral wrappings around the equatorial region and Type II sensory neurons employ flower spray endings towards the peripheral ends of the fiber. γ -MNs innervate the peripheral ends of the intrafusal fibers via flower-spray endings as well. The peripheral ends of the intrafusal fibers slowly relax or contract under the control of γ -MNs. These γ -MNs modulate the tension, sensitivity, and length of the intrafusal fibers so muscle spindles can maintain constant sensitivity during dynamic muscle action and prevent overextension, which can lead to undue stress on the muscle as well as tendon and joint damage(87). Unlike α motoneurons, γ -MNs do not directly induce muscle tissue contraction or relaxation but modulate the sensitivity of the muscle spindle instead(86), which then modifies the activity of α -motoneurons (α -MN) and subsequent muscle contraction. Human-based *in vitro* models for the innervation of extrafusal fibers by α -MNs and intrafusal fibers by proprioceptive sensory neurons have been established, but an *in vitro* model for the innervation of intrafusal fibers by γ -MNs has yet to be developed, despite being crucial for proper function of the neuromuscular system. Development and incorporation of this γ -motoneuron - intrafusal fiber system into the reflex arc would provide a better platform for the study of neuromuscular development, prosthetic design, relevant diseases and the evaluation of potential drug candidates.

Investigations surrounding γ -MN interactions have been sparse due to the nature of the cell types involved, and the lack of *in vitro* studies demonstrating this particular cellular interaction, especially with human cells. Although γ -MNs have a specific function in the neuromuscular system, their developmental similarity to α -MNs has made it difficult to identify them for study. γ -MNs originate in the ventral spinal cord along with three subtypes of α -MNs(86, 87). Recently, molecular markers have become available for identifying γ -MNs in co-culture with α -MNs from murine tissue(89-94). However, functional data of postnatal *in vitro* γ -MNs has yet to be observed and no human systems have been studied.

Utilization of human reflex arc test platforms with the inclusion of γ -MNs could allow for more appropriate analysis of neuromuscular diseases, particularly in relation to proprioceptive function. This is specifically applicable for Spinal Muscular Atrophy (SMA) research. The mechanism for SMA progression in murine models indicated a difference in motoneuron subtype (α versus γ) survival rates compared to analysis of human cells(95). These data imply that animal models may be insufficient to recapitulate the human form of the disease and more accurate, reproducible, and modular models are needed to fully understand the mechanisms of disease onset and progression. There is also a distinct possibility that this circuit can be involved in neuropathic pain in some cases(96) and a model system that could investigate this possibility should significantly advance our understandings in this field. In this study, we aimed to develop a de novo defined human-based functional *in vitro* fusimotor system in which the innervation of intrafusal fibers by γ -MNs was evaluated by both immunocytochemical and electrophysiological approaches.

Results

Morphological analysis

Human intrafusal fibers were co-cultured with human motoneurons (MNs) on trimethoxysilylpropyldiethylenetriamine (DETA) coated glass coverslips in serum-free medium. This surface modification has been used as a means of providing a surface amenable for the proliferation and maturation of an array of cell types for long term experimentation(7, 13-15, 34, 36, 37, 79, 81, 82, 97-102) Figure 9 indicates the protocol for cell expansion and differentiation for developing the co-culture and more detail can be found in Guo *et al.*(15) and Guo *et al.*(36). Cellular proliferation and differentiation of intrafusal fibers and neurons were temporally monitored via phase contrast microscopy and assessed via morphological analysis as shown in Figure 10. Intrafusal fibers and neurons were identified in the culture by their unique morphological features. Chain fibers have long segments of aligned nuclei in the equatorial region and bag fibers have a large cluster of nuclei in the center of the fiber, which tapers down to thin myotube endings used to anchor both ends of the elongated cell within the spindle *in vivo*(44). Phase contrast images demonstrated both chain and bag morphologies of intrafusal fibers. Direct physical contacts observed morphologically between intrafusal fibers and neurons indicated possible intrafusal fiber innervation by MNs (Figure 10 F-G).

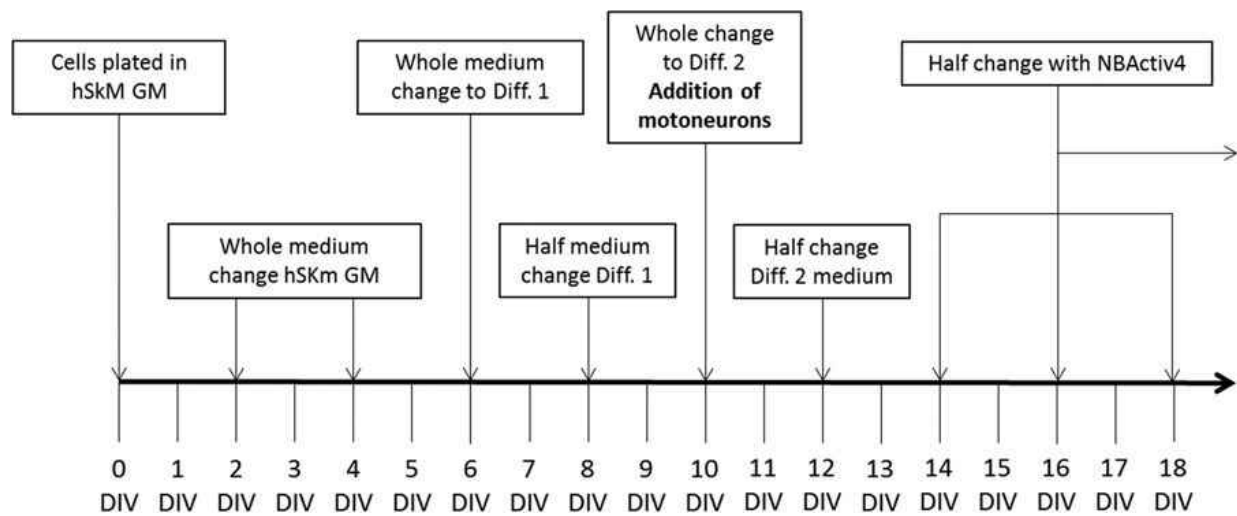


Figure 9: The cell culture scheme for the differentiation of the human intrafusal fibers derived from satellite cells. MNs added on day 10 of the culture were subjected to 2–10 DIV differentiation.

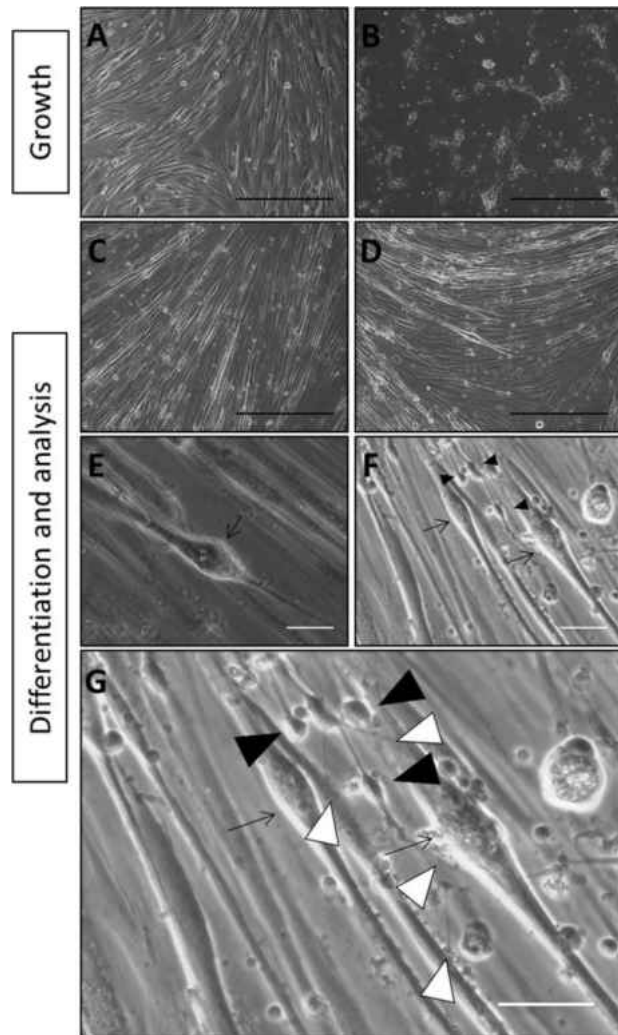


Figure 10: Phase contrast analysis of the human skeletal muscle and motoneurons. **(A)** Human muscle at 4 DIV. **(B)** Human MNs at 4 DIV. **(C and D)** Human muscle cultured without **(C)** and with **(D)** MNs at 17 DIV. **(E and F)** Morphological confirmation of intrafusal fibers in both muscle only **(E)** and muscle and MNs co-cultures **(F)**. **(G)** An enlarged view of image F to demonstrate the contacts of axon terminals with intrafusal fibers. Intrafusal fibers are indicated with **arrows** and MNs are indicated with black arrowheads. Neuromuscular contacts are indicated with white arrowheads. Black scale bars are 500 μ M. White scale bars are 50 μ M.

Immunocytochemical analysis

After maturation, at approximately day 15 of the human muscle and MN co-culture, cells were immunostained utilizing the molecular markers for both intrafusal fibers and γ -MNs (Table 3). The general marker used to identify muscle fibers in the cultures was All myosin heavy chain (AllMyHC). Neurofilament, a neuronal cytoskeleton marker, was used to non-specifically identify neurons. Intrafusal fibers were identified using pERB2 and EGR3. ErbB2 is a receptor tyrosine kinase for neuregulin, a molecule released by neurons as part of the intrafusal induction mechanism during differentiation(103). Upon the binding of neuregulin to ERB2, the receptor becomes phosphorylated (pErbB2)(104), leading to an increase in the transcription factor EGR3, which initiates the expression of genes for intrafusal differentiation(105). Immunocytochemistry indicated positive identification of both bag and chain intrafusal fibers (Figure 11).

Table 3: Listing of primary antibodies used to characterize γ -motoneurons, intrafusal fibers and the co-cultures.

Antibody	Target	Host Species	Dilution/ Concentration	Source	Catalog Number
All MyHC	All muscle	Mouse	1:10	Developmental studies hybridoma bank	A4. 1025
Phospho-erbB2	Intrafusal fibers, activated NRG receptors	Rabbit	2 μ g/ml	Millipore	06-229
EGR3	Intrafusal fibers, transcription factor	Rabbit	1:100	Santa Cruz Biotechnology	SC-191
Erry	γ -MNs	Mouse	1:100	Perseus Proteomics	PD-H6812-00
α-Bungarotoxin	Acetylcholine receptors	N/A	1:100	Thermo Fisher	B13422
Neurofilament	Neuronal cytoskeleton	Chicken	1:1000	Millipore	AB5539

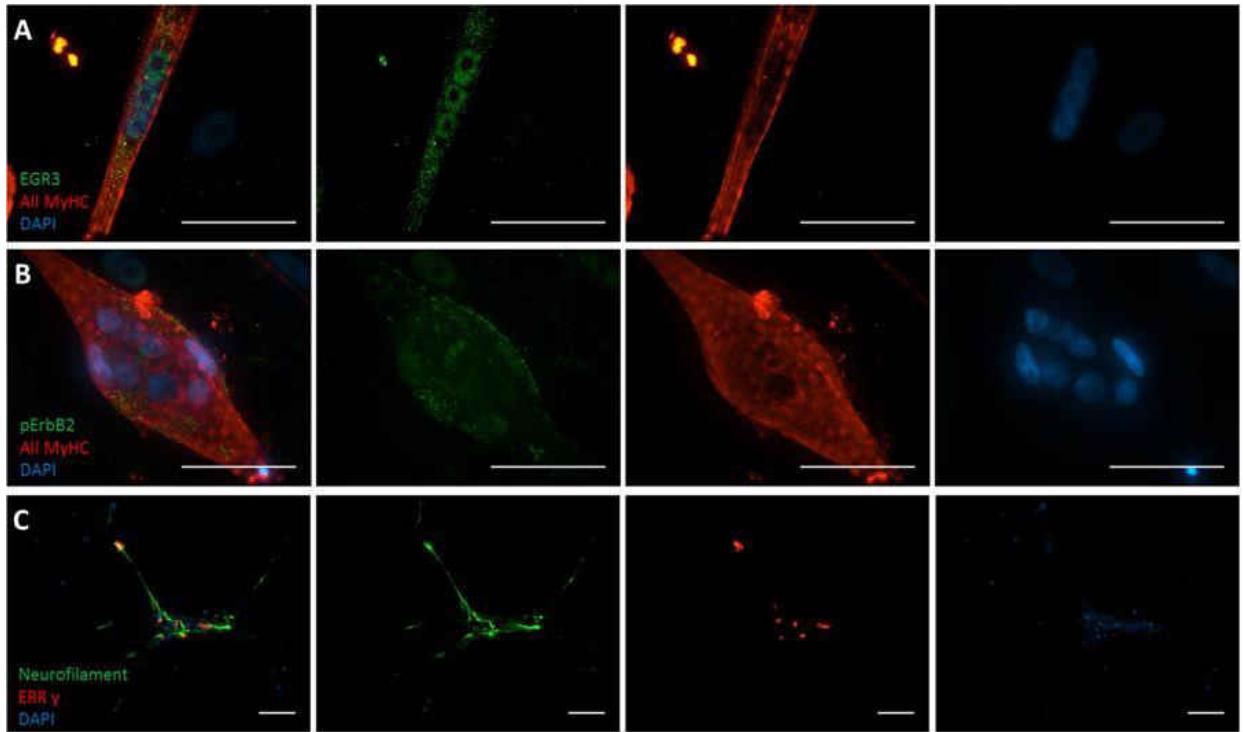


Figure 11: Immunocytochemical analysis of intrafusal fibers and γ -MNs. (**A** and **B**) Intrafusal fibers were identified with the antibodies against EGR3 (**A**) and pErbB2 (**B**). Myotubes were visualized with the antibody against All Myosin Heavy Chains, and nuclei were identified by DAPI (**A** and **B**). A sample image of a chain fiber is shown in panel A and bag fiber in panel B. (**C**) Motoneuron cultures were stained with Neurofilament and γ -MNs were additionally stained with an antibody against ERR γ . Scale bars are 50 μ M.

Very few markers have been reported for γ -MNs, but ERR γ (95) was found to be the most robust. Other markers were evaluated, including Wnt7a (marker for γ -MNs) and NeuN (marker for α -MNs), but did not have as robust and repeatable of a signal as ERR γ (Figure 11). γ -MNs were recognized by positive immunostaining for ERR γ and the axonal terminals were visualized with neurofilament (Figure 12 A). Since the cultures used have a mixed population, γ -MNs were quantified in a motoneuron preparation and it was found to have

3.63% γ -MNs ($\pm 0.86\%$). Previous work has shown these cultures contain about 20% of motoneurons(101) so the MN culture consisted of about 18% γ -MNs in the culture. Recent literature from *in vivo* animal studies has also shown that γ -MN innervation of intrafusal fibers is an acetylcholine (ACh)-based neuromuscular interaction(106). In order to detect the possible innervation of intrafusal fibers by γ -MNs in the co-culture, intrafusal fibers were visualized by fluorescently-labeled bungarotoxin (BTX), a toxin that specifically binds to ACh receptors (Fig. 4). The close apposition of γ -MN axonal terminals or soma with the ACh receptor -positive intrafusal fibers were frequently observed under high definition confocal microscopy, demonstrating immunocytochemical evidence for the potential innervation of intrafusal fibers by γ -MNs. These interactions were quantified as 53.4% ($\pm 7.59\%$) of all neuromuscular appositions. Considering the low percentage of γ -MNs in the motoneuron only culture, interactions between intrafusal fibers and γ -MNs appear to be enhanced over interactions between intrafusal fibers and other neuron types in the culture. This may imply a selective mechanism to promote NMJs between γ -MNs and intrafusal fibers.

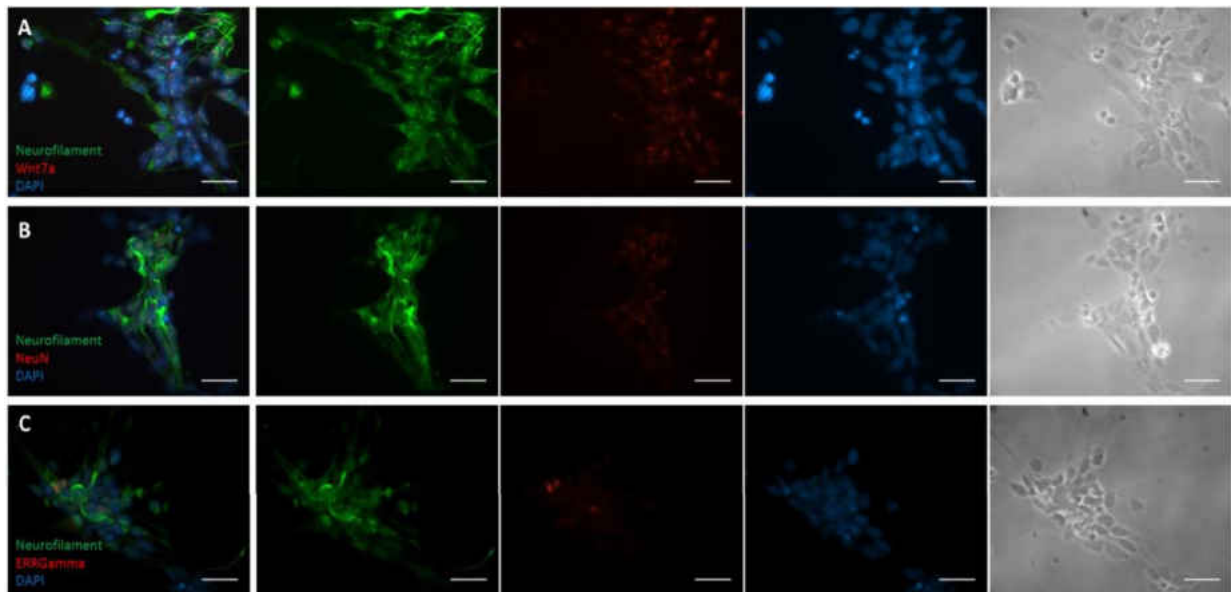


Figure 12: Immunocytochemical analysis of motoneuron only cultures. Markers for Wnt7a (Abcam ab100792) (A) NeuN (Millipore MAB377) (B) and ERRGamma (C) immunocytochemistry in motoneuron only controls. Scale bars are 50 μ M.

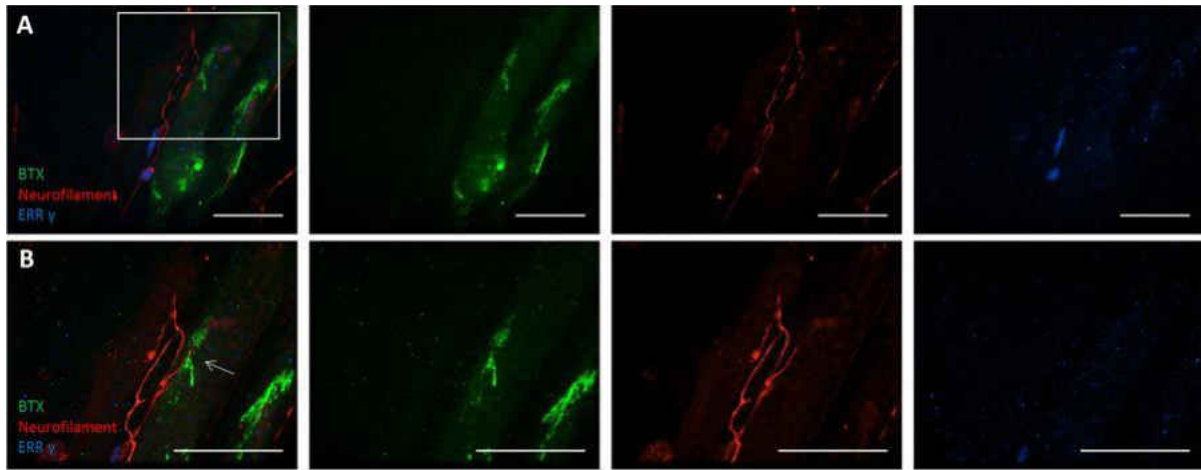


Figure 13: Immunocytochemical analysis of intrafusal fibers and motoneurons co-cultures.

(A) Co-cultures were stained with Bungarotoxin (BTX), Neurofilament, and ERR γ . (B) High definition image for the boxed area in (A) indicates a close apposition of an axonal terminal from a γ -MN with BTX-488 patches (white arrow). Scale bars are 50 μ M.

RNA expression analysis

Immunocytochemistry results for γ -MN percentage in the MN cultures were confirmed by quantitative PCR analysis. RNA expression of $ERR\gamma$ was examined in human motoneuron cultures, utilizing the undifferentiated neural progenitors (human spinal cord stem cells, or SCSCs) as the control. There was found to be a 5.3 fold increase in $ERR\gamma$ expression in differentiated human motoneurons compared to the control (Figure 14). This confirmed the increase in expression levels of the γ -MN specific marker $ERR\gamma$ in the immunocytochemical data, demonstrating the presence of γ -MNs in the heterogeneous culture.

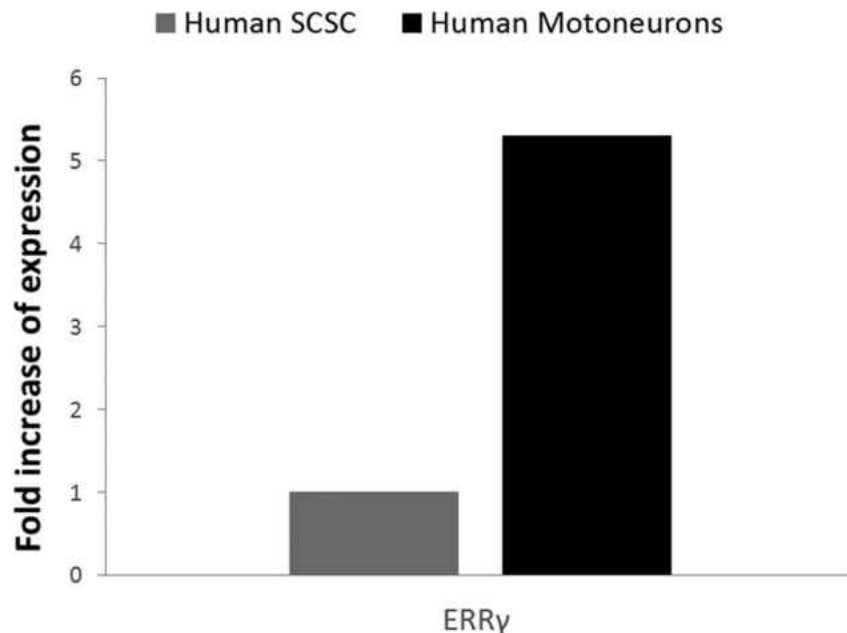


Figure 14: Quantitative PCR: Quantification of $ERR\gamma$ in the motoneuron culture compared to that in their undifferentiated precursors, human SCSCs

Electrophysiological analysis

The immunocytochemical evidence strongly suggested that the stimulation of γ -MNs would lead to electrophysiological activity in the intrafusal fibers. In order to determine if the innervations identified immunocytochemically were functional, patch-clamp electrophysiological recordings were performed on intrafusal fibers (15–30 days in vitro (DIV)). Glutamate is an excitatory neurotransmitter that has been previously used to stimulate neurons in co-cultures with muscle without directly initiating myotube contraction(13). The electrophysiological response to the addition of glutamate, both with and without MNs in the culture, was recorded from intrafusal fibers, identified by their morphological characteristics, in the co-culture (Figure 15 A,B). Theoretically, the intrafusal fiber, if innervated, should be excited upon glutamate addition, while those not innervated should not be affected. As indicated, bursts of myotube action potentials (APs) were induced in multiple intrafusal fibers upon glutamate addition, suggesting innervation by γ -MNs (Figure 15 C). To confirm that the increased AP firing was initiated by ACh-mediated innervation, a blocking agent for ACh mediated synaptic transmission, curare, was applied after increased firing was initiated by glutamate treatment(13). Immediate cessation of electrophysiological activity was observed (Figure 15 D). This demonstrated the functional innervation of the intrafusal fibers by γ -MNs. As a control, the same experiment was performed on intrafusal fibers in the absence of MNs where no significant change of activity was detected. Quantification of the co-cultures indicated that 28 out of 34 intrafusal fibers were excited upon glutamate addition, while only 1 out of 23 muscle-only controls were excited (p value = 0.2.17e-9) (Figure 16). The few intrafusal fibers not excited in the co-culture may not have been innervated, resulting in a lack of response to MN activity. This

data confirms not only the formation of functional synapses but also demonstrates a high percentage of γ -MN innervation of the intrafusal fibers under these co-culture conditions.

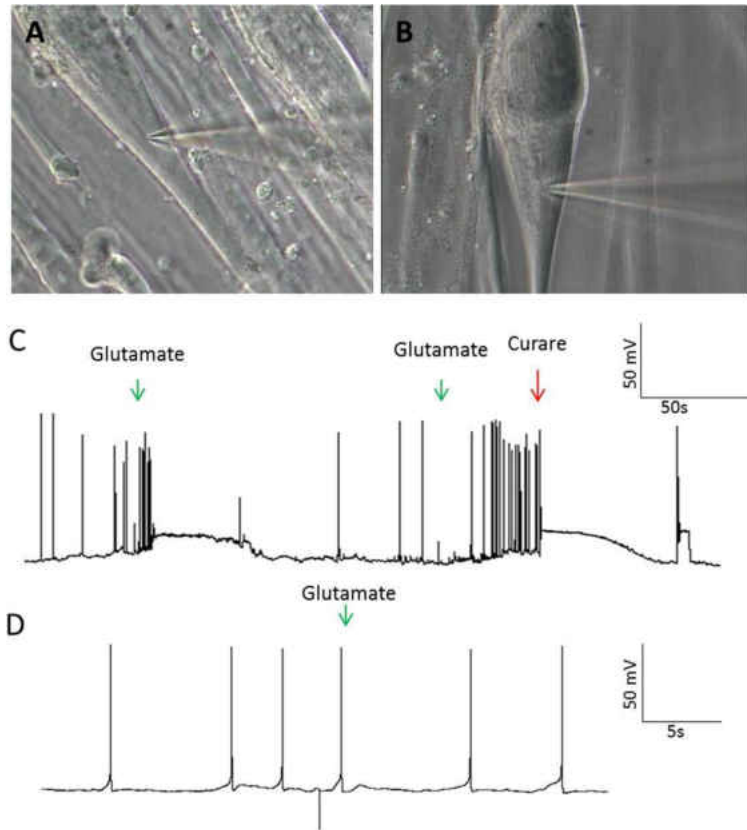


Figure 15: Patch-clamp analysis of intrafusal fibers. (A,B) Representative bright field microscopy of patched intrafusal cells in motoneuron-muscle co-cultures (A) and muscle only controls (B). (C,D) Gap-free recordings from patched intrafusal fibers in motoneuron–muscle co-cultures (C) and muscle only controls (D). Addition of glutamate (marked with green arrows) in the co-culture elicited increased activity and addition of curare (marked with red arrow) terminated activity (C) but no activity change was induced by either of them in intrafusal fibers in the muscle culture alone (D).

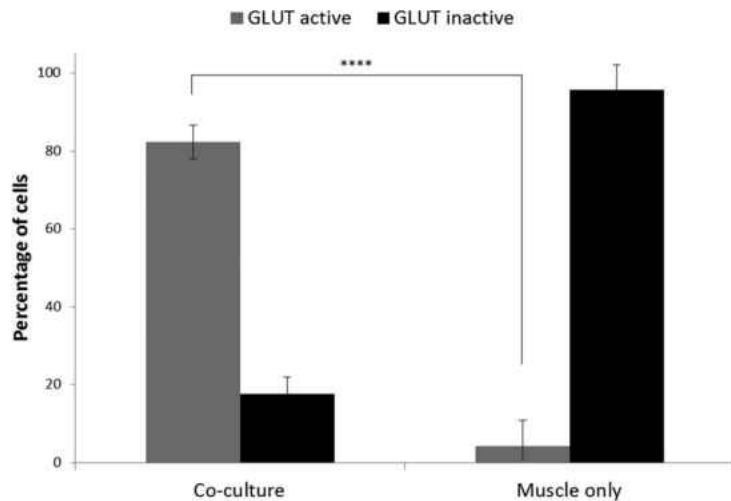


Figure 16: Statistical analysis. Percentages of glutamate responding and glutamate nonresponding intrafusal fibers in muscle-motoneuron co-culture conditions and muscle only conditions. P value = 2.17e-9.

Discussion

We have developed a human-based *in vitro* fusimotor system in which functional innervation of intrafusal fibers by γ -MNs was demonstrated by morphological, immunocytochemical and electrophysiological analysis. Neither the culture of human γ -MNs nor their innervation by intrafusal fibers has previously been shown *in vitro*. The recapitulation of the spindle fusimotor circuit *in vitro* with human cells provides a defined model to investigate the physiology of this circuit, which is otherwise extremely difficult to observe for human systems. The use of MNs and muscle derived from iPSCs also offers the possibility for their incorporation into human-on-a-chip systems designed for the investigation of patient specific neuromuscular diseases and deficits.

The functional sensory circuits, especially human based systems, have previously not been extensively investigated *in vitro* and γ -MN identification and functional innervation had not

been demonstrated with human cells at all. Here, a co-culture of human intrafusal fibers and human MNs was established to evaluate the interactions between these two important cell types from the sensory portion of the reflex arc. Initial morphological analysis via phase contrast microscopy indicated the two cell types were compatible in a serum-free defined system and formed close physical contacts suggesting synaptic interactions.

Immunocytochemical analysis confirmed the identity of the cell types in these intercellular interactions. Intrafusal fibers stained positive for pERB2 and EGR3, while the γ -MNs were identified by immunostaining with a γ -MN specific marker ERR γ (87, 89, 93).

Electrophysiological analysis confirmed functional interactions between the γ -MNs and intrafusal fibers. γ -MNs were stimulated using the neurotransmitter glutamate. The majority of intrafusal fibers in co-culture demonstrated increased excitation upon the application of glutamate (28 out of 34), while only one intrafusal fiber in the monoculture responded.

Furthermore, the glutamate-induced responses were terminated by the application of curare, a competitive antagonist of acetylcholine receptors. These data indicate functional innervation of human intrafusal fibers by human γ -MNs in our defined *in vitro* system.

It should be pointed out that a single intrafusal fiber in monoculture conditions exhibited AP firing upon exposure to glutamate. The presence of glutamate receptors on muscle fibers is known and has been researched(107, 108). Multiple mechanisms have been proposed regarding the function of glutamate receptors in muscle tissue, but none of which correspond to direct action potential generation(109-114). Actually, a similar response was recorded from another intrafusal fiber in a muscle-only culture by adding media instead of glutamate (data not shown), indicating the addition event itself could non-specifically induce muscle

excitation, although very rarely. To further confirm the muscle was not directly excited by glutamate in our system, glutamate dosage experiments (data not shown) were performed on muscle only cultures to evaluate the responsiveness of intrafusal fibers to increasing concentrations of glutamate. The lack of glutamate mediated electrical activity in these cultures, even at concentrations far higher than used in experiments reported here, demonstrates the lack of direct response to glutamate. This evidence confirms that the single cell responsive to glutamate was not the result of a glutamate induced electrophysiological mechanism in this human model.

Study of the entire functional reflex arc is essential to understand and further investigate many neuromuscular disorders, predominantly Amyotrophic Lateral Sclerosis (ALS) and Spinal Muscular Atrophy (SMA). In both reports the sparing of γ -MNs were reported in mice models as well as peripheral neuropathies(95, 115). Most existing *in vitro* systems used to study these diseases only investigate the motor perspective of neuromuscular interactions. However, utilization and especially integration of sensory components is essential to investigate complicated neuromuscular diseases by the inclusion of afferent mechanisms. Additionally, the sensory portion of the reflex arc has been of interest to the field of pain research(96). Drug discovery has been moving towards more repeatable and high-throughput organ-on-a-chip *in vitro* systems recently for use in preclinical compound evaluation to improve drug discovery efficiency(1, 8, 9, 76-80). These systems provide a highly controllable and repeatable platform that can be tailored to more human-specific diseases by utilizing patient-derived iPSCs. Incorporation of γ -MN and intrafusal interactions to such systems will allow for a more complete and refined model for simulating neuromuscular diseases and testing a multitude of drug response variables.

Materials and Methods

Surface modification

18 mm round glass coverslips (VWR, 48380-046) were cleaned and functionalized by exposure to an oxygen plasma generated by a Harrick plasma cleaner (model PDC-32G) utilizing high purity oxygen gas. The surfaces were then submersed in a reaction solution of 1% v/v of trimethoxysilylpropyldiethylenetriamine (DETA, United Chemical Technologies, Inc., T2910-KG) in dry toluene (VWR, BDH1151-4LG) and heated to just below the boiling point of toluene over a period of 30 minutes. The reaction vessel was removed from heat and allowed to cool for 30 minutes, and then rinsed in 3 serial toluene baths. Next, the surfaces were placed in dry toluene and heated to just below the boiling point of toluene over a period of 30 minutes. After the second heating step, the surfaces were cured in an oven at approximately 110 °C overnight (~15 hr). Derivatized surfaces were characterized by contact angle goniometry, with a 5 µL droplet of water, and by X-ray photoelectron spectroscopy using a Thermo Scientific ESCALAB 220i-XL instrument with aluminum K α X-rays and a 90° take-off angle(97, 98).

Cell culture

Human intrafusal fibers were differentiated from human satellite cells provided as a gift from Dr. Herman Vandenburg. Human skeletal muscle stem cells (hSKM SCs)/progenitors were isolated and proliferated as described in Thorrez *et al.*(68) Briefly, the primary human skeletal muscle cells (hSKMs) were isolated by needle biopsy(116) and expanded in the myoblast growth medium (MGM; SkGM (Cambrex Bio Science, Walkersville, MD) plus 15% (v/v) fetal bovine serum. Biopsies were performed on adult volunteers according to procedures

approved by the Institutional Clinical Review Board of the Miriam Hospital and were performed in accordance with the relevant guidelines and regulations. All samples, from the study participation and publication of images, were obtained with informed consent and de-identified before being sent to UCF. Cell preparations averaged 70% myogenic content based on desmin-positive staining(117). The differentiation protocol was adapted from our protocol for extrafusal fiber differentiation by inclusion of specific factors to facilitate intrafusal differentiation(15). Specifically, thawed satellite cells from liquid nitrogen were plated onto glass coverslips at a density of 100 cells per mm². The cells were given a whole medium change of human skeletal growth medium every two days until confluent. Upon confluence, the medium was fully switched to differentiation 1 medium (DMEM (Invitrogen 11775-040), Insulin (Sigma I9278) at 10 µg/ml, BSA (Sigma A9418) at 500 µg/ml, and EGF (Invitrogen 13247-051) at 10 ng/ml)(36) and fed every 2 days for 4 days. At this point, the medium was switched to differentiation 2 medium (described in detail in Guo *et al.*(15)) and MNs were added to co-cultures at 50 cells per mm². The cells were fed every two days with differentiation 2 medium and maintained for four days. After this point, the medium was given a half change with NBActive4 differentiation medium. The cells were maintained in this medium for the remainder of the culture and fed every two days until 15–30 DIV total when they were analyzed via electrophysiology or fixed for immunocytochemical analysis.

Human Motoneurons were differentiated from spinal cord stem cells (SCSCs) NSI566RSC according to a previous report(37). Specifically, thawed SCSC cells (0.5 E6) from liquid nitrogen were plated onto a T-25 cell culture flask coated with Poly-D-Lysine. The cells were supplemented with bFGF every day and fed every other day with N2B medium. Upon confluence, the cells were trypsinized with 0.05% Trypsin and the reaction was inhibited with

the addition of 0.2% Trypsin inhibitor (final 0.05%). The cells were replated onto a permanox dish (Diameter 60 mm) coated with Poly-D-Lysine and fibronectin. Cells were initially plated in priming medium and fed on day 2 of culture with a half change of medium. On day 4 the medium was half changed with human MN medium. The cells were maintained in the permanox dish for about 10 days. At this point cells were again trypsinized and purified via an Optiprep concentration gradient (Optiprep diluted to 30% [v/v] utilizing Neurobasal with and without phenol red (ThermoFisher Cat#21103-049 and Cat#12348-017, respectively) and then made to 9.5, 7.0, 6.0, and 5.5% for fractions 1–4, bottom to top sequentially [v/v] in Neurobasal, with fractions 1 and 3 containing phenol red and fractions 2 and 4 lacking phenol red for optimizing visualization of the fractions). The cells were plated into DETA coated glass coverslips for less than 10 days before being trypsinized (as described above) and replated onto either muscle cultures or control DETA coated glass coverslips. At this point the neurons either underwent exposure to intrafusal differentiation media (co-cultures) or were maintained in human MN medium (monocultures).

Immunocytochemistry

Cells on coverslips were fixed with 4% paraformaldehyde diluted in PBS solution for 15 minutes, then rinsed with PBS (phosphate buffered saline) for 5, 10, and 15 minutes and stored until staining in PBS. Cells were permeabilized with 0.1% Triton X-100 for 15 minutes then incubated for 1–2 hours at room temperature in blocking buffer (5% Donkey serum +0.5% BSA in PBS) to prevent nonspecific binding. Fixed and permeabilized cells were incubated overnight with primary antibodies (diluted in blocking buffer) at 4 °C. Antibodies used and their concentrations are listed in Table 3. The cells were rinsed with PBS for

5 minutes, 0.01% Triton X-100 for 10 minutes and PBS for 15 minutes, and then subjected to incubation with the secondary antibodies (1:250 diluted in blocking buffer) for 1–2 hours at room temperature. The cells were then rinsed with PBS for 5 minutes, 0.01% Triton X-100 for 10 minutes and PBS for 15 minutes and mounted onto glass slides using ProLong Gold Antifade Mountant with DAPI (Thermo Fisher P36931) or Vectashield mounting medium for fluorescence (Vector laboratories, Burlingame, CA) and imaged using a Zeiss LSM 510 confocal microscope.

Quantitative polymerase chain reaction

Human motoneurons and human spinal cord stem cells were harvested for RNA extraction at less than 10 days *in vitro*. The RNA extraction was done utilizing the Aurum™ Total RNA Mini Kit (Biorad 7326820). RT-PCR was performed using the iTaq™ Universal SYBR® Green One-Step Kit (Biorad 1725150). Reaction volumes was 25 µl total (12.5 µl 2X SYBR® Green reaction mix, 0.75 µl forward primer at 10 µM, 0.75 reverse primer at 10 µM, 1.0 µl iTaq DNA polymerase, 10 ng RNA template, and enough water to fill the remaining volume). Reactions were incubated at 50 °C for 10 minutes, 95 °C for 5 minutes, 95 °C for 10 seconds and 55 °C for 30 seconds cycled 40 times, and underwent melt curve analysis (95 °C for 1 minute, 55 °C for 1 minute, and 55 °C to 95 °C for 80 cycles for 10 seconds, increasing 0.5 °C each cycle). ERRγ (Forward: 5'-AGGAAAACCTATGGGGAATG-3'; Reverse: 5'-GGAGCAAATGAAATGTGGGTG-3') expression was evaluated along with β-actin (Forward: 5'-CCCCATTGAACACGGCATTG-3'; Reverse: 5'-ACGACCAGAGGCATACAGG-3') as a positive control and template free β-actin reactions as negative controls. Samples were run in triplicate along with β-actin positive controls and

template free negative controls. An MJ mini thermal cycler (Biorad) and Opticon Monitor software (Biorad) were used. Expression levels were corrected with β -actin levels.

Electrophysiology

Whole-cell patch clamp recordings were performed in a recording chamber on the stage of an upright microscope (Axioscope FS2, Carl Zeiss, Göttingen, Germany). The patch-clamp recording chamber was filled with the same medium as utilized for cell culture. The intracellular solution composition was (in mM): K-gluconate 140, NaCl 4, CaCl₂ 0.5, MgCl₂ 1, EGTA 1, HEPES acid 5, HEPES base 5, Na₂ATP 5. Patch pipettes were prepared (borosilicate glass, BF150-86-10; Sutter, Novato, CA) with a Sutter P97 pipette puller. Pipette resistance was 4–10 M Ω for intracellular patch clamp recordings. Experiments were performed with a Multi clamp 700B (Axon Instruments, Foster City, CA, USA) amplifier. Signals were filtered at 2 kHz and digitized at 20 kHz with an Axon Digidata 1322 A interface. Action potentials were recorded in current-clamp mode under gap free conditions at zero holding potential. The series resistance was in the range of 5–10 M Ω and was compensated by 60% on-line. Leak currents were subtracted using a standard P/4 protocol. Before seals were established on the cells, offset potentials were nulled. Capacitance subtraction was used in all recordings. All intrafusal fibers chosen in co-culture conditions were in proximity to MNs identified via morphological analysis. To test whether the patched intrafusal fiber was innervated, glutamate was added in 30 μ l doses of 200 mM to the extracellular solution in the vicinity of the patched intrafusal fiber. When excited, the MNs would excite innervated muscle fibers and the excitation was recorded. Once repetitive firing was consistent, curare was added in 30 μ l doses of 500 μ M to the extracellular solution.

Statistical analysis

The proportion of active intrafusal fibers that showed electrical activity in response to glutamate was compared between muscle only and co-cultured conditions by categorizing each patched cell as responsive or unresponsive and organized into a contingency table, followed by statistical analysis via Fisher's Exact Test ($\alpha = 0.05$). 57 cells were patched across multiple coverslips and platings. The standard error of the mean for each proportion was calculated for the binomial distribution. γ -MN quantification data was taken from 20 view fields from each of three separate coverslips spanning over two separate platings. For γ -motoneuron- intrafusal fiber interaction quantification, two separate co-culture coverslips from two separate platings were stained with ERR γ , BTX488, and neurofilament. Intrafusal fibers positive for BTX488 staining that had contact with neuronal processes positive for neurofilament that lead to an identifiable soma were counted. Standard deviations were calculated and expressed as percent error.

CHAPTER FOUR: DIFFERENTIATION OF HUMAN INTRAFUSAL FIBERS FROM INDUCED PLURIPOTENT STEM CELLS

The work in this chapter was submitted for publication as follows.

Colón, A., Badu-Mensah, A., Guo, X., Goswami, A., Hickman, J.J. Differentiation of intrafusal fibers from human induced pluripotent stem cells. ACS Neuroscience. June 14, 2019.

J.J.H. and A.C. performed the experimental design, A.C. performed the differentiation from myoblasts to mature myotubes, all immunocytochemistry, all imaging, executed statistical analysis, arranged the figures, and wrote the manuscript. A.B. performed all differentiation of iPSCs into myoblasts and provided feedback on the manuscript and experimental design. X.G. contributed significantly to the manuscript, experimental design, and data interpretation. A.G. provided the DETA modified glass coverslips. J.J.H. directed the work and edited the manuscript until it was finalized.

Introduction

Animal models have never been an optimal route for modeling human disease states and physiology (1, 76). The differences between human and animal physiology have often caused failures in drug trials, leading to a slow and expensive drug discovery process (76). Furthermore, regulatory bodies have been emphasizing more ethical standards for drug discovery, moving toward more animal-free designs. As a result, “body-on-a-chip” testing platforms have become a major interest to drug companies, research scientists, practicing clinicians, and related regulatory bodies. These platforms integrate microelectromechanical systems (MEMS) and specific cell types to have functional phenotypic models of single and multi-organ systems. This allows for the evaluation of the pathology of specific diseases as well as the response of these specific cells

to drug treatments (77). While several human-based cell lines are available for integration into these “body-on-a-chip” systems, there are certain challenges regarding maintenance, reproducibility, and clinical relevance for diseases with genetic variances. Induced pluripotent stem cells (iPSCs) have found increasing significance in the development of phenotypic models for many diseases due to their ease of use, significant clinical relevance and in many cases the lack of relevant animal models (11). These cells are obtained from human biopsy or blood samples and are treated with defined factors to drive their developmental stage back to pluripotency (118). They can then be re-differentiated into multiple cell lineages, allowing for the phenotypic evaluation of specific genotypes and their physiological manifestations and drug responsiveness. The integration of these cell types into “body-on-a-chip” technology is essential for developing testing platforms designed for use in preclinical drug candidate evaluation and use in personalized medicine and treatment plan optimization applications.

The neuromuscular reflex arc is composed of four cell types: motoneurons, sensory neurons, extrafusal fibers, and intrafusal fibers. Motoneurons send efferent signals to the contractile extrafusal fibers, modulating the contraction, relaxation, and tension of the muscle tissue.

Embedded in the extrafusal skeletal muscle tissue is the muscle spindle composed of intrafusal fibers. The subtypes of intrafusal fibers have distinct morphological characteristics. Bag fibers have a large collection of nuclei in the equatorial region with a tapering to each anchoring fiber end (44). Chain fibers have a collection of nuclei in close proximity composed of a single row with a narrow cytosol (44). The muscle spindle is the sensory organ of muscle tissue and sends afferent proprioceptive information to the central nervous system via sensory neurons (44, 88, 119). Additionally, these muscle spindles can be innervated by gamma motoneurons to aid in compensating for muscle length and maintaining spindle sensitivity (86).

This multi-cell reflex arc system has been previously evaluated by integrating the cellular compounds of the arc with MEMS devices (14-16, 34, 81, 83, 120) to model the complex structure and physiology of the neuromuscular reflex arc (5, 7, 13, 14, 99, 121-124). However, current technologies have limitations that warrants research improvements and increased sophistication of the platforms. One of the most useful hybrid devices is the incorporation of extrafusal (7, 13, 99, 123, 125) and intrafusal (14) fibers with silicon cantilever platforms to record or activate myofiber function. Recent techniques have used commercially available cell lines which can aid in the investigation of basic physiology but fail to address genetic components of neuromuscular diseases such as amyotrophic lateral sclerosis (ALS) and spinal muscular atrophy (SMA). These diseases have several genetic variants, each of which have relatively unique molecular differences (126, 127). Integration of iPSCs into existing cantilever-based testing platforms would allow for real-time functional investigation of these genetic differences and how they influence force output and connectivity aberrations due to specific mutations. Motoneurons, (128) sensory neurons, (129) and extrafusal fibers, (130) have each been previously derived from iPSCs. However, the differentiation of intrafusal fibers from iPSCs is yet to be demonstrated.

Intrafusal fiber differentiation *in vivo* is primarily regulated by neuregulin (NRG), a factor secreted by sensory neurons during neuromuscular development (16, 35, 40). Once NRG interacts with ErbB2 receptors in the undifferentiated myoblasts, this receptor becomes phosphorylated (phospho-erbB2 or pErbB2) (16). This phosphorylation leads to the induction of intrafusal fiber specific transcription factors, such as Egr3, (16, 35) and the differentiation of these myofibers into intrafusal fibers (16, 35). Addition of NRG *to in vitro* cultures to increase activation of this pathway has been previously utilized to increase the amount of intrafusal fibers

in both human (15, 16) and rat (34) myoblast cell lines. In this work, NRG supplementation to the culture medium was sufficient to drive iPSC-derived myoblasts toward intrafusal fiber differentiation. The morphology and ErbB2 phosphorylation levels was evaluated to confirm intrafusal fiber identity. Additionally, these cells were grown and differentiated on trimethoxysilylpropyldiethylenetriamine (DETA) coated surfaces, a self-assembling monolayer compatible with “body-on-a-chip” systems. These cells can later be integrated into existing neuromuscular platforms, along with other related human iPSC-derived cell lines for a more complete investigation of human physiology, disease pathology, and drug discovery.

Results

Morphological analysis and quantification of bag fibers

Myoblasts derived from iPSCs were differentiated on DETA modified and collagen coated glass coverslips using an extrafusal-centered muscle differentiation protocol and an intrafusal-centered protocol (130) (Figure 17). Cells were fixed and evaluated at 15-20 days *in vitro* for bag fiber specific morphology by phase contrast imaging. Some myofibers from the extrafusal differentiation protocol showed some intrafusal-like morphology, including myotubes with collections of nuclei consistent with both bag and chain fiber morphologies (Figure 18 B and E). However, the majority of intrafusal-like fiber morphologies in these cultures were largely atypical in size and structure and very few bag fibers could be distinguished. Numerous myofibers from the intrafusal differentiation protocol using the iPSC-derived myoblasts indicated typical bag and chain intrafusal fiber morphologies (Figure 18 C and F) which matched the positive controls of intrafusal fibers derived from human satellite cells used in previous experiments (15, 16) (Figure 18 A and D). There was a significant increase in morphologically identifiable bag fibers in the iPSC-derived myoblasts treated with the intrafusal-specific protocol (Figure 18 G) ($p = 0.002$). This evidence suggests that activation of the NRG signaling pathway can induce intrafusal fiber differentiation from iPSC-derived myoblasts as also seen with human and rat satellite cells. It also indicates that the iPSC-derived myoblasts can generate both intrafusal and extrafusal fibers upon proper induction. Further analysis was performed to confirm the identity of the intrafusal fibers in the culture conditions.

Table 4: Medium formulations used to differentiate intrafusal fibers from induced pluripotent stem cells

Reagent	Final Concentration/Amount	Source	Catalog Number
Differentiation Medium 1			
DMEM High Glucose, Pyruvate	N/A	Invitrogen	11995-065
EGF recombinant human protein (hEGF)	10 ng/ml	Invitrogen	PHG0314
Insulin	10 µg/ml	Sigma Aldrich	I9278
Bovine Serum Albumin (BSA)	500 µg/ml	Sigma Aldrich	A9418
Neuregulin	100 µg/ml	R&D Systems	396-HB-050
Agrin	100 ng/ml	R&D Systems	550-AG
Laminin	1 µg/ml	ThermoFisher	23017015
Differentiation Medium 2			
Neurobasal	N/A	ThermoFisher	21103-049
B27	1X	ThermoFisher	17504001
Glutamax	1X	ThermoFisher	35050-061
NaCl (4M)	~31.2 mM for 270-280 mOsm	Sigma Aldrich	S3014-1KG
GDNF	10 ng/ml	Cell Sciences	CRG400E
BDNF	20 ng/ml	Cell Sciences	CRB600D
CNTF	5 ng/ml	Cell Sciences	CRC400B

NT3	20 ng/ml	Cell Sciences	CRN500D
Reagent	Final Concentration/Amount	Source	Catalog Number
NT4	20 ng/ml	Cell Sciences	CRN501C
Vitronectin	100 ng/ml	Sigma Aldrich	V8379-50ug
IGF-1	10 ng/ml	Sigma Aldrich	I3769-100ug
cAMP	1 μ M	Sigma Aldrich	A9501-1G
Shh	50 ng/ml	R&D Systems	1845-SH-100
RA	0.1 μ M	Sigma Aldrich	R2625
Agrin	100 ng/ml	R&D Systems	550-AG
Laminin	1 μ g/ml	ThermoFisher	23017015
NGF	100 ng/ml	R&D Systems	256-GF-100
NRG	100 ng/ml	R&D Systems	396-HB-050

Table 5: Medium formulations used to differentiate extrafusal fibers from induced pluripotent stem cell derived myoblasts

Reagent	Final Concentration/Amount	Source	Catalog Number
DK-HI Medium			
DMEM/F12 (1:1)	N/A	Gibco	21041-025
Knockout Serum Replacement (KSR)	150ul/ml	ThermoFisher	10828028
HGF	10 ng/ml	PeproTech	315-23-20UG
IGF	2 ng/ml	Sigma Aldrich	I1271-MG
β -mercaptoethanol	99mM	Gibco	21985-023
MEM Non-essential Amino Acids	1X	Gibco	11140-050
N2 Medium			
DMEM/F12 (1:1)	N/A	Gibco	21041-025
Insulin-Transferrin-Fetuin	1X	Gibco	41400-45
L-Glutamine	1X	Gibco	25030-081
N2 supplement	1X	Gibco	17502-048

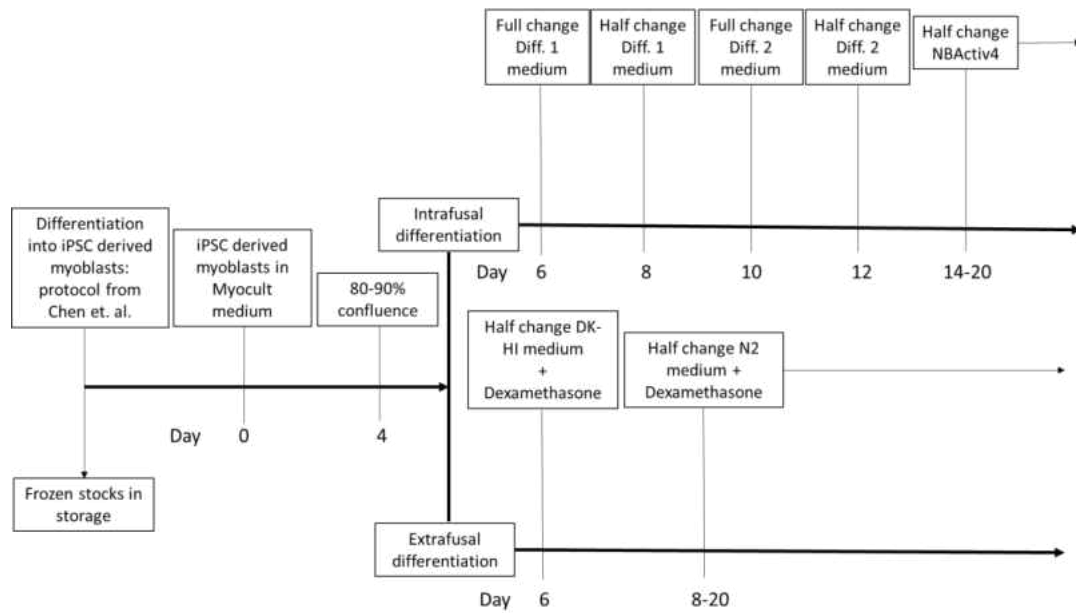


Figure 17: Cell culture protocol. Cells were differentiated into myoblasts from a previous protocol and frozen into stocks. Cells were then expanded and treated with either intrafusal fiber differentiation or extrafusal fiber differentiation.

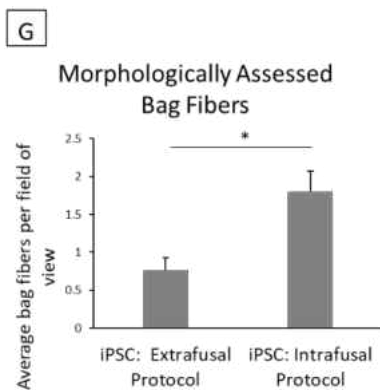
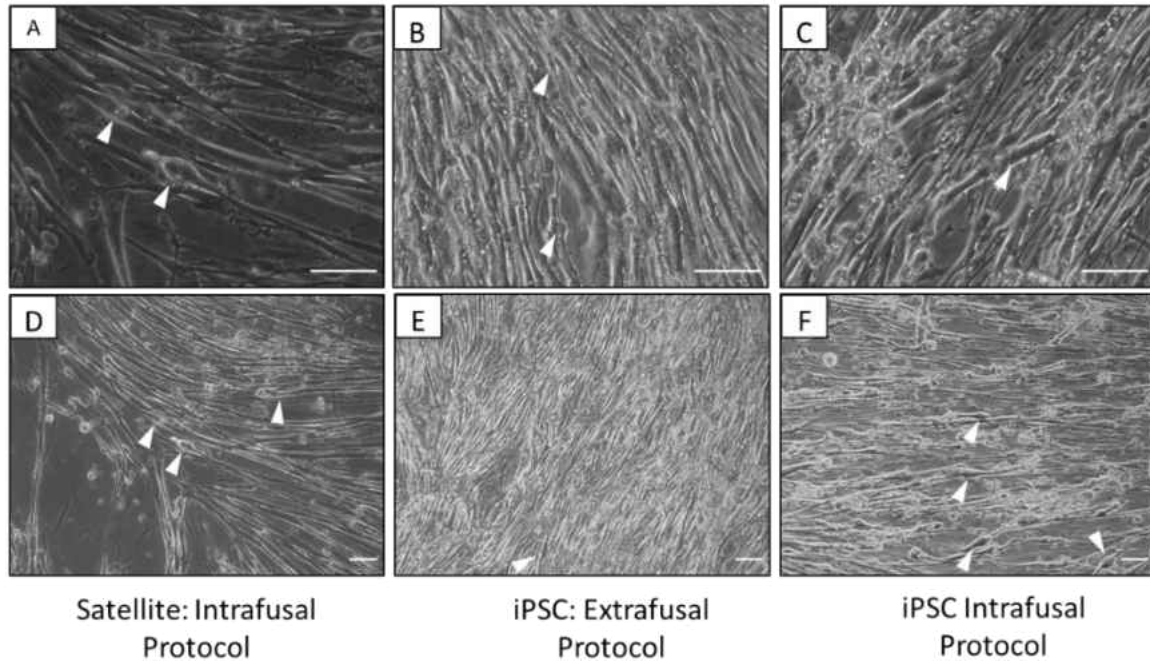
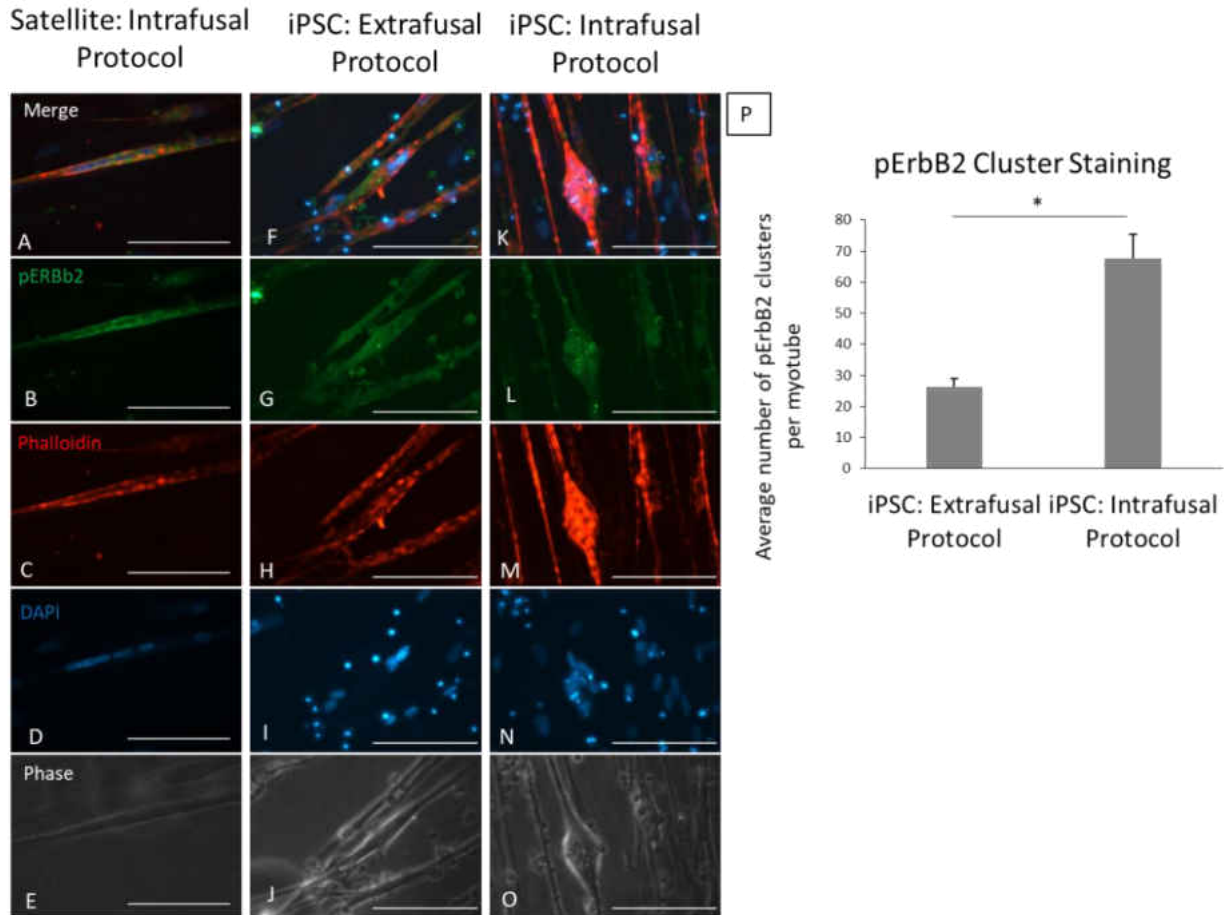


Figure 18: Phase Contrast Analysis. Morphological comparison between Intrafusal fibers derived from satellite cells and iPSC myoblasts treated with different differentiation protocols. A) and D) Cultures of satellite cells treated with an intrafusal induction protocol. B) and E) Cultures of iPSC myoblasts treated with an extrafusal-centered differentiation protocol C) and F) Cultures of iPSC myoblasts treated with an intrafusal induction protocol. White arrowheads show cells with intrafusal morphology. G) Quantification of morphologically assessed bag fibers. (Error bars=SEM, $p=0.002$). All scale bars are 100 microns.

Immunocytochemical analysis

To investigate the role of NRG and other differentiation factors on the induction of intrafusal fibers in iPSCs, we evaluated the phosphorylation of ErbB2 in cultures treated with and without an intrafusal differentiation specific protocol. Immunocytochemistry was performed to evaluate the level of phosphorylation of ErbB2 receptors to determine the phenotype of the muscle fibers. iPSC-derived myoblasts were differentiated on DETA modified and collagen coated glass coverslips using an extrafusal-centered muscle differentiation protocol and an intrafusal-centered protocol. Cells were fixed at 15-20 days *in vitro* and evaluated for pErbB2 staining. Myofibers found in both satellite-derived cultures and iPSC-derived cultures treated with the intrafusal differentiation protocol exhibited typical pErbB2 staining. Numerous clusters of receptors throughout the membrane were observed (Figure 19 A-E and 19 K-O). However, the iPSC-derived myoblasts treated with extrafusal differentiation had significantly fewer clusters of pErbB2 (Figure 19 F-J, P) ($p=0.00054$). This contrast indicates specific enhancement of the NRG signaling pathway in these myofibers under intrafusal induction conditions. To further confirm the increased induction of intrafusal fibers through NRG activation, cells were evaluated by S46 staining. S46 is a slow myosin heavy chain specific for intrafusal fibers (131). iPSC-derived myoblast cultures treated with the extrafusal-specific protocol had significantly fewer s46 positive cells than the iPSC-derived myoblast cultures treated with the intrafusal differentiation protocol (Figure 20 K) ($p=0.03$). These data indicate a lack of natural development of intrafusal fibers using an extrafusal differentiation protocol and an increase in the amount of intrafusal fibers using the intrafusal protocol due to an increased activation of the ErbB2 receptor mediated pathway in response to NRG and other intrafusal differentiation factors.



*Figure 19: Immunocytochemical Analysis of the myotubes induced under different conditions. Molecular comparison between ErbB2 phosphorylation in Intrafusal fibers derived from satellite cells and iPSC cells treated with different differentiation protocols. A-E) Cultures of satellite cells treated with an intrafusal induction protocol. F-J) Cultures of iPSC cells treated with an extrafusal-centered differentiation protocol K-O) Cultures of iPSC cells treated with an intrafusal induction protocol. P) Quantification of pERBb2 clustering within iPSC cultures. (Error bars are SEM, ***p=0.00054). All scale bars are 100 microns.*

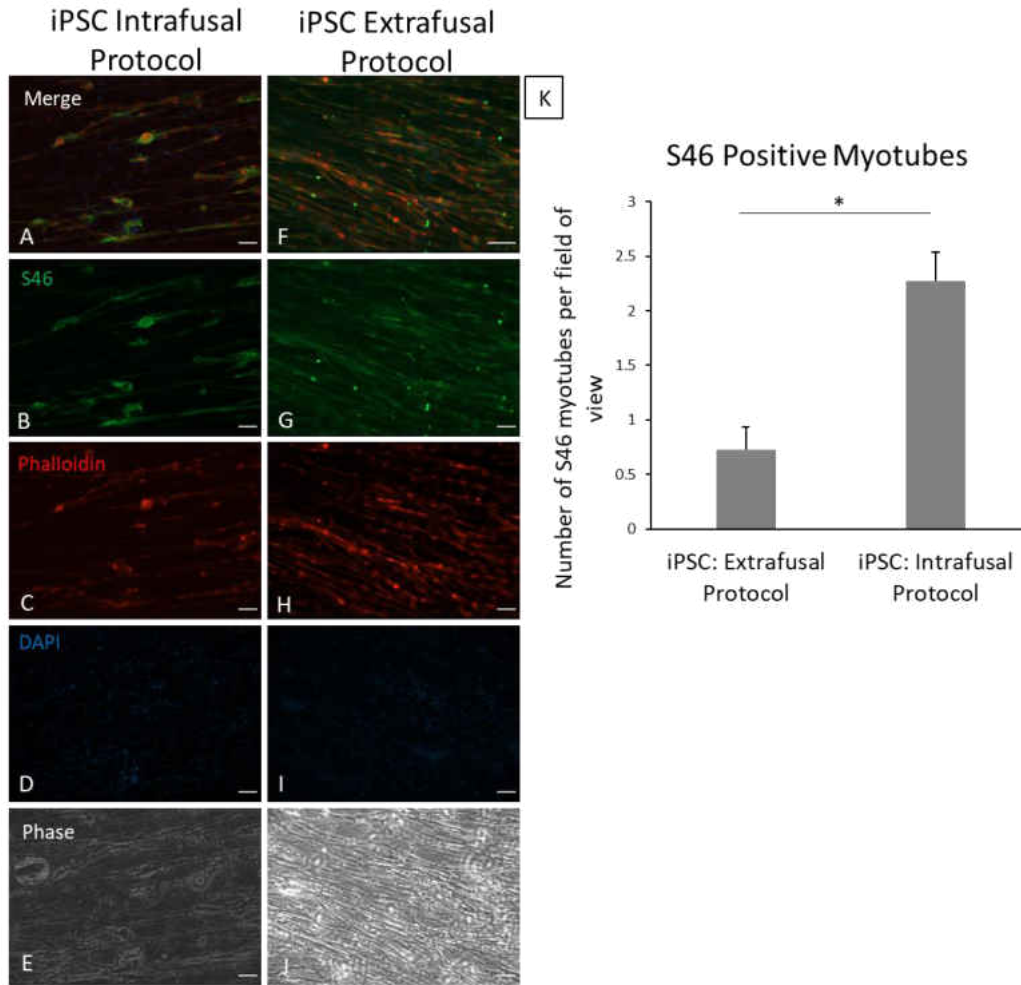


*Figure 20: Immunocytochemical Analysis of the myotubes induced under different conditions. Molecular comparison between s46 expression in Intrafusal fibers derived from iPSC cells treated with different differentiation protocols. (Error bars are SEM, *p=0.03) All scale bars are 100 microns.*

Discussion

This work demonstrates the induction of intrafusal fibers from iPSCs that now enables a range of investigations into various disease models of the spinal stretch reflex arc. Previous work has demonstrated the differentiation of human muscle from iPSCs, however, this is the first study targeting the differentiation of intrafusal fibers from iPSCs demonstrating successful differentiation supported by morphological and immunocytochemical evidence. These cells can now be integrated into existing “body-on-a-chip” testing platforms for a more thorough evaluation of the neuromuscular reflex arc, neuromuscular diseases, and for predicting drug efficacy and safety in clinical trials. For example, numerous compounds are known to mediate specific effects on the muscle spindle, including its activity (132) development, (133) and the ability to propagate pain to the central nervous system (134). Having a platform for functional evaluation of these activities in an *in vitro* setting will allow for more thorough preclinical evaluations in an attempt to reduce clinical trial failures.

Recent evaluations of the neuromuscular reflex arc have used “body-on-a-chip” testing platforms to elucidate functionally relevant data for predictions of human physiology and drug efficacy, safety, and toxicity. These systems have investigated the efferent neuromuscular processes of exercise (135) and contraction (13) as well as afferent innervation of intrafusal fibers by sensory neurons (14, 15). To enable these *in vitro* investigations to be more clinically relevant, iPSCs show great promise due to their ability to model specific patient physiology, especially for disease phenotypes. As shown in previous publications, iPSCs can be differentiated into extrafusal fibers, (130) motoneurons, (128) and sensory neurons (129) but the differentiation of intrafusal fibers from human iPSCs has not been reported. This work demonstrates the differentiation of iPSC-derived intrafusal fibers, further advancing “body-on-a-chip” technology

to deliver disease-specific, or even patient-specific, results without sacrificing inappropriate animal models.

In previous work, NRG has been used to induce the differentiation of intrafusal fibers from both rat (34) and human cell lines (15). While these cells can be used to determine certain basic aspects of physiology, the use of disease specific iPSCs is becoming more experimentally significant for the progression of drug and disease studies into clinical trials. This work outlines the induction of intrafusal fibers from iPSCs using the administration of NRG and other intrafusal fiber inducing factors. Upon treatment with an intrafusal-specific protocol the average quantity of iPSC-derived bag fibers per field of view increased from 0.76 ± 0.17 to 1.8 ± 0.27 (mean \pm SEM) (Figure 18). Additionally, the morphologies present in the iPSC-derived intrafusal fiber cultures more closely resembled those in previous publications (14-16, 34, 44) (Figure 18). This data suggests NRG-mediated differentiation has occurred in the iPSC-derived myoblast cultures. Immunocytochemistry for pERbB2 and S46 was used to further confirm the activation of the NRG signaling pathway and the increased induction of intrafusal fibers. Each of these markers have been previously used as an indicator for intrafusal fiber identity (16, 131). An increase in the average level of phosphorylation of the ErbB2 receptors of individual myotubes from 26.2 ± 2.84 to 67.5 ± 7.81 (mean \pm SEM) (Figure 19) and an increase in the number of myotubes positive for S46 staining from 0.73 ± 0.21 to 2.28 ± 0.26 (mean \pm SEM) (Figure 20), confirms increased differentiation of intrafusal fibers in a human iPSC-derived culture using this protocol. A similar increase in both immunocytochemical markers demonstrates that the intrafusal-specific differentiation protocol induced increased differentiation of the iPSC-derived myotubes. A slightly lower increase derived from phase quantification could be due to the fact that only bag fibers were counted for the intrafusal quantification under phase

contrast microscopy. It should be noted that the amount of intrafusal fibers present within muscle tissue is highly variable and the reasons for which have yet to be fully understood(136-138).

Further evaluation of this differentiation system will drive current understanding toward a more efficient differentiation process.

This work is the first evidence indicating that NRG can be used to drive human iPSC- derived myoblasts toward the intrafusal fiber lineage. The incorporation of iPSC-derived intrafusal fibers into existing neuromuscular testing platforms will allow for a more clinically relevant method for disease pathology analysis and drug discovery testing. By incorporating iPSCs derived from genetic mutant variants, it is now possible to identify the specific roles of these mutations on muscle spindles; a first for neuromuscular diseases such as ALS and SMA where the involvement of mechanosensation in disease progression is known but not yet fully elucidated (139, 140).

Materials and Methods

Surface modification

Glass coverslips (18mm round, VWR, 48380-046) were cleaned and functionalized by a Harrick plasma cleaner (model PDC-32G) by expose to an oxygen plasma from high purity oxygen gas. The coverslips were submerged in a reaction solution of 1% v/v trimethoxysilylpropyltriethylenetriamine (DETA, United Chemical Laboratories, Inc., T2910-KG) in dry toluene (VWR, BDH1151-4LG) and heated for 30 minutes to just below the boiling point of toluene (110.6°C). The vessel was then removed from heat and allowed to cool at room temperature for 30 minutes. Next the coverslips were rinsed in 3 serial toluene baths and submerged in dry toluene and heated for 30 minutes to just under the boiling point of toluene. The surfaces were then removed and cured overnight (~15hrs) in an oven at approximately 110°C. Surfaces were characterized by goniometry and X-ray photoelectron spectroscopy (XPS) to verify the

DETA functionalization according to Das et. al. 2006 (7). Goniometry characterization was performed by contact angle goniometry with a 5 μ l droplet of water. XPS characterization was performed with a Thermo Scientific ESCALAB 220i-XL instrument with aluminum K α X-rays and a 90° take off angle.

Satellite cell culture

Satellite cells were cultured according to previously published techniques (68) (Figure 17, Table 4). Briefly, cells were plated at ~200 cells per mm² and expanded in Lonza human skeletal growth medium (Lonza, CC3160 or CC-3246 plus 10mM L-glutamine and CC-4139) supplemented with 15% FBS on 18mm round coverslips that were DETA modified then Collagen (ThermoFisher, A1048301, 60 μ g/ml) coated until the cells reached ~80-90% confluency. Cells were then given a full medium change into differentiation medium 1 and given a half change of differentiation medium 1 two days after differentiation was initiated. After four days of differentiation, cells were given a full medium change of differentiation medium 2 and then a half change of differentiation medium 2 two days after the culture was switched to differentiation medium 2. After four days in differentiation medium 2, cells were fed with a half change of NBActiv4 (Brainbits, NB4-500) medium supplemented with 1X antibiotic/antimycotic (ThermoFisher, 15240062) every other day until the culture was ready for analysis (10-15 days after differentiation).

iPSC extrafusar cell culture

iPSCs were obtained from Coriell Institute for Medical Research (Camden, New Jersey). Cells were cultured according to previously published techniques (130) until the myoblast stage and then frozen as stocks in liquid nitrogen with 10% DMSO (Figure 17). Cells were then expanded

and differentiated as previously published.⁽¹³⁰⁾ Briefly, cells were plated at ~200 cells per mm² and expanded in Myocult medium (Stemcell Technologies, 36253 and 5982) on 18mm coverslips that were DETA modified then Collagen (ThermoFisher, A1048301, 60 ug/ml) coated until cells reached ~80-90% confluency. Cells were then given a half medium change with DK-HI supplemented with dexamethasone. Two days after feeding with DK-HI, cultures were given a half medium change of N2 medium (Table 5). Cultures were fed every other day until the culture was ready for analysis (10-15 days after differentiation).

iPSC intrafusal cell culture

IPSCs were obtained from Coriell Institute for Medical Research (Camden, New Jersey). Cells were cultured according to previously published techniques ⁽¹³⁰⁾ until the myoblast stage and then frozen as stocks in liquid nitrogen with 10% DMSO. Myoblasts were then expanded as previously published ⁽¹³⁰⁾ and differentiated using a modified protocol. Myoblasts were cultured according to previously published techniques ⁽¹⁵⁾. Briefly, myoblasts were plated at ~200 cells per mm² and expanded in Myocult medium (Stemcell Technologies, 36253 and 5982) on 18mm round coverslips that were DETA modified then Collagen (ThermoFisher, A1048301, 60 ug/ml) coated until cells reached ~80-90% confluency. Cells were then given a full medium change into differentiation medium 1 and then a half change of differentiation medium 1 two days after differentiation was initiated. After four days of differentiation, cells were given a full medium change of differentiation medium 2 and then a half change of differentiation medium 2 two days after the culture was switched to differentiation medium 2. After four days in differentiation medium 2, cells were fed with a half change of NBActiv4 (Brainbits, NB4-500)

medium supplemented with 1X antibiotic/antimycotic (ThermoFisher, 15240062) every other day until the cultures were ready for analysis (10-15 days after differentiation).

Immunocytochemistry-pErbB2 and phalloidin

Cells were fixed with 4% paraformaldehyde for 15 minutes and then rinsed 2 times with phosphate buffered saline (PBS) and stored in a third wash of PBS until immunocytochemical treatment (~0-14 days). Before immunocytochemistry, cells were treated with a blocking solution (donkey serum and 10% BSA in PBS) for 2 hours then treated with rabbit-anti-pErbB2 488 antibody (EMD Millipore, 16-235, 1:250 dilution) and Phalloidin 568 (Fisher Scientific, A12380, 1:40 dilution) for 2 hours. Cells were rinsed with PBS for 5 minutes, then rinsed with PBS and DAPI for 10 minutes and then rinsed with PBS for 15 minutes. Glass coverslips were mounted onto glass slides using ProLong™ gold antifade mounting medium (ThermoFisher, P36931). Slides were imaged using a Zeiss Axioskop 2 Mot plus spinning disk confocal microscope.

Immunocytochemistry-S46 and phalloidin

Cells were fixed with 4% paraformaldehyde for 15 minutes and then rinsed 2 times with phosphate buffered saline (PBS) and stored in a third wash of PBS until immunocytochemical treatment (~0-14 days). Before immunocytochemistry, cells were permeabilized with 0.1% Triton X-100 for 15 minutes and treated with a blocking solution (donkey serum and 10% BSA in PBS) for 2 hours. Cells were then treated with Mouse-anti-S46 antibody (Developmental Studies Hybridoma Bank, S46-s) overnight. The next day, cells were rinsed for 5, 10, and 15

minutes with PBS and treated with donkey-anti-mouse 488 Alexa Fluor® antibody (ThermoFisher, A21202, 1:250 dilution) and Phalloidin 568 (1:40 dilution) for 2 hours. Cells were then rinsed with PBS for 5 minutes, rinsed with PBS and DAPI for 10 minutes and rinsed with PBS for 15 minutes. Glass coverslips were then mounted onto glass slides using ProLong™ gold antifade mounting medium (ThermoFisher, P36931). Slides were imaged using a Zeiss Axioskop 2 Mot plus spinning disk confocal microscope.

Image analysis

Quantification of intrafusal morphology was performed across three separate cultures for the two iPSC-derived myoblast differentiation protocols. Within each culture, five random phase contrast images were taken from each of the two replicate coverslips for each protocol, for a total of 30 images per condition. A nested statistical design was employed, in which the 5 replicate images in each coverslip were nested in the independent coverslip samples ($n = 6$ coverslips). Images for pErbB2 and S46 quantification were obtained similarly to those for the intrafusal morphology, with $n = 6$ coverslips across 3 cultures and $n = 8$ coverslips across 4 cultures, respectively, each with 5 replicate images. For each quantification, two tailed t-tests ($\alpha = 0.05$, $n = 6$ or 8 coverslips) were performed to compare the numbers of intrafusal fibers per field of view, numbers of pErbB2 clusters per myotube, and numbers of S46 positive myotubes per field of view between the two differentiation protocols. Error bars in each figure are presented as standard error of the mean (SEM).

CHAPTER FIVE: INVESTIGATION OF NOCICEPTIVE MUSCLE SPINDLE ACTIVITY

Introduction

The muscle spindle has largely been studied for its involvement in neuromuscular communication efficiency and proprioception. However, increasing evidence suggests its involvement in neuropathic pain, a term used to describe nerve damage resulting in the perception of pain (141). This damage can result in sensitization of the nerve endings and allodynia, or a painful response to a typically non painful stimulus (141). Many links exist between neuropathic pain and afferent skeletal muscle activity (96, 142-147), some suggesting nociceptor-mediated pain originating in the muscle spindle (17). The exact mechanisms involved are of great research interest for as their investigation could lead to therapeutic innovations for pain. Thus far, multiple afferent cells, including, intrafusal fibers (96, 143), nociceptors (144), and other sensory neurons (143) have been linked to the propagation of pain signals from the muscle tissue. To have a complete *in vitro* model of the human neuromuscular reflex arc, it is important to have these functionalities represented in an *in vitro* platform.

Nociceptors are sensory neurons specialized for the perception of noxious stimuli (141). They are present in a wide variety of tissues including skin, muscles, joints and fascia (148). Recent research has allowed for the characterization of many nociceptive agonists including heat, changes in pH, and specific molecules. Of particular interest to this work, capsaicin, a well characterized nociceptive agonist is the molecule found in spicy peppers that gives them their “hot” flavor (149). This molecule binds to transient potential receptor vanilloid-1 (TRPV1) found on nociceptors(150). This binding opens the nonspecific TRPV1 receptor which allows for a dramatic influx of calcium and sodium ions, evoking the perception of pain. However, if the

TRPV1 ion channel is exposed to capsaicin for a long enough time period, the associated neuron gets flooded with calcium and can no send action potentials, leading to a sensation of numbness (149). This mechanism is widely utilized in clinical settings as a method of delivering pain relief with the topical application of capsaicin (151). In an *in vitro* setting, this mechanism can be used to confirm likely nociceptive capabilities of the cell type in question. This work demonstrates the use of capsaicin on human neural progenitor-derived sensory neurons to evaluate nociceptive capability. Integration of these nociceptors into the existing platform for neuromuscular reflex arc will incorporate a perspective on pain when evaluating neuromuscular activity in regard to normal, diseased, and drug treatment conditions.

As described in Chapter 1, intrafusal fibers are the sensory component of skeletal muscle tissue. These fibers form a collection called a muscle spindle which is innervated by both afferent and efferent neurons. This spindle is embedded within skeletal muscle tissue and mediates afferent muscular perception (44). However, recent research suggests its potential role in the propagation of pain perception, including injury and inflammation, particularly in regard to the presence of the TRPV1 ion channel (142, 145, 147, 152-155). This work investigates the potential for intrafusal fibers of initiating the propagation of noxious stimuli to the CNS.

The confirmation of nociceptive activity *in vitro* is difficult to define. There is no method of interrogating neurons for “pain” or how much of the sensation would be perceived by the CNS. Therefore, it is important to carefully investigate and utilize a functional analog to demonstrate the involvement of pain within an *in vitro* testing platform for the neuromuscular reflex arc. First, nociceptive capability must be demonstrated in the cells themselves. Later, they can be fully integrated into the existing neuromuscular testing platform. Here we demonstrate nociceptive activity in neurons derived from commercially available human neural progenitor

(hnp1) cells and the possible nociceptive involvement of human intrafusal fibers. This is a first step toward integrating more complex pain-linked disease states to the neuromuscular reflex arc testing platform.

Results

Immunocytochemical analysis of hNP1-derived sensory neurons

To confirm the presence of nociceptive cells in hNP1-derived sensory neurons, we evaluated the presence of nociceptive membrane channels on the membranes of the mature cells with immunocytochemistry. HNP1 cells were expanded and differentiated using an adapted protocol from previous methods (15). The differentiation protocol yields a mixed population of sensory neurons, therefore further analysis was required to confirm nociceptive identity. Once the cells reached maturity, they were fixed and evaluated by immunocytochemistry for the presence of TRPV1, the receptor for capsaicin, and the high-affinity receptor tyrosine kinase A (TRKA) both of which are found selectively on nociceptors(156). A correlation between TRPV1 and TRKA expression was observed (Figure 21), suggesting that the cells positive for both markers are indeed nociceptors. Functional analysis of the TRPV1 channel will further confirm their nociceptive identity.

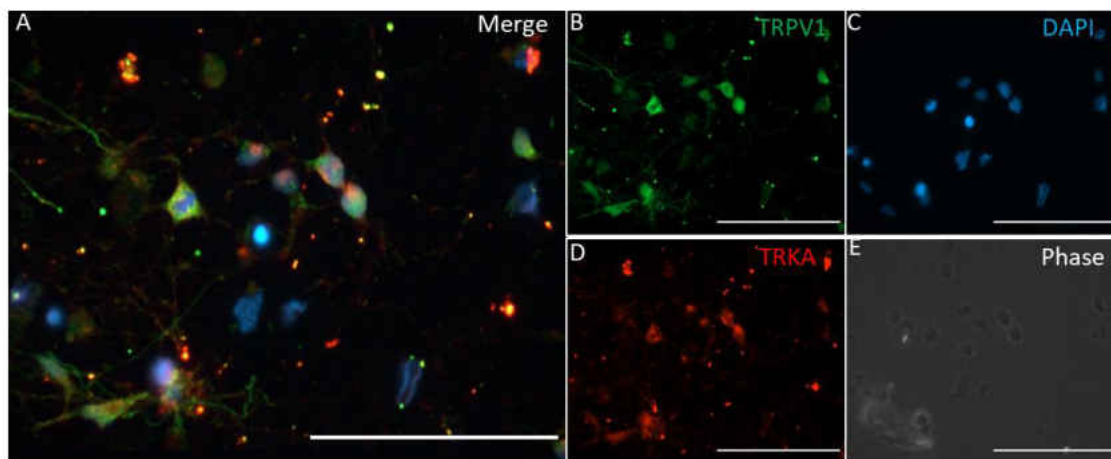


Figure 21: Immunocytochemical analysis of hNP1-derived neurons. Evaluation of TRPV1 and TRKA expression in hNP1-derived neurons. All scale bars are 100 microns.

Functional evaluation of hNP1-derived neurons

To determine the nociceptive functionality of these cells, they were treated with capsaicin, a known nociceptive agonist for the TRPV1 channel. HNP1 cells were expanded and differentiated as with the immunocytochemical evaluation. Upon maturity, cells were replated onto custom microelectrode arrays (cMEAs), allowed to recover for 3-5 days and evaluated using a customized amplifier unit along with customized detection software. Upon application of 2 μ M capsaicin, a likely response was observed (Figure 22). This demonstrates a coordination with neuronal firing and the administration of this nociceptive agonist, suggesting *in vitro* nociceptive functional activity and further confirming the nociceptive population within the hNP1-derived sensory neurons.

Electrophysiological responses detected from a cMEA

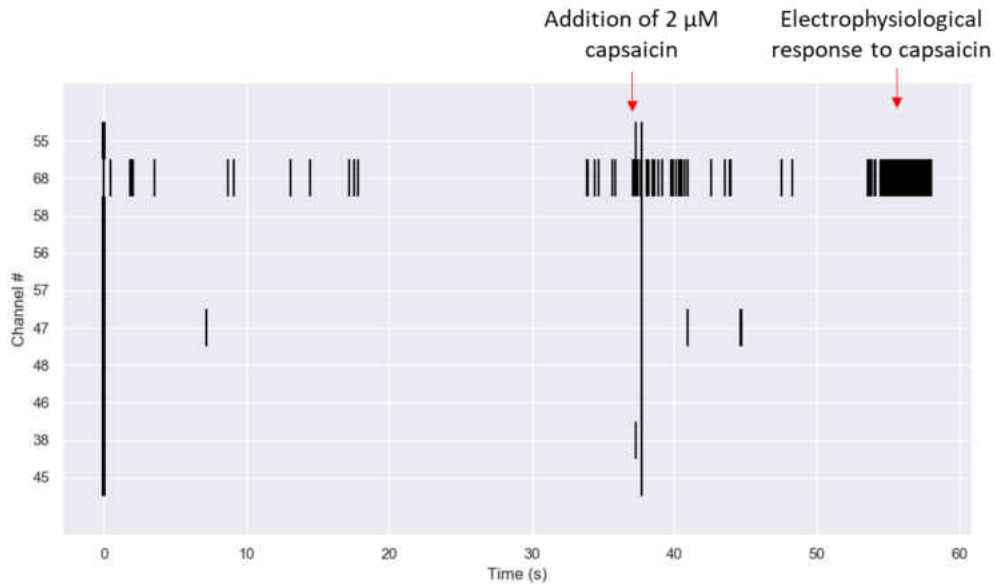


Figure 22: Raster plot demonstrating the electrophysiological response of hNP1-derived neurons to capsaicin

Immunocytochemical evaluation of intrafusal fibers

To determine the potential involvement of intrafusal fibers in pain, these cells must be evaluated for known mediators of nociception. Human skeletal muscle myoblasts were expanded and differentiated according to previous methods. Upon maturation, cells were fixed and evaluated by immunocytochemistry for the presence of TRPV1. The intrafusal cultures demonstrated a co-staining of TRPV1 and S46, a known indicator of intrafusal fiber identity (131) (Figure 23). The presence of a well-known nociceptive mediator both in the nuclei and on the cellular membrane suggests a possible role of human muscle spindles in nociception.

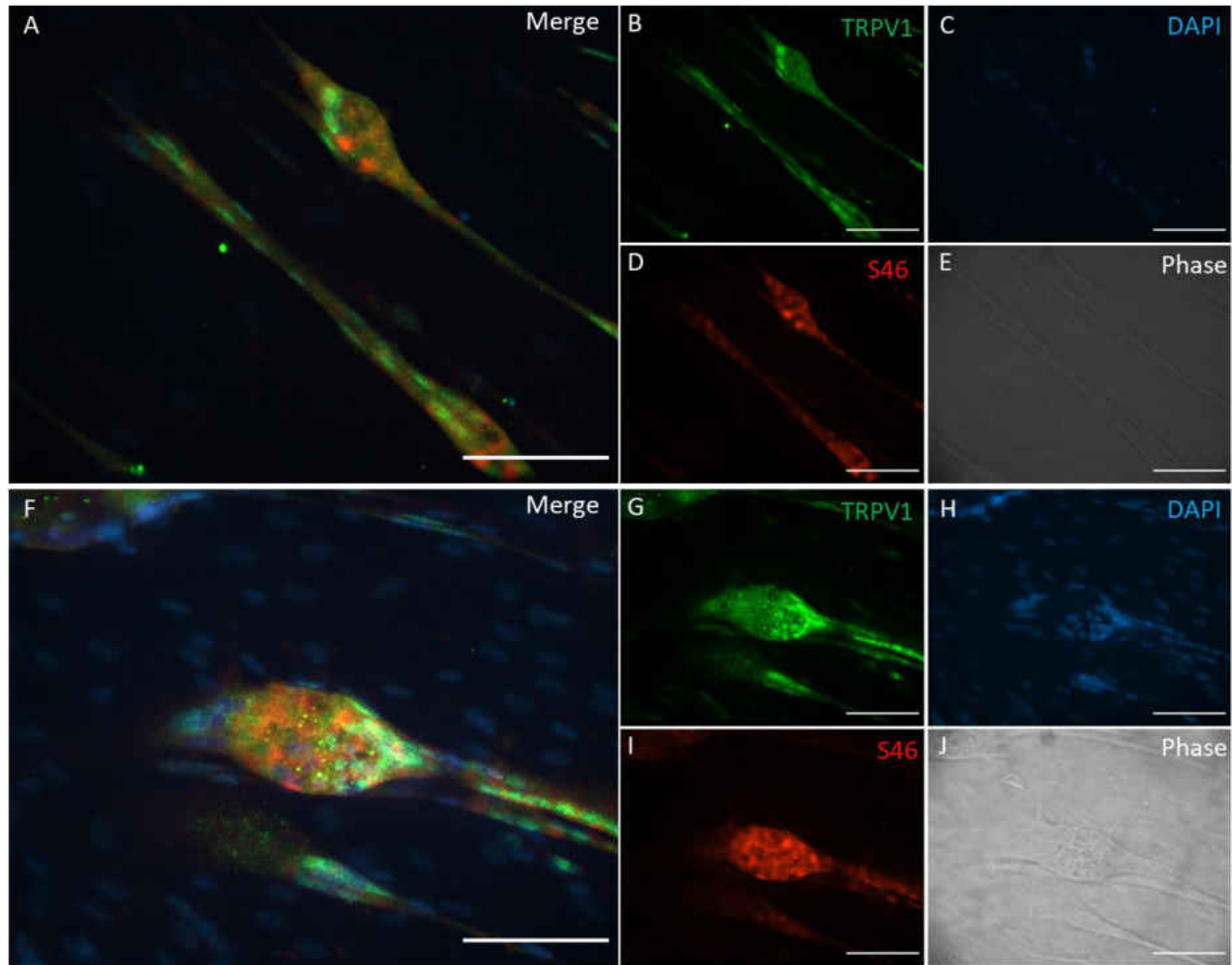


Figure 23: Immunocytochemical analysis of human skeletal muscle. Cultures were evaluated for TRPV1 and S46. All scale bars are 100 microns.

Discussion

This work demonstrates the potential for interrogation of pain on an *in vitro* neuromuscular reflex arc testing platform. Evidence of immunocytochemical markers and the functional evaluation of nociceptive activity within hNP1-derived sensory neurons suggests the incorporation of these cells into an existing neuromuscular evaluation platform will allow for an opportunity to evaluate pain *in vitro*. Additionally, the presence of TRPV1 on in multiple locales (membrane and nuclei) of intrafusal fibers suggests a role of this cell type in nociception. Both

cell types can easily be integrated into existing neuromuscular testing platforms for a potential new way to evaluate pain *in vitro*.

Materials and Methods

Surface preparation

Glass coverslips (18mm round, VWR, 48380-046) were cleaned and functionalized by a Harrick plasma cleaner (model PDC-32G) by exposure to an oxygen plasma from high purity oxygen gas. Coverslips and cMEAs were submerged in a reaction solution of 1% v/v trimethoxysilylpropyldiethylenetriamine (DETA, United Chemical Laboratories, Inc., T2910-KG) in dry toluene (VWR, BDH1151-4LG) and heated for 30 minutes on a hot plate to just below the boiling point of toluene (110.6°C). The vessel was then removed from heat and allowed to cool at room temperature for 30 minutes. Next the surfaces were rinsed in 3 serial toluene baths and submerged in dry toluene and heated for 30 minutes on a hot plate to just under the boiling point of toluene. The surfaces were then removed and cured overnight (~15hrs) in an oven at approximately 110°C. Surfaces were characterized by goniometry and X-ray photoelectron spectroscopy (XPS) to verify the DETA functionalization according to Das et. al. 2006 (7). Goniometry characterization was performed by contact angle goniometry with a 5 µl droplet of water. XPS characterization was performed with a Thermo Scientific ESCALAB 220i-XL instrument with aluminum K α X-rays and a 90° take off angle. Surfaces were then sterilized with 70% Ethanol and allowed to dry under sterile laminar flow. The cMEAs were then assembled into custom polymethylmethacrylate and polydimethylsiloxane housing systems. The surfaces were next coated with poly-ornathine (15 µg/ml, Sigma, P3655) overnight. The next day, the surfaces were rinsed twice with PBS and coated with laminin (1 µg/ml Invitrogen

23017-015) and fibronectin (10 µg/ml EMD Millipore FC010) overnight. The next morning the surfaces were rinsed twice with PBS and were ready for cell seeding.

Human neural progenitor cell expansion and differentiation

Human neural progenitor (STEMEZ™ hNP1,) were obtained from Neuromics (Edina, Minnesota) and expanded in RenCell medium (EMD Millipore, SCM005) supplemented with basic fibroblast growth factor (20ng/ml, R&D, 233-FB) and epidermal growth factor (20ng/ml, R&D, 236-EG) on Matrigel coated polystyrene (Corning Life Sciences, 354230). Matrigel was incubated on polystyrene at a 1:100 dilution in DMEM : F12 (Gibco, 21041-025) for one hour at room temperature. Cells were given a full medium change every other day until ~90% confluence was reached. Cells were then replated onto poly-ornathine/ fibronectin/ laminin, coated coverslips with 0.05% trypsin and 0.2% trypsin inhibitor. Cells were fed every other day with RenCell medium until ~90% confluency was reached. Differentiation was then initiated with a full change of 100% KSR medium (knockout DMEM, ThermoFisher, 10829018; knockout serum replacement, 150 µl/ml, ThermoFisher, 10828028; 2 mM L-glutamine, Gibco, 25030-081; antibiotic/antimycotic, 1X, ThermoFisher, 15240-062; MEM Non-essential amino acids, 1X, Gibco 11140-050; 55 µM β-mercaptoethanol, Gibco, 21985-023) supplemented with 100 nM LDN (Tocris, 6053/10) and 10 µM SB431542 (Tocris, 1614/1) at day 1 of differentiation. On day 3, cells were given a full medium change of 100% KSR medium supplemented with 100 nM LDN, 10 µM SB431542, 3 µM CHIR99021 (Tocris, 4423/10), 10 µM SU5402 (Tocris, 3300), and 10 µM DAPT (2643/10). On day 5, cells were given a full change of 75% KSR medium and 25% N2B Medium (DMEM/F-12, phenol red free, ThermoFisher, 21041-025; 200 µg/ml Human Apo-transferrin, R&D, 3188-AT; 25 µg/ml Insulin, Millipore, 407709; 1.56 mg/ml D-(+)-glucose, anhydrous, Sigma, G-7012) supplemented with 100 nM LDN, 10 µM SB431542, 3 µM

CHIR99021 , 10 μ M SU5402 , and 10 μ M DAPT. On day 7, cells were given a full change of 50% KSR medium and 50% N2B Medium supplemented with 100 nM LDN, 10 μ M SB431542, 3 μ M CHIR99021 , 10 μ M SU5402 , and 10 μ M DAPT. On day 9, cells were given a full change of 25% KSR medium and 75% N2B Medium Supplemented with 100 nM LDN, 10 μ M SB431542, 3 μ M CHIR99021 , 10 μ M SU5402 , and 10 μ M DAPT. On day 1, cells were given a full change of 100% N2B Medium Supplemented with 100 nM LDN, 10 μ M SB431542, 3 μ M CHIR99021 , 10 μ M SU5402 , and 10 μ M DAPT. .On day 13, cells were given a full medium change with N2B medium supplemented with 25 ng/ml human-b-NGF (R&D, 256-GF), 25 ng/ml BDNF (Cell Sciences, CRB600B), and 25 ng/ml GDNF(CRG400B). On day 15, cells undergoing electrophysiological analysis were replated onto Poly-ornathine/laminin/fibronectin coated cMEAs Cells were fed every 3-4 days in this final medium until cells were ready for analysis (~5-15 days).

Electrophysiological Evaluation of hNP1 cells

Once hNP1 cells reached maturity (10-15 days post differentiation) cells were replated onto custom cMEAs within housings and recovered for 3-5 days. The housings were then attached to a custom amplifier circuit to observe and record electrical signals detected from the neurons. First, 10 μ l warmed medium was added as a negative control then capsaicin (1-2 μ M ,Fisher Scientific, ICN202757) was added at recorded time points and electrophysiological response was recorded on a custom software program.

Human Intrafusal fiber differentiation

Human skeletal muscle was obtained from Lonza (CC-2580) and expanded in Lonza human skeletal growth medium (CC-3160) supplemented with 15% FBS until ~70-80% confluence was reached. Then the medium was fully switched to differentiation 1 medium (DMEM (Invitrogen 11775-040), Insulin (Sigma I9278) at 10 µg/ml, BSA (Sigma A9418) at 500 µg/ml, and EGF (Invitrogen 13247-051) at 10 ng/ml)(36) and fed every 2 days for 4 days. At this point, the medium was switched to differentiation 2 medium (described in detail in Guo *et al.*(15)) and MNs were added to co-cultures at 50 cells per mm². The cells were fed every two days with differentiation 2 medium and maintained for four days. After this point, the medium was given a half change with NBActive4 differentiation medium. The cells were maintained in this medium for the remainder of the culture and fed every two days until 15–30 DIV total when they were analyzed via immunocytochemical analysis.

Immunocytochemical analysis

Upon maturation, cells were fixed with 4% paraformaldehyde for 15 minutes then rinsed three times with PBS. At this point, cells were either stored in PBS for 0-14 days or incubated with permeabilization solution for 15 minutes (Triton X-100) and then blocking solution (5% Donkey serum +0.5% BSA in PBS) for 2 hours to prevent nonspecific binding. Cells were then incubated with primary antibodies overnight (Rabbit anti TRKA, 1:100 Abcam, ab8871 or Guinea Pig-anti-TRPV1, 1:100, Invitrogen PA1-29770). The next day cells were rinsed three times with PBS and incubated with secondary antibodies (Goat-anti-Guinea Pig-488 Alexa Fluor, ThermoFisher A-11073 or Donkey-anti-Rabbit 568 AlexaFluor, ThermoFisher, A10042) in a 1:250 dilution for 1-2 hours. Cells were then rinsed for 5 minutes in PBS, 10 minutes in PBS

with DAPI (1:1000, ThermoFisher D1306), and 15 minutes with PBS then mounted onto glass coverslips using ProLong™ gold antifade mounting medium. Slides were imaged using a Zeiss Axioskop 2 Mot plus spinning disk confocal microscope.

CHAPTER SIX: PIEZOELECTRIC BIOMEMS CANTILEVER FOR MEASUREMENT OF MUSCLE CONTRACTION AND FOR ACTUATION OF MECHANOSENSITIVE CELLS

The work in this chapter was submitted for publication as follows. This work will also be included in the doctoral dissertation of Elizabeth Coln.

Coln, E., Colón, A., Long, C., Narasimhan Sriram, N., Esch, M., Prot, J.M., Elbrecht, D., Wang, Y., Jackson, M., Shuler, M., Hickman, J.J. Piezoelectric BioMEMS cantilever for measurement of muscle contraction and for actuation of mechanosensitive cells. MRS Communications. June 11, 2019.

JJH, MLS, CJL conceived and designed the experiments; CJL, ME, JMP, and YW fabricated the device; AC and DHE performed the experiments; EAC, AC, CJL, NNS, MJ analyzed the data; EAC, AC, DHE, CJL, and JJH prepared the manuscript.

Introduction

Microcantilever sensors have been increasingly used in biomedical microelectromechanical systems (bioMEMS) devices to measure small scale mechanical movement and are typically silicon-based cantilevers due to availability and easy integration with silicon-based technology.(157) One application of these microcantilever sensors is in the determination of contractile force of cardiac and skeletal muscle tissues using in vitro “body-on-a-chip systems”.(10, 158-162) These “body-on-a-chip” systems integrate biology and engineering to measure the biochemical, mechanical, and physiological responses of organ analogues to predict human response to drug and chemical exposure.(158, 159, 163, 164) The existing

microcantilever sensors in “body-on-a-chip” systems utilize imaging methods or optical laser deflection of cantilevers for calculating contractility(157, 159) and rely on imaging methods or expensive optical detection components.(165, 166) Since piezoelectric materials have high sensitivity and the ability to convert mechanical energy to an electrical signal, they have been used in a variety of microscale sensor systems such as pressure sensors and chemical sensors,(167-169) and as biosensors to detect biological targets, such as microbes, proteins, viruses, and nucleic acids.(170) Additionally, the ability of piezoelectric materials to convert electrical signals to mechanical energy has led to their use as microactuators.(171) However, these biosensor methods are based on shifts in the resonance frequencies to measure changes in mass on the surface and are not suited for measuring dynamic force changes. Extending the use of piezoelectric materials to cantilever-based muscle contraction bioMEMS devices would enable a direct electrical readout of muscle contraction. Moreover, these cantilevers could also be used in reverse as actuators to impose a stress on tissues attached to the device, specifically the sensory portion of the reflex arc. The stretch reflex arc refers to how the central nervous system senses and responds to peripheral stimuli to regulate skeletal movement and is composed of skeletal muscle, the muscle spindle, motoneurons, and sensory neurons. The sensory portion is composed of intrafusal fibers embedded in the muscle tissue of the muscle spindle and proprioceptive sensory neurons.(172-174) Development of an in vitro sensory circuit of the reflex arc would improve the overall understanding of the mechanosensitive feedback, allowing opportunities to create more physiologically relevant systems and for investigation of neuromuscular diseases.

This present study details the design and fabrication of a piezoelectric bioMEMS cantilever which can act as either a sensing element for muscle contraction or as an actuator to apply

mechanical force to cells. This device incorporates a piezoelectric element composed of a thin film of aluminum nitride (AlN) on top of the cantilever sandwiched between two platinum electrodes. As a sensor, bending of the piezoelectric cantilever caused by contracting iPSC-derived cardiac muscle grown on the cantilever surface produced a voltage across the piezoelectric element, which was measured by an external amplifier. As an actuator, a periodic voltage was applied to the piezoelectric cantilevers and the resultant bending was measured using an optical beam displacement method. This bioMEMS system has the advantage of being able to acquire a direct electrical signal from the cantilever with a simple system setup for high content systems and may offer the advantage of high-throughput data collection by integration with current robotic screening systems in drug discovery.

Experimental Details

Design and fabrication of piezoelectric cantilevers

Piezoelectric cantilever devices were fabricated at the Cornell Nanoscale Science & Technology Facility (Ithaca, NY) using standard microfabrication processes. Each chip included 16 individual microscale cantilevers each 100 μm wide, 750 μm long, and 4 μm thick with a total chip size of 17 mm x 14 mm. The 5-inch photomasks for each layer to produce the piezoelectric cantilevers were designed using L-edit layout editor (Tanner). For production of the devices, silicon oxide and silicon nitride layers were grown via Plasma Enhanced Chemical Vapor Deposition (PECVD) (GSI PECVD System, Novanta, Inc., Bedford, MA); metal layers (titanium and platinum) were deposited via electron-beam evaporation (CHA Mark 50 e-Beam Evaporator, CHA Industries, Fremont, CA); the aluminum nitride (AlN) was sputtered using an aluminum target in a nitrogen plasma environment (ATC Orion Sputter Deposition Tool, AJA International,

Inc., Scituate, MA); oxide and nitride layers were etched via reactive ion etching (RIE) (Oxford PlasmaLab 80+ RIE System, Oxford Instruments, Concord, MA); the silicon device and handle layers were etched via deep reactive ion etching (DRIE) (Unaxis 770 Deep Silicon Etcher, Plasma-Therm, St. Petersburg, FL), and photolithography was performed using a Karl Suss MA6 Mask Aligner (Suss Microtec SE, Garching, Germany). The fabrication process, starting from a silicon-on-insulator wafer with a 4 μm thick $\langle 100 \rangle$ silicon device layer, 1-2 μm buried oxide layer, and 500 μm handle wafer, is shown in Figure 24, and focuses on the production, patterning, and electrical isolation of the sandwich structure of AlN between two platinum electrodes. A 1.5 μm thick silicon dioxide layer and 300 nm silicon nitride layer were deposited via PECVD on the back and front (device) sides of the wafer, respectively. The piezoelectric element consisting of an aluminum nitride layer sandwiched between two platinum electrodes was produced by evaporation and liftoff of the bottom metal layer (10 nm titanium and 50 nm platinum) (Figure 24A), followed by reactive sputtering of 300 nm of aluminum nitride (Figure 24B) and evaporation of a second electrode identical in composition and thickness to the first. Both the aluminum nitride and top electrode layers were patterned via a liftoff process (Figure 24C). An insulation layer of silicon oxide and silicon nitride was deposited on top of the device layer, including the piezoelectric element (Figure 24D). The insulation layer was patterned via RIE to expose the contact pads and allow etching to define the cantilevers (Figure 24E). DRIE was then used to define the cantilevers in the device layer silicon. To release the cantilevers and open a window through the wafer to the cantilevers, the oxide on the backside of the wafer was etched using RIE to create an etch mask for the DRIE process, which was used to perform a through etch of the handle wafer to the cantilevers. Buffered hydrofluoric acid (HF) was used to remove the buried oxide layer to fully release the cantilevers (Figure 24F). Each final cantilever

is 100 μm wide and 750 μm long, with a piezoelectric cantilever element 80 μm wide and 730 μm long on the top of the silicon cantilever. In the piezoelectric cantilever chip design (Figure 25A), each cantilever has an independent contact pad for the top and bottom platinum layers, and these contact pads are connected to an external amplifier. A JEOL 6400 scanning electron microscope (JOEL USA, Inc., Peabody, MA) was used to measure cantilever dimensions (Figure 25B).

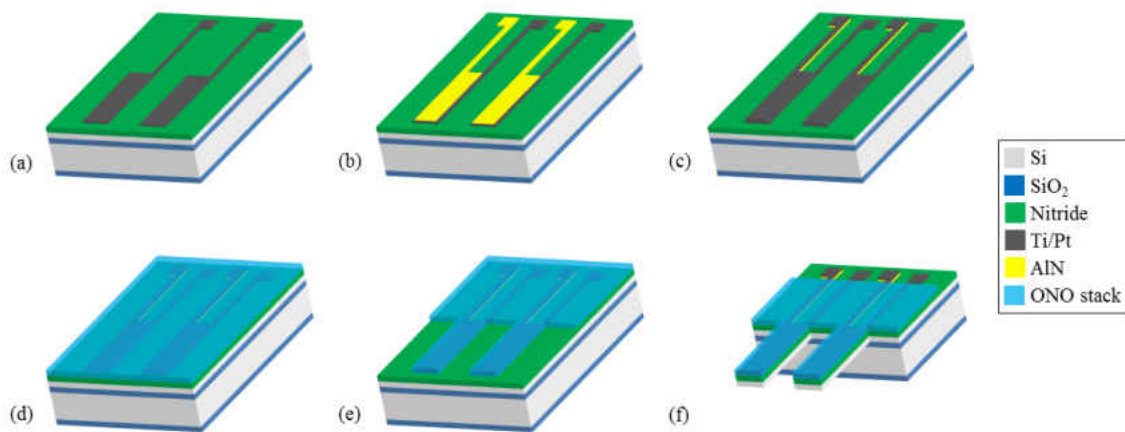


Figure 24: Fabrication of piezoelectric cantilevers. (a) Ti/Pt bottom electrodes and contact pads were deposited on an SOI wafer with insulation layers on the front and backside and patterned via liftoff. (b) Piezoelectric AlN was reactively sputtered and patterned via liftoff. (c) Top metal electrodes and contact pads were deposited and patterned via liftoff. (d) Top insulation layer (ONO) was deposited via PECVD. (e) The insulation layer was patterned by RIE. (f) The front and backside were etched via DRIE to define and release the cantilevers, followed by an HF dip to remove the buried oxide layer.

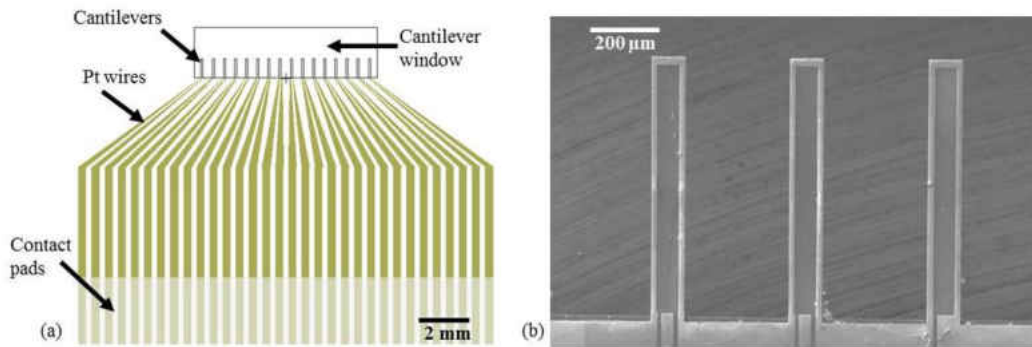


Figure 25: Piezoelectric cantilever chip layout (a) Piezoelectric cantilever chip design showing location of cantilevers, wires, and contact pads. (b) SEM image of piezoelectric cantilevers showing top surface of platinum and SiO₂ insulation. Because the cantilever chip was not coated with a separate conductive layer, the piezoelectric element and platinum wires appear darker, as the adjacent insulation layers charge slightly under the electron beam.

Surface modification of piezoelectric cantilevers

Piezoelectric cantilevers were chemically modified with a diethylenetriamine (DETA)-containing silane using previously published methods to enhance cell adhesion and functional development.^(159, 175-177) Following chemical modification, the chips were incubated in human fibronectin (50 μg/mL) in phosphate buffered saline (PBS) at 37°C for 30 minutes just prior to cell plating to adsorb the fibronectin to the DETA surface for cell attachment.

Cell culture on the piezoelectric cantilevers and housing system assembly

Commercially available, cryogenically preserved, human induced pluripotent stem cell (iPSC) derived cardiomyocytes (iCell Cardiomyocytes, #CMC-100-110-005, Cellular Dynamics

International, Madison, WI) were plated onto piezoelectric cantilevers (2200 cells/mm²) in a serum-free medium according to previously published methods that described culturing these cells on non-piezoelectric bioMEMS cantilevers.^(158-160, 176) These cardiomyocytes in our serum-free culture system express a mature phenotype, have robust electrical and mechanical function, and show appropriate functional changes in response to drug compounds.^(159, 160, 178, 179) Every 2 days, one-half of the medium was replaced with fresh medium. The piezoelectric chips with cultured cardiomyocytes were maintained for 7 days prior to assembling into housings. System housings and gaskets were manufactured from 6 mm thick transparent poly(methylmethacrylate) (PMMA) (McMaster-Carr, Elmhurst, IL) and 0.5 mm thick poly(dimethylsiloxane) (Grace Bio-Labs, Bend, OR), respectively. Both housings and gaskets were designed in Eagle (Autodesk) software and laser cut using a Versalaser PLS 75W laser cutter (Universal Laser Systems, Scottsdale, AZ). The piezoelectric cantilevers were assembled within the PMMA top and bottom plates, with the gaskets sealing the contact pads from the cantilever area, which contained 500 μ L of serum-free medium.

Contractile force measurement with piezoelectric cantilevers

A microelectrode array (MEA) amplifier (MEA 1040, Multichannel Systems, Reutlingen, Germany) was interfaced to the piezoelectric cantilever chip in the housing via a custom printed circuit board and was used to record the electrical output from the piezoelectric cantilevers. For contractile force experiments, piezoelectric cantilever chips cultured with cardiomyocytes were assembled into system housings with 500 μ L serum-free medium over the piezoelectric cantilevers. The force of the beating cardiomyocytes bent the cantilevers, producing a mechanical stress in the piezoelectric aluminum nitride, in turn generating an electric potential

difference across the two electrodes (Figure 26C top panel). This voltage was measured by the amplifier and recorded in real-time using a commercially available data acquisition software package (MC_Rack, Multichannel Systems, Reutlingen, Germany), and the voltage data was analyzed with Clampfit (Axon Instruments) software (Figure 26B and C top panel). To demonstrate the ability of the piezoelectric cantilever sensors to detect changes in cardiomyocyte function, the cardiomyocytes were dosed with 3 μ M epinephrine to increase the beat frequency during the recording (Figure 26C, bottom panel).

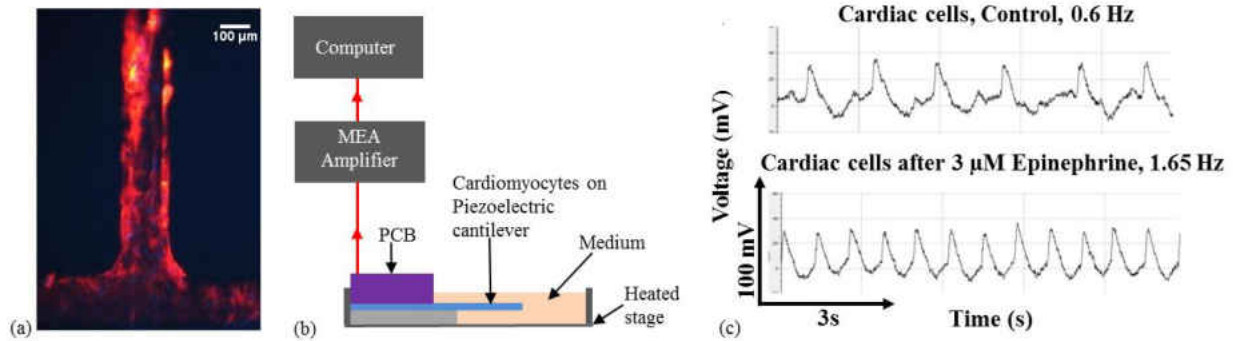


Figure 26: Sensing of muscle contraction using piezoelectric cantilevers. (a) Confocal image of skeletal muscle on a piezoelectric cantilever, with myosin heavy chain shown in red and DAPI in blue. (b) Schematic of recording setup for cardiomyocyte force measurements using piezoelectric cantilevers. (c) Measurement of cardiomyocytes on piezoelectric cantilevers showing control (top) and after treatment with addition of 3 μ m epinephrine (bottom).

Immunocytochemical imaging of cardiomyocytes on piezoelectric cantilevers

Piezoelectric cantilevers were prepared for immunocytochemistry using methods that previously described staining these cells on non-piezoelectric cantilevers and coverslips.^(173, 177) Briefly, cells on the piezoelectric cantilevers were fixed with a 4% (vol/vol) paraformaldehyde/PBS

solution for 15 minutes at room temperature, then rinsed 3X with PBS. Cardiomyocytes were permeabilized for 15 minutes with 0.1% Triton X-100 and then blocked with 5% donkey serum + 0.5% bovine serum albumin in PBS for 1-2 hours at room temperature. Cells were incubated overnight at 4°C with a mouse anti-myosin heavy chain primary antibody (Developmental Studies Hybridoma Bank, Iowa City, IA) diluted in blocking buffer. The cells were rinsed with PBS for 5 minutes, 0.01% Triton X-100 for 10 minutes, and PBS for 15 minutes. The cells were incubated with Alexa Fluor 594 (Invitrogen, Carlsbad, CA) secondary antibodies (1:250 diluted in blocking buffer) for 1-2 hours at room temperature. The stained samples were then rinsed with PBS for 5 minutes, 0.01% Triton X-100 and DAPI (Thermo Fisher P36931) for 10 minutes and PBS for 15 minutes and imaged using a Zeiss LSM 510 confocal microscope (Figure 26 A).

Detection system for actuation of piezoelectric cantilevers

For actuation experiments, acellular piezoelectric cantilever chips were assembled into system housings with 500 μ L of PBS and interfaced through a custom printed circuit board (PCB) to a Model 2100 Isolated Pulse Stimulator (A-M systems, Sequim, WA) (Figure 27A). A single cantilever was stimulated at a time by connecting the two electrode pads to the stimulator through the PCB. Two pulse shapes were applied to the piezoelectric cantilever: a monophasic square pulse (5V, 150 ms duration, and 0.6 Hz), and a biphasic square pulse (\pm 5V, 300 ms duration, and 0.6 Hz). A previously described optical detection system (158-160, 177) was used to measure the deflection of the piezoelectric cantilever. In this system, a 635 nm laser (CPS635F, Thorlabs, Newton, NJ) and linear effect photodetector (PSD9, Thorlabs, Newton, NJ) were located under a fixed stage and were aligned such that the laser was focused onto the tip of the underside of the cantilever (Figure 27A). The laser was subsequently reflected onto the

center of the photodetector to measure the deflections of the cantilevers as a change in position of the reflected laser spot on the photodetector. The deflection at the tip of the cantilever was then determined using methods described in Pirozzi, et al. for this system.(180)

To understand the cantilever deflection when stimulated electrically as an actuator, a mathematical relationship between the input pulses and the average deflection signals was developed (Figure 27B and C). The deflection curves for the monophasic stimuli were averaged, as were those for the biphasic stimuli. The induced strain in a piezoelectric material is approximately linearly proportional to the electric field across the piezoelectric element, as shown in Equation (1), where ε is the strain in the piezoelectric material, d is the piezoelectric coefficient, and E is the electric field for the inverse effect.

$$\varepsilon = d \times E \quad (1)$$

However, the electric field across the element is related not only to the voltage applied to the electrode pads and geometric configuration, but also the resistive and capacitive elements in the circuit, including those of the piezoelectric aluminum nitride element. The input voltage is effectively filtered in a similar way as a low pass RC filter in producing the actuation. As all of the input voltage changes used in this study were step functions (increasing and decreasing), the differential equation for the effect of an RC filter has a simple time-domain solution, forming the basis of Equation (2):

$$\Delta\delta = A\Delta V_{pulse}(1 - e^{-t/\tau}) \quad (2)$$

where $\Delta\delta$ is the change in position (deflection) of the tip of the cantilever, A is the parameter relating the voltage across the AlN element to the cantilever deflection and is related to the piezoelectric coefficient and physical layout of the device, ΔV_{pulse} is the change in voltage of the input step function, t is the time since the square wave initiation, and τ is the time constant of the

circuit. The measured deflection from the optical detection system was fit to Equation (2) using a least-squares regression method to determine A and τ .

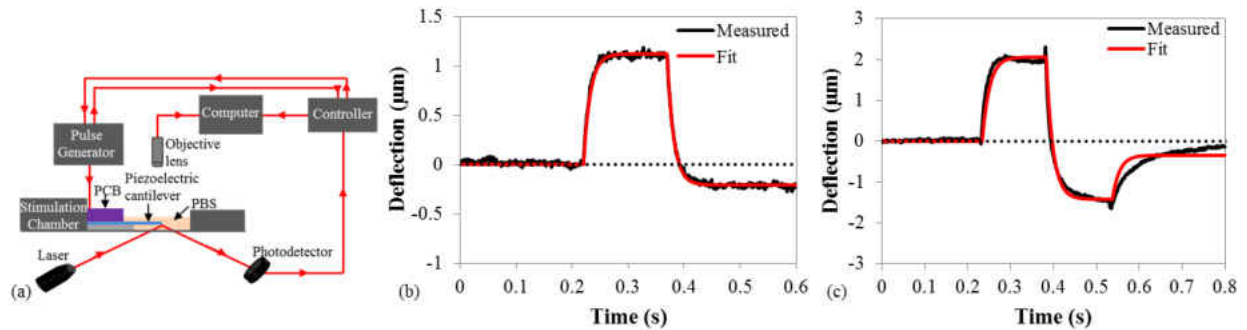


Figure 27: Actuation of piezoelectric cantilevers. (a) Schematic of optical deflection system. (b) Piezoelectric cantilever actuation under a 5V monophasic 150 ms stimulation pulse. (c) Piezoelectric cantilever actuation under a $\pm 5\text{V}$ biphasic (total duration 300 ms) stimulation pulse. Slight offset observed at end of actuation in (a) and (b) due to baseline drift in raw data (Figure 28).

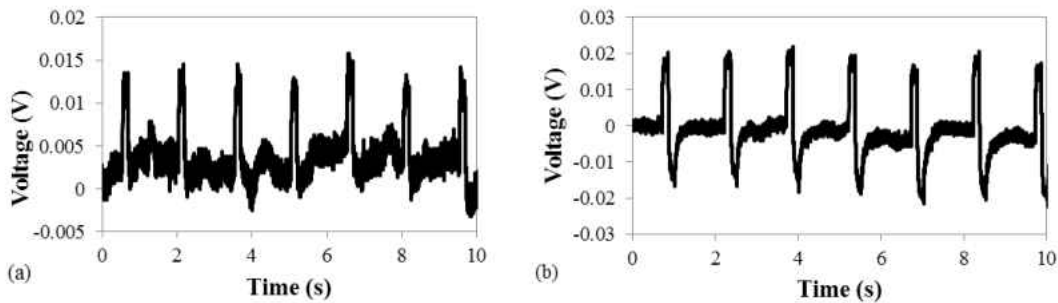


Figure 28: Raw data from actuation of piezoelectric cantilevers. (a) Piezoelectric cantilever actuation under a 5V monophasic 150 ms stimulation pulse. (b) Piezoelectric cantilever actuation under a $\pm 5\text{V}$ biphasic (total duration 300 ms) stimulation pulse.

Results and Discussion

Piezoelectric sensing for cardiomyocyte force measurements

To demonstrate that the piezoelectric cantilevers could produce electrical signals from cardiomyocyte contraction, human iPSC-derived cardiac muscle was grown on the piezoelectric cantilevers in the serum-free medium. Confocal microscopy of the cardiomyocytes on the piezoelectric cantilevers (Figure 26A) shows the cardiomyocytes integrated on the top of the cantilever surface, with a muscle-specific structural protein myosin heavy chain (red) and nuclei (blue) visible. These cardiomyocytes formed a syncytium of contracting cardiomyocytes, and this syncytium beat spontaneously due to the presence of pacemaker cells in the culture. Using the direct piezoelectric effect, the piezoelectric cantilevers converted the mechanical strain caused by the cardiomyocyte contraction into an electrical output. Figure 26B shows a simplified schematic of the MEA amplifier system setup used for cardiomyocyte force measurements. The real-time, continuous electrical signals generated by the piezoelectric AIN, in response to the cardiomyocyte tissue bending of the cantilever, were recorded when the PCB was connected to an external amplifier. To demonstrate that the system was capable of measuring changes in cardiomyocyte function, 3 μ M epinephrine was added to the medium to increase beat frequency of the cardiomyocytes.⁽¹⁸¹⁾ Upon addition of epinephrine, the change in cardiomyocyte beat frequency was clearly observed, with an increase in frequency by a factor of more than two. Figure 26C indicates clear peak shapes with measurable amplitude and frequency for both the spontaneous cardiomyocyte contractions (top) and for the cardiomyocyte contractions induced by the addition of epinephrine (bottom).

Actuation of piezoelectric cantilevers

The ability of the piezoelectric cantilevers to serve as actuators for applying mechanical stress to tissue constructs was evaluated using an optical beam displacement method (Figure 27A) to measure the deflection of the piezoelectric cantilever under a periodic waveform of applied voltage. Using the inverse piezoelectric effect, when the electric signal was applied to the piezoelectric aluminum nitride element, the aluminum nitride converted the electrical pulse into a mechanical deformation, causing the cantilever to bend. The actuation of the piezoelectric cantilevers was modeled electrically following a simple RC circuit,⁽¹⁸²⁾ and captures the capacitance of the platinum/aluminum nitride/platinum stack as well as the bulk resistance of the aluminum nitride and the resistance of the wires and other series elements in the circuit. Because of the effective resistance and capacitance of the circuit, the shape of the input actuation signal was not exactly reflected in the actuated cantilever beam. A transfer function model relating the output deflection to the input voltage signal was determined to better understand the behavior of the piezoelectric cantilevers as actuating elements and to help determine input functions to produce desired deflection waveforms. Figures 27A and 27C show the recorded cantilever deflection (black) of the 5V monophasic square wave input and 5V biphasic square wave, respectively, and the modeled transfer function (red) for each stimulation input. In both the monophasic and biphasic stimulations, the modeled transfer function very closely resembles the stimulated actuation signal. There is a slight offset in the actuation signals for both the monophasic and biphasic stimulations due the baseline drift in the raw data as shown in Figures 28A and 28B, respectively. Fitting these two models separately, the monophasic and biphasic models had an average τ of 0.014s, and average A of 0.31 $\mu\text{m}/\text{V}$.

For use with mechanosensitive cells, such as intrafusal skeletal muscle fibers innervated by sensory neurons as part of the stretch reflex arc, simple functions, such as square waves, are not sufficient to mimic physiological strain profiles needed to trigger sensory neuron action potentials. Instead, an isometric contraction profile would be desired to stretch the intrafusal fibers to activate the mechanoreceptors in the sensory neuron's axons to initiate an action potential. The transfer function between time-dependent input voltage and time-dependent deflection, developed here, could be used to generate the required input waveform to produce the desired output deflection. Equation (3) relates the required applied voltage waveform to the desired voltage across the piezoelectric element for an arbitrary waveform:

$$V_{applied}(t) = \tau \frac{dV_{AIN}(t)}{dt} + V_{AIN}(t) \quad (3)$$

where $V_{applied}(t)$ is the input voltage waveform, τ is the time constant (0.014s), and $V_{AIN}(t)$ is the voltage across the AIN element. As the deflection of the cantilever tip is related to the voltage across the AIN element according to the inverse piezoelectric effect (Equation 4):

$$\delta(t) = AV_{AIN}(t), \quad (4)$$

Equation (3) can be modified to relate the output deflection and voltage applied as time series (Equation 5):

$$V_{applied}(t) = \frac{1}{A} \left(\tau \frac{d\delta(t)}{dt} + \delta(t) \right) \quad (5)$$

where $\delta(t)$ is the desired deflection of the tip of the cantilever, and A and τ are as in Equation (2). For an arbitrary desired actuation profile ($\delta(t)$) such as to mimic an isometric muscle contraction, Equation (5) can be used to determine the input voltage waveform needed. This indicates that the piezoelectric system could be used to stimulate intrafusal fibers to generate action potentials in sensory neurons.

Conclusion

This work demonstrates the development of a new method using piezoelectric cantilevers to measure contractile muscle force generation in human cells by acquiring a real-time, continuous and direct electrical signal generated in the piezoelectric AIN, caused by the muscle tissue bending the cantilever. This sensor was able to detect spontaneous cardiac muscle contraction with enough sensitivity to observe changes in contraction frequency induced by the addition of epinephrine. The piezoelectric cantilevers were additionally shown to function as actuators, with a defined filtering effect of the input signal to cantilever deflection. The actuation experiments enabled the determination of coefficients relating the input voltage waveform to cantilever deflection, which can be used to determine the required input voltage waveforms to produce a desired arbitrary actuation profile. The ability of these piezoelectric cantilevers to actuate opens the opportunity for use with mechanosensitive cells, such as those in the sensory segment of the stretch reflex arc to stretch intrafusal fibers. These piezoelectric cantilever devices, which were designed to be incorporated into “body-on-a-chip” systems, have the potential to enable functional experiments with mechanosensitive tissue structures such as those in the stretch reflex arc, to incorporate these tissues into “body-on-a-chip” devices, and to increase the throughput of measurements of cardiac and skeletal muscle mechanical function in “body-on-a-chip” devices for basic physiological investigations, pharmaceutical compound development, toxin detection, neurological and muscular disease modeling for therapeutic development, and predictive toxicology.^(183, 184) Integration of human skeletal muscle fibers on the piezoelectric cantilevers would enable a more robust method to study the human central nervous system and improve understanding of spinal cord injuries, diseases such as amyotrophic lateral sclerosis (ALS),

CHAPTER SEVEN: GENERAL DISCUSSION

Animal models have proven insufficient for demonstrating human, molecular biology, and clinical response to drugs (1, 76). Movement toward more human-based preclinical testing platforms is becoming more essential for accurate predictions of human biology and drug testing. Also, many governing bodies have chosen to move away from animal models and move closer to more ethical human-based *in vitro* testing platforms for drug safety evaluation and product development. As a solution to these issues, “body-on-a-chip” technology has become increasingly prevalent in human-based research. This technology integrates MEMS technology with human-based cell culture to develop platforms for elucidating functional data based on specific organ systems (77). Development of these systems to incorporate multiple facets of human health enables the rapid and efficient progression of human disease research and drug discovery.

Multiple *in vitro* platforms already exist for various investigative pathways. The neuromuscular reflex arc, however, is a particularly challenging system to recapitulate in an animal-free platform. In the *in vivo* reflex arc, both descending and ascending neuromuscular pathways interact to form complex interactions with the CNS and the environment. While many of these intracellular interactions and cell types have been demonstrated in other *in vitro* platforms, this work describes the first functional evidence of γ -motoneuron innervation *in vitro*, the only demonstration of intrafusal fiber differentiation from the increasingly clinically relevant iPSCs, and insights as to how to incorporate complex aspects of afferent signaling into “body-on-a-chip” technology.

The complexity of the neuromuscular reflex arc yields itself to misunderstandings, particularly regarding cellular communication. Outside of this work, motoneuron innervation of extrafusal

fibers (13, 37, 82), sensory neuron innervation of intrafusal fibers (14, 15), and interactions between motoneurons and sensory neurons (81) has been established. However, γ -motoneuron innervation of intrafusal fibers had not been demonstrated. This important cellular interaction is vital for the accurate sensation and proprioception of skeletal muscle (87). To establish a complete model of the neuromuscular reflex arc, γ - motoneuron contribution must be considered. This work demonstrates both molecular and functional evidence of human γ -motoneuron innervation *in vitro*. Co-culture conditions were established for the survival of both human motoneurons and intrafusal fibers (Figures 11, 12, and 15). Upon morphological analysis, these cultures had developed close cell to cell interactions indicative of innervation (Figure 10 G). As a confirmation of communication ability, the cultures were stained to confirm the identities of the cell types involved and to establish molecular evidence of innervation (Figures 11 and 13). Furthermore, functional evidence was established by stimulating the motoneurons to send signals to the intrafusal fibers which they innervated (Figure 15). Collectively, these data show the *in vitro* establishment of γ -motoneuron innervation of intrafusal fibers. This interaction can now become integrated into current neuromuscular reflex arc testing platforms for a more detailed perspective on neuromuscular responses to drug treatment, disease states, and development.

Current neuromuscular evaluation platforms can evaluate certain aspects of human biology such as exercise (135) and therapeutics (124). However, certain neuromuscular diseases, such as ALS and SMA, have genetic components that are difficult to functionally recapitulate *in vitro* or even in animal models. Therefore iPSCs are gaining demand for their use in evaluation of genetic diseases. In relation to the neuromuscular reflex arc, extrafusal fibers (130), motoneurons (128), and sensory neurons (129) have been differentiated from iPSCs but this work is the first demonstration of intrafusal fiber differentiation with morphological (Figure 18) and

immunocytochemical (Figures 19 and 20) evidence. Establishment of this cell line permits the integration of these cells into neuromuscular reflex arc testing platforms for analysis of afferent related dysfunction, development, and drug response.

Several aspects of the afferent spindle signal, including the muscle spindle and nociceptors, can be linked to the sensation of pain (141, 143, 144, 147, 148, 153). Therefore, it is vital to consider these aspects when developing a preclinical model to evaluate potentially pain-related disease states and drug testing. This work evaluates the potential for integrating nociceptors and intrafusal fibers into a pain-centered neuromuscular reflex arc testing platform. Sensitization of nociceptor endings within the muscle spindle has been of recent interest (17). Potential interactions between nociceptors and other cells more frequently found in the muscle spindle may possibly explain some of the more elusive aspects of neuropathic pain generation.

Establishment of neuropathic pain *in vitro* is a current challenge for pain research. While it is not possible to interrogate cells for level of pain perception, neuropathic-related neuronal activity is possible to demonstrate. This work shows the electrophysiological response of nociceptor marker positive sensory neurons to a common nociceptive agonist, capsaicin, establishing a potential for *in vitro* pain analysis (Figure 22). Additionally, the expression of pain-related receptors on intrafusal fibers suggests a possible role in noxious afferent signaling (Figure 23).

Afferent signaling interrogation presents as a challenging aspect of neuromuscular reflex arc research. While sensory neurons can receive and send signaling in a variety of ways (81), intrafusal fibers must be mechanically stimulated (185). To overcome this challenge, aluminum nitride, a piezoelectric material, can be integrated into existing cantilever systems for mechanical stimulation of intrafusal fibers. This work outlines a method for developing the first mechanically interrogative neuromuscular reflex arc testing platform, allowing for the

mechanical stimulation of intrafusal fibers and observation of subsequent signal propagation.

This advancement enhances the investigational capabilities of *in vitro* functional analysis, particularly regarding complex neuromuscular interactions.

Collectively, these data demonstrate a significant advancement in the field of afferent neuromuscular activity research. Integration of γ -motoneurons, iPSC-derived intrafusal fibers, human-derived nociceptors, and mechanical interrogation into existing *in vitro* research allows for substantial advancement in animal-free preclinical analyses.

LIST OF REFERENCES

1. C. M. Sakolish, M. B. Esch, J. J. Hickman, M. L. Shuler, G. J. Mahler, Modeling Barrier Tissues In Vitro: Methods, Achievements, and Challenges. *EBioMedicine* **5**, 30-39 (2016).
2. C. Oleaga, C. Bernabini, A. S. Smith, B. Srinivasan, M. Jackson, W. McLamb, V. Platt, R. Bridges, Y. Cai, N. Santhanam, B. Berry, S. Najjar, N. Akanda, X. Guo, C. Martin, G. Ekman, M. B. Esch, J. Langer, G. Ouedraogo, J. Cotovio, L. Breton, M. L. Shuler, J. J. Hickman, Multi-Organ toxicity demonstration in a functional human in vitro system composed of four organs. *Sci Rep* **6**, 20030 (2016).
3. C. Oleaga, A. Lavado, A. Riu, S. Rothemund, C. Carmona-Moran, K. Persaud, A. Yurko, J. Lear, N. Sriram Narasimhan, C. Long, F. Sommerhage, L. Richard Bridges, Y. Cai, C. Martin, M. Schnepfer, A. Goswami, R. Note, J. Langer, S. Teissier, J. J. Hickman, *Long-Term Electrical and Mechanical Function Monitoring of a Human-on-a-Chip System*. (2018), vol. 29.
4. M. Stancescu, P. Molnar, C. W. McAleer, W. McLamb, C. J. Long, C. Oleaga, J. M. Prot, J. J. Hickman, A phenotypic in vitro model for the main determinants of human whole heart function. *Biomaterials* **60**, 20-30 (2015).
5. Y. I. Wang, C. Oleaga, C. J. Long, M. B. Esch, C. W. McAleer, P. G. Miller, J. J. Hickman, M. L. Shuler, Self-contained, low-cost Body-on-a-Chip systems for drug development. *Experimental biology and medicine (Maywood, N.J.)* **242**, 1701-1713 (2017).
6. D. E. C.J.L. C.W. McAleer, T. Sasserath, L.R. Bridges, J.W. Rumsey, C. Martin, M. Schnepfer, Y. Wang, F. Schuler, A.B. Roth, C. Funk, M.L. Shuler, J.J. Hickman, Reconfigurable Multi-Organ System for the Evaluation of Anti-Cancer Therapeutics on Efficacy and Off-Target Toxicity. *accepted to Sci. Trans. Med*, (2019).
7. M. Das, C. A. Gregory, P. Molnar, L. M. Riedel, K. Wilson, J. J. Hickman, A defined system to allow skeletal muscle differentiation and subsequent integration with silicon microstructures. *Biomaterials* **27**, 4374-4380 (2006).
8. M. B. Esch, A. S. Smith, J. M. Prot, C. Oleaga, J. J. Hickman, M. L. Shuler, How multi-organ microdevices can help foster drug development. *Advanced drug delivery reviews* **69-70**, 158-169 (2014).
9. J. H. Sung, M. B. Esch, J. M. Prot, C. J. Long, A. Smith, J. J. Hickman, M. L. Shuler, Microfabricated mammalian organ systems and their integration into models of whole animals and humans. *Lab on a chip* **13**, 1201-1212 (2013).
10. A. Smith, C. Long, K. Pirozzi, S. Najjar, C. McAleer, H. Vandenburg, J. Hickman, A multiplexed chip-based assay system for investigating the functional development of human skeletal myotubes in vitro. *Journal of Biotechnology* **185**, 15-18 (2014).
11. M. Arbab, S. Baars, N. Geijsen, Modeling motor neuron disease: the matter of time. *Trends in Neurosciences* **37**, 642-652 (2014).
12. S. Schiaffino, A. C. Rossi, V. Smerdu, L. A. Leinwand, C. Reggiani, Developmental myosins: expression patterns and functional significance. *Skeletal muscle* **5**, 1 (2015).
13. A. S. Smith, C. J. Long, K. Pirozzi, J. J. Hickman, A functional system for high-content screening of neuromuscular junctions in vitro. *Technology* **1**, 37-48 (2013).

14. J. W. Rumsey, M. Das, A. Bhalkikar, M. Stancescu, J. J. Hickman, Tissue engineering the mechanosensory circuit of the stretch reflex arc: sensory neuron innervation of intrafusal muscle fibers. *Biomaterials* **31**, 8218-8227 (2010).
15. X. Guo, A. Colon, N. Akanda, S. Spradling, M. Stancescu, C. Martin, J. J. Hickman, Tissue engineering the mechanosensory circuit of the stretch reflex arc with human stem cells: Sensory neuron innervation of intrafusal muscle fibers. *Biomaterials* **122**, 179-187 (2017).
16. A. Colón, X. Guo, N. Akanda, Y. Cai, J. J. Hickman, Functional analysis of human intrafusal fiber innervation by human γ -motoneurons. *Sci Rep* **7**, 17202 (2017).
17. J. V. Partanen, T. A. Ojala, J. P. Arokoski, Myofascial syndrome and pain: A neurophysiological approach. *Pathophysiology : the official journal of the International Society for Pathophysiology* **17**, 19-28 (2010).
18. A. Maier, Development and regeneration of muscle spindles in mammals and birds. *The International journal of developmental biology* **41**, 1-17 (1997).
19. H. H. Chen, S. Hippenmeyer, S. Arber, E. Frank, Development of the monosynaptic stretch reflex circuit. *Current opinion in neurobiology* **13**, 96-102 (2003).
20. J. X. Liu, P. O. Eriksson, L. E. Thornell, F. Pedrosa-Domellof, Myosin heavy chain composition of muscle spindles in human biceps brachii. *The journal of histochemistry and cytochemistry : official journal of the Histochemistry Society* **50**, 171-183 (2002).
21. E. R. Andrechek, W. R. Hardy, A. A. Girgis-Gabardo, R. L. Perry, R. Butler, F. L. Graham, R. C. Kahn, M. A. Rudnicki, W. J. Muller, ErbB2 is required for muscle spindle and myoblast cell survival. *Mol Cell Biol* **22**, 4714-4722 (2002).
22. X. J. Chen, E. N. Levedakou, K. J. Millen, R. L. Wollmann, B. Soliven, B. Popko, Proprioceptive sensory neuropathy in mice with a mutation in the cytoplasmic Dynein heavy chain 1 gene. *The Journal of neuroscience : the official journal of the Society for Neuroscience* **27**, 14515-14524 (2007).
23. P. J. Stapley, L. H. Ting, M. Hulliger, J. M. Macpherson, Automatic postural responses are delayed by pyridoxine-induced somatosensory loss. *The Journal of neuroscience : the official journal of the Society for Neuroscience* **22**, 5803-5807 (2002).
24. K. G. Pearson, J. E. Misiaszek, M. Hulliger, Chemical ablation of sensory afferents in the walking system of the cat abolishes the capacity for functional recovery after peripheral nerve lesions. *Experimental brain research* **150**, 50-60 (2003).
25. A. B. Serman, H. H. Schaumburg, A. K. Asbury, The acute sensory neuronopathy syndrome: a distinct clinical entity. *Annals of neurology* **7**, 354-358 (1980).
26. R. Forget, Y. Lamarre, Rapid elbow flexion in the absence of proprioceptive and cutaneous feedback. *Human neurobiology* **6**, 27-37 (1987).
27. J. D. Cole, E. M. Sedgwick, The perceptions of force and of movement in a man without large myelinated sensory afferents below the neck. *The Journal of Physiology* **449**, 503-515 (1992).
28. J. Cole, J. Paillard, in *The Body and the Self*, J. L. Bermudez, A. J. Marcel, N. M. Eilan, Eds. (MIT Press, 1995), pp. 245--266.
29. J. Izawa, S. E. Pekny, M. K. Marko, C. C. Haswell, R. Shadmehr, S. H. Mostofsky, Motor learning relies on integrated sensory inputs in ADHD, but over-selectively on

- proprioception in autism spectrum conditions. *Autism research : official journal of the International Society for Autism Research* **5**, 124-136 (2012).
30. A. Conte, N. Khan, G. Defazio, J. C. Rothwell, A. Berardelli, Pathophysiology of somatosensory abnormalities in Parkinson disease. *Nature reviews. Neurology* **9**, 687-697 (2013).
 31. G. Abbruzzese, A. Berardelli, Sensorimotor integration in movement disorders. *Movement disorders : official journal of the Movement Disorder Society* **18**, 231-240 (2003).
 32. M. H. Cameron, F. B. Horak, R. R. Herndon, D. Bourdette, Imbalance in multiple sclerosis: a result of slowed spinal somatosensory conduction. *Somatosensory & motor research* **25**, 113-122 (2008).
 33. E. B. Torres, R. W. Isenhower, J. Nguyen, C. Whyatt, J. I. Nurnberger, J. V. Jose, S. M. Silverstein, T. V. Papatomas, J. Sage, J. Cole, Toward Precision Psychiatry: Statistical Platform for the Personalized Characterization of Natural Behaviors. *Frontiers in neurology* **7**, 8 (2016).
 34. J. W. Rumsey, M. Das, J. F. Kang, R. Wagner, P. Molnar, J. J. Hickman, Tissue engineering intrafusal fibers: dose- and time-dependent differentiation of nuclear bag fibers in a defined in vitro system using neuregulin 1-beta-1. *Biomaterials* **29**, 994-1004 (2008).
 35. C. Jacobson, D. Duggan, G. Fischbach, Neuregulin induces the expression of transcription factors and myosin heavy chains typical of muscle spindles in cultured human muscle. *Proc Natl Acad Sci U S A* **101**, 12218-12223 (2004).
 36. X. Guo, K. Greene, N. Akanda, A. Smith, M. Stancescu, S. Lambert, H. Vandeburgh, J. Hickman, In vitro Differentiation of Functional Human Skeletal Myotubes in a Defined System. *Biomaterials science* **2**, 131-138 (2014).
 37. X. Guo, M. Gonzalez, M. Stancescu, H. Vandeburgh, J. J. Hickman, Neuromuscular junction formation between human stem cell-derived motoneurons and human skeletal muscle in a defined system. *Biomaterials* **32**, 9602-9611 (2011).
 38. X. Guo, S. Spradling, M. Stancescu, S. Lambert, J. J. Hickman, Derivation of sensory neurons and neural crest stem cells from human neural progenitor hNP1. *Biomaterials* **34**, 4418-4427 (2013).
 39. M. Das, J. W. Rumsey, C. A. Gregory, N. Bhargava, J. F. Kang, P. Molnar, L. Riedel, X. Guo, J. J. Hickman, Embryonic motoneuron-skeletal muscle co-culture in a defined system. *Neuroscience* **146**, 481-488 (2007).
 40. Q. Ma, Z. Chen, I. del Barco Barrantes, J. L. de la Pompa, D. J. Anderson, neurogenin1 is essential for the determination of neuronal precursors for proximal cranial sensory ganglia. *Neuron* **20**, 469-482 (1998).
 41. S. Williams, C. Jacobson, alpha-Dystroglycan is essential for the induction of Egr3, a transcription factor important in muscle spindle formation. *Developmental neurobiology* **70**, 498-507 (2010).
 42. L. F. Mavrinskaya, Development of muscle spindles in man. *Neuroscience Translations* **2**, 529-535 (1968).
 43. S. Hippenmeyer, N. A. Shneider, C. Birchmeier, S. J. Burden, T. M. Jessell, S. Arber, A role for neuregulin1 signaling in muscle spindle differentiation. *Neuron* **36**, 1035-1049 (2002).

44. L. E. Thornell, L. Carlsson, P. O. Eriksson, J. X. Liu, C. Osterlund, P. Stal, F. Pedrosa-Domellof, Fibre typing of intrafusal fibres. *Journal of anatomy* **227**, 136-156 (2015).
45. S. Schiaffino, C. Reggiani, Fiber types in mammalian skeletal muscles. *Physiol Rev* **91**, 1447-1531 (2011).
46. D. L. McWhorter, J. M. Walro, S. A. Signs, J. Wang, Expression of alpha-cardiac myosin heavy chain in normal and denervated rat muscle spindles. *Neuroscience letters* **200**, 2-4 (1995).
47. S. Britsch, The neuregulin-I/ErbB signaling system in development and disease. *Advances in anatomy, embryology, and cell biology* **190**, 1-65 (2007).
48. W. G. Tourtellotte, C. Keller-Peck, J. Milbrandt, J. Kucera, The transcription factor Egr3 modulates sensory axon-myotube interactions during muscle spindle morphogenesis. *Developmental biology* **232**, 388-399 (2001).
49. W. G. Tourtellotte, J. Milbrandt, Sensory ataxia and muscle spindle agenesis in mice lacking the transcription factor Egr3. *Nat Genet* **20**, 87-91 (1998).
50. H. Ogawa, Y. Yamashita, in *Progress in Brain Research*, W. Hamann, A. Iggo, Eds. (Elsevier, 1988), vol. 74, pp. 63-68.
51. J. Van Hees, J. Gybels, C nociceptor activity in human nerve during painful and non painful skin stimulation. *Journal of neurology, neurosurgery, and psychiatry* **44**, 600-607 (1981).
52. H. Wissing, H. A. Braun, K. Schäfer, in *Progress in Brain Research*, W. Hamann, A. Iggo, Eds. (Elsevier, 1988), vol. 74, pp. 99-107.
53. A. B. Vallbo, R. S. Johansson, Properties of cutaneous mechanoreceptors in the human hand related to touch sensation. *Human neurobiology* **3**, 3-14 (1984).
54. J. M. Aimonetti, V. Hospod, J. P. Roll, E. Ribot-Ciscar, Cutaneous afferents provide a neuronal population vector that encodes the orientation of human ankle movements. *The Journal of Physiology* **580**, 649-658 (2007).
55. A. B. Vallbo, K. E. Hagbarth, B. G. Wallin, Microneurography: how the technique developed and its role in the investigation of the sympathetic nervous system. *J Appl Physiol (1985)* **96**, 1262-1269 (2004).
56. N. Kakuda, M. Nagaoka, Dynamic response of human muscle spindle afferents to stretch during voluntary contraction. *The Journal of Physiology* **513 (Pt 2)**, 621-628 (1998).
57. N. Kakuda, Response of human muscle spindle afferents to sinusoidal stretching with a wide range of amplitudes. *The Journal of Physiology* **527 Pt 2**, 397-404 (2000).
58. P. Malik, N. Jabakhanji, K. E. Jones, An Assessment of Six Muscle Spindle Models for Predicting Sensory Information during Human Wrist Movements. *Frontiers in computational neuroscience* **9**, 154 (2015).
59. J. N. Sanes, K. H. Mauritz, M. C. Dalakas, E. V. Evarts, Motor control in humans with large-fiber sensory neuropathy. *Human neurobiology* **4**, 101-114 (1985).
60. M. H. Cameron, S. Lord, Postural control in multiple sclerosis: implications for fall prevention. *Current neurology and neuroscience reports* **10**, 407-412 (2010).
61. N. Jain, K. C. Catania, J. H. Kaas, Deactivation and reactivation of somatosensory cortex after dorsal spinal cord injury. *Nature* **386**, 495-498 (1997).

62. R. W. van Deursen, G. G. Simoneau, Foot and ankle sensory neuropathy, proprioception, and postural stability. *The Journal of orthopaedic and sports physical therapy* **29**, 718-726 (1999).
63. H. Z. Lefumat, R. C. Miall, J. D. Cole, L. Bringoux, C. Bourdin, J. L. Vercher, F. R. Sarlegna, Generalization of force-field adaptation in proprioceptively-deafferented subjects. *Neuroscience letters* **616**, 160-165 (2016).
64. L. Bringoux, C. Scotto Di Cesare, L. Borel, T. Macaluso, F. R. Sarlegna, Do Visual and Vestibular Inputs Compensate for Somatosensory Loss in the Perception of Spatial Orientation? Insights from a Deafferented Patient. *Frontiers in human neuroscience* **10**, 181 (2016).
65. J. Cole, Rehabilitation after sensory neuronopathy syndrome. *Journal of the Royal Society of Medicine* **91**, 30-32 (1998).
66. M. Das, N. Bhargava, C. Gregory, L. Riedel, P. Molnar, J. J. Hickman, Adult rat spinal cord culture on an organosilane surface in a novel serum-free medium. *In vitro cellular & developmental biology. Animal* **41**, 343-348 (2005).
67. M. Das, P. Molnar, H. Devaraj, M. Poeta, J. J. Hickman, Electrophysiological and morphological characterization of rat embryonic motoneurons in a defined system. *Biotechnology progress* **19**, 1756-1761 (2003).
68. L. Thorrez, J. Shansky, L. Wang, L. Fast, T. VandenDriessche, M. Chuah, D. Mooney, H. Vandenburgh, Growth, differentiation, transplantation and survival of human skeletal myofibers on biodegradable scaffolds. *Biomaterials* **29**, 75-84 (2008).
69. J. V. Hennessey, J. A. Chromiak, S. Della Ventura, J. Guertin, D. B. MacLean, Increase in percutaneous muscle biopsy yield with a suction-enhancement technique. *J Appl Physiol (1985)* **82**, 1739-1742 (1997).
70. C. Powell, J. Shansky, M. Del Tatto, D. E. Forman, J. Hennessey, K. Sullivan, B. A. Zielinski, H. H. Vandenburgh, Tissue-engineered human bioartificial muscles expressing a foreign recombinant protein for gene therapy. *Hum Gene Ther* **10**, 565-577 (1999).
71. G. Lee, S. M. Chambers, M. J. Tomishima, L. Studer, Derivation of neural crest cells from human pluripotent stem cells. *Nature protocols* **5**, 688-701 (2010).
72. B. X. Gao, L. Ziskind-Conhaim, Development of ionic currents underlying changes in action potential waveforms in rat spinal motoneurons. *J Neurophysiol* **80**, 3047-3061 (1998).
73. J. Liu, J. W. Rumsey, M. Das, P. Molnar, C. Gregory, L. Riedel, J. J. Hickman, Electrophysiological and immunocytochemical characterization of DRG neurons on an organosilane surface in serum-free medium. *In vitro cellular & developmental biology. Animal* **44**, 162-168 (2008).
74. T. Xu, P. Molnar, C. Gregory, M. Das, T. Boland, J. J. Hickman, Electrophysiological characterization of embryonic hippocampal neurons cultured in a 3D collagen hydrogel. *Biomaterials* **30**, 4377-4383 (2009).
75. R. Z. Sabirov, S. Morishima, in *Patch Clamp Techniques: From Beginning to Advanced Protocols*, Y. Okada, Ed. (Springer Japan, Tokyo, 2012), pp. 415-431.
76. G. J. Mahler, M. B. Esch, T. Stokol, J. J. Hickman, M. L. Shuler, Body-on-a-chip systems for animal-free toxicity testing. *Alternatives to laboratory animals : ATLA* **44**, 469-478 (2016).

77. A. S. Smith, C. J. Long, B. J. Berry, C. McAleer, M. Stancescu, P. Molnar, P. G. Miller, M. B. Esch, J. M. Prot, J. J. Hickman, M. L. Shuler, Microphysiological systems and low-cost microfluidic platform with analytics. *Stem cell research & therapy* **4 Suppl 1**, S9 (2013).
78. J. H. Sung, B. Srinivasan, M. B. Esch, W. T. McLamb, C. Bernabini, M. L. Shuler, J. J. Hickman, Using physiologically-based pharmacokinetic-guided "body-on-a-chip" systems to predict mammalian response to drug and chemical exposure. *Experimental biology and medicine (Maywood, N.J.)* **239**, 1225-1239 (2014).
79. *Neural Engineering: From Advanced Biomaterials to 3D Fabrication Techniques*, (Springer International Publishing 2016, 2016), pp. 261-298
80. F. Zheng, F. Fu, Y. Cheng, C. Wang, Y. Zhao, Z. Gu, Organ-on-a-Chip Systems: Microengineering to Biomimic Living Systems. *Small* **12**, 2253-2282 (2016).
81. X. Guo, J. E. Ayala, M. Gonzalez, M. Stancescu, S. Lambert, J. J. Hickman, Tissue engineering the monosynaptic circuit of the stretch reflex arc with co-culture of embryonic motoneurons and proprioceptive sensory neurons. *Biomaterials* **33**, 5723-5731 (2012).
82. X. Guo, M. Das, J. Rumsey, M. Gonzalez, M. Stancescu, J. Hickman, Neuromuscular junction formation between human stem-cell-derived motoneurons and rat skeletal muscle in a defined system. *Tissue engineering. Part C, Methods* **16**, 1347-1355 (2010).
83. M. Das, J. W. Rumsey, N. Bhargava, M. Stancescu, J. J. Hickman, A defined long-term in vitro tissue engineered model of neuromuscular junctions. *Biomaterials* **31**, 4880-4888 (2010).
84. L. Kokontis, L. Gutmann, Current treatment of neuromuscular diseases. *Archives of Neurology* **57**, 939-943 (2000).
85. M. S. Kinch, An analysis of FDA-approved drugs for neurological disorders. *Drug discovery today* **20**, 1040-1043 (2015).
86. N. Stifani, Motor neurons and the generation of spinal motor neuron diversity. *Frontiers in Cellular Neuroscience* **8**, (2014).
87. K. C. Kanning, A. Kaplan, C. E. Henderson, Motor neuron diversity in development and disease. *Annual review of neuroscience* **33**, 409-440 (2010).
88. J. X. Liu, L. E. Thornell, F. Pedrosa-Domellof, Muscle spindles in the deep muscles of the human neck: a morphological and immunocytochemical study. *The journal of histochemistry and cytochemistry : official journal of the Histochemistry Society* **51**, 175-186 (2003).
89. S. Ashrafi, M. Lalancette-Hébert, A. Friese, M. Sigrist, S. Arber, N. A. Shneider, J. A. Kaltschmidt, Wnt7A identifies embryonic gamma-motor neurons and reveals early postnatal dependence of gamma-motor neurons on a muscle spindle-derived signal. *The Journal of neuroscience : the official journal of the Society for Neuroscience* **32**, 8725-8731 (2012).
90. I. J. Edwards, G. Bruce, C. Lawrenson, L. Howe, S. J. Clapcote, S. A. Deuchars, J. Deuchars, Na⁺/K⁺ ATPase alpha1 and alpha3 isoforms are differentially expressed in alpha- and gamma-motoneurons. *The Journal of neuroscience : the official journal of the Society for Neuroscience* **33**, 9913-9919 (2013).

91. A. Enjin, N. Rabe, S. T. Nakanishi, A. Vallstedt, H. Gezelius, F. Memic, M. Lind, T. Hjalt, W. G. Tourtellotte, C. Bruder, G. Eichele, P. J. Whelan, K. Kullander, Identification of novel spinal cholinergic genetic subtypes disclose Chodl and Pitx2 as markers for fast motor neurons and partition cells. *The Journal of comparative neurology* **518**, 2284-2304 (2010).
92. A. Friese, J. A. Kaltschmidt, D. R. Ladle, M. Sigrist, T. M. Jessell, S. Arber, Gamma and alpha motor neurons distinguished by expression of transcription factor Err3. *Proceedings of the National Academy of Sciences* **106**, 13588-13593 (2009).
93. N. A. Shneider, M. N. Brown, C. A. Smith, J. Pickel, F. J. Alvarez, Gamma motor neurons express distinct genetic markers at birth and require muscle spindle-derived GDNF for postnatal survival. *Neural development* **4**, 42 (2009).
94. A. Enjin, K. E. Leão, S. Mikulovic, P. Le Merre, W. G. Tourtellotte, K. Kullander, Sensorimotor function is modulated by the serotonin receptor 1d, a novel marker for gamma motor neurons. *Molecular and Cellular Neuroscience* **49**, 322-332 (2012).
95. R. A. Powis, T. H. Gillingwater, Selective loss of alpha motor neurons with sparing of gamma motor neurons and spinal cord cholinergic neurons in a mouse model of spinal muscular atrophy. *Journal of anatomy* **228**, 443-451 (2016).
96. J. P. Lund, S. Sadeghi, T. Athanassiadis, N. Caram Salas, F. Auclair, B. Thivierge, I. Arsenault, P. Rompre, K. G. Westberg, A. Kolta, Assessment of the potential role of muscle spindle mechanoreceptor afferents in chronic muscle pain in the rat masseter muscle. *PLoS one* **5**, e11131 (2010).
97. M. Das, P. Molnar, C. Gregory, L. Riedel, A. Jamshidi, J. J. Hickman, Long-term culture of embryonic rat cardiomyocytes on an organosilane surface in a serum-free medium. *Biomaterials* **25**, 5643-5647 (2004).
98. M. S. Ravenscroft, K. E. Bateman, K. M. Shaffer, H. M. Schessler, D. R. Jung, T. W. Schneider, C. B. Montgomery, T. L. Custer, A. E. Schaffner, Q. Y. Liu, Y. X. Li, J. L. Barker, J. J. Hickman, Developmental Neurobiology Implications from Fabrication and Analysis of Hippocampal Neuronal Networks on Patterned Silane-Modified Surfaces. *Journal of the American Chemical Society* **120**, 12169-12177 (1998).
99. M. Das, K. Wilson, P. Molnar, J. J. Hickman, Differentiation of skeletal muscle and integration of myotubes with silicon microstructures using serum-free medium and a synthetic silane substrate. *Nature protocols* **2**, 1795-1801 (2007).
100. M. Das, J. W. Rumsey, N. Bhargava, M. Stancescu, J. J. Hickman, Skeletal muscle tissue engineering: a maturation model promoting long-term survival of myotubes, structural development of the excitation-contraction coupling apparatus and neonatal myosin heavy chain expression. *Biomaterials* **30**, 5392-5402 (2009).
101. X. Guo, K. Johe, P. Molnar, H. Davis, J. Hickman, Characterization of a Human Fetal Spinal Cord Stem Cell Line NSI-566RSC and Its Induction to Functional Motoneurons. *Journal of tissue engineering and regenerative medicine* **4**, 181-193 (2010).
102. A. S. T. Smith, C. J. Long, K. Pirozzi, J. J. Hickman, A functional system for high-content screening of neuromuscular junctions in vitro. *Technology* **1**, 37-48 (2013).
103. M. Leu, E. Bellmunt, M. Schwander, I. Farinas, H. R. Brenner, U. Muller, Erbb2 regulates neuromuscular synapse formation and is essential for muscle spindle development. *Development (Cambridge, England)* **130**, 2291-2301 (2003).

104. S. A. Jo, X. Zhu, M. A. Marchionni, S. J. Burden, Neuregulins are concentrated at nerve-muscle synapses and activate ACh-receptor gene expression. *Nature* **373**, 158-161 (1995).
105. M. Oliveira Fernandes, W. G. Tourtellotte, Egr3-dependent muscle spindle stretch receptor intrafusal muscle fiber differentiation and fusimotor innervation homeostasis. *The Journal of neuroscience : the official journal of the Society for Neuroscience* **35**, 5566-5578 (2015).
106. Y. Zhang, M. Wesolowski, A. Karakatsani, V. Witzemann, S. Kroger, Formation of cholinergic synapse-like specializations at developing murine muscle spindles. *Developmental biology* **393**, 227-235 (2014).
107. T. A. Mays, J. L. Sanford, T. Hanada, A. H. Chishti, J. A. Rafael-Fortney, Glutamate receptors localize postsynaptically at neuromuscular junctions in mice. *Muscle Nerve* **39**, 343-349 (2009).
108. M. Francolini, G. Brunelli, I. Cambianica, S. Barlati, A. Barbon, L. La Via, B. Guarneri, F. Boroni, A. Lanzillotta, C. Baiguera, M. Ettorre, M. Buffelli, P. Spano, F. Clementi, M. Pizzi, Glutamatergic reinnervation and assembly of glutamatergic synapses in adult rat skeletal muscle occurs at cholinergic endplates. *J Neuropathol Exp Neurol* **68**, 1103-1115 (2009).
109. G. S. Bewick, B. Reid, C. Richardson, R. W. Banks, Autogenic modulation of mechanoreceptor excitability by glutamate release from synaptic-like vesicles: evidence from the rat muscle spindle primary sensory ending. *The Journal of Physiology* **562**, 381-394 (2005).
110. K. E. Personius, B. S. Slusher, S. B. Udin, Neuromuscular NMDA Receptors Modulate Developmental Synapse Elimination. *The Journal of neuroscience : the official journal of the Society for Neuroscience* **36**, 8783-8789 (2016).
111. H. Nishimaru, C. E. Restrepo, J. Ryge, Y. Yanagawa, O. Kiehn, Mammalian motor neurons corelease glutamate and acetylcholine at central synapses. *Proc Natl Acad Sci U S A* **102**, 5245-5249 (2005).
112. A. K. Urzaev, S. T. Magsumov, G. I. Poletayev, E. E. Nikolsky, F. Vyskocil, Muscle NMDA receptors regulate the resting membrane potential through NO-synthase. *Physiological research* **44**, 205-208 (1995).
113. M. Combes, P. Poindron, N. Callizot, Glutamate protects neuromuscular junctions from deleterious effects of beta-amyloid peptide and conversely: an in vitro study in a nerve-muscle coculture. *Journal of neuroscience research* **93**, 633-643 (2015).
114. A. I. Malomuzh, M. R. Mukhtarov, A. Urzaev, E. E. Nikol'skii, F. Vyskocil, The effects of glutamate on spontaneous acetylcholine secretion processes in the rat neuromuscular synapse. *Neuroscience and behavioral physiology* **32**, 577-582 (2002).
115. M. Lalancette-Hebert, A. Sharma, A. K. Lyashchenko, N. A. Shneider, Gamma motor neurons survive and exacerbate alpha motor neuron degeneration in ALS. *Proc Natl Acad Sci U S A* **113**, E8316-e8325 (2016).
116. J. V. Hennessey, J. A. Chromiak, S. Dellaventura, J. Guertin, D. B. Maclean, Increase in percutaneous muscle biopsy yield with a suction-enhancement technique. *Journal of Applied Physiology* **82**, 1739-1742 (1997).

117. C. Powell, J. Shansky, M. DelTatto, D. E. Forman, J. Hennessey, K. Sullivan, B. A. Zielinski, H. H. Vandenburg, Tissue engineered human bioartificial muscles expressing a foreign recombinant protein for gene therapy. *Human Gene Therapy* **10**, 565-577 (1999).
118. K. Takahashi, S. Yamanaka, Induction of pluripotent stem cells from mouse embryonic and adult fibroblast cultures by defined factors. *Cell* **126**, 663-676 (2006).
119. I. A. Boyd, The Response of Fast and Slow Nuclear Bag Fibres and Nuclear Chain Fibres in Isolated Cat Muscle Spindles to Fusimotor Stimulation, and the Effect of the Intrafusal Contraction on the Sensory Endings. *Quarterly Journal of Experimental Physiology and Cognate Medical Sciences* **61**, 203-253 (1976).
120. X. Guo, F. Sommerhage, C. McAleer, C. Martin, C. Long, Y. Wang, N. Santhanam, A. Colon, C. O. Sancho, J. Hickman, in *Neural Engineering: From Advanced Biomaterials to 3D Fabrication Techniques*, L. G. Zhang, D. L. Kaplan, Eds. (Springer International Publishing, Cham, 2016), pp. 261-298.
121. K. L. Pirozzi, C. J. Long, C. W. McAleer, A. S. Smith, J. J. Hickman, Correlation of embryonic skeletal muscle myotube physical characteristics with contractile force generation on an atomic force microscope-based bio-microelectromechanical systems device. *Applied physics letters* **103**, 83108 (2013).
122. A. S. Smith, C. J. Long, K. Pirozzi, S. Najjar, C. McAleer, H. H. Vandenburg, J. J. Hickman, A multiplexed chip-based assay system for investigating the functional development of human skeletal myotubes in vitro. *Journal of biotechnology* **185**, 15-18 (2014).
123. A. S. Smith, C. J. Long, C. McAleer, N. Bobbitt, B. Srinivasan, J. J. Hickman, Utilization of microscale silicon cantilevers to assess cellular contractile function in vitro. *Journal of visualized experiments : JoVE*, e51866 (2014).
124. N. Santhanam, L. Kumanchik, X. Guo, F. Sommerhage, Y. Cai, M. Jackson, C. Martin, G. Saad, C. W. McAleer, Y. Wang, A. Lavado, C. J. Long, J. J. Hickman, Stem cell derived phenotypic human neuromuscular junction model for dose response evaluation of therapeutics. *Biomaterials* **166**, 64-78 (2018).
125. M. Das, P. Molnar, C. Gregory, L. Riedel, J. J. Hickman, Long-term culture of embryonic rat cardiomyocytes on an organosilane surface in a serum free medium. *Biomaterials* **25**, 5643-5647 (2004).
126. A. E. Volk, J. H. Weishaupt, P. M. Andersen, A. C. Ludolph, C. Kubisch, Current knowledge and recent insights into the genetic basis of amyotrophic lateral sclerosis. *Medizinische Genetik : Mitteilungsblatt des Berufsverbandes Medizinische Genetik e.V* **30**, 252-258 (2018).
127. W. D. Arnold, D. Kassar, J. T. Kissel, Spinal muscular atrophy: diagnosis and management in a new therapeutic era. *Muscle Nerve* **51**, 157-167 (2015).
128. F. Bianchi, M. Malboubi, Y. Li, J. H. George, A. Jerusalem, F. Szele, M. S. Thompson, H. Ye, Rapid and efficient differentiation of functional motor neurons from human iPSC for neural injury modelling. *Stem cell research* **32**, 126-134 (2018).
129. M. Z. P. Guimaraes, R. De Vecchi, G. Vitoria, J. K. Sochacki, B. S. Paulsen, I. Lima, F. Rodrigues da Silva, R. F. M. da Costa, N. G. Castro, L. Breton, S. K. Rehen, Generation of iPSC-Derived Human Peripheral Sensory Neurons Releasing Substance P Elicited by TRPV1 Agonists. *Frontiers in molecular neuroscience* **11**, 277 (2018).

130. J. Chal, Z. Al Tanoury, M. Hestin, B. Gobert, S. Aivio, A. Hick, T. Cherrier, A. P. Nesmith, K. K. Parker, O. Pourquie, Generation of human muscle fibers and satellite-like cells from human pluripotent stem cells in vitro. *Nature protocols* **11**, 1833-1850 (2016).
131. J. Kucera, J. M. Walro, Origin of intrafusal fibers from a subset of primary myotubes in the rat. *Anat Embryol (Berl)* **192**, 149-158 (1995).
132. D. R. Maxwell, E. A. Sumpter, A comparison of the actions of some drugs on decerebrate rigidity, muscle spindle activity and alpha-adrenoceptors. *British journal of pharmacology* **50**, 355-363 (1974).
133. J. Kucera, J. M. Waldro, Treatment with beta bungarotoxin blocks muscle spindle formation in fetal rats. *Development (Cambridge, England)* **110**, 483-489 (1990).
134. K. Yoshida, R. Kaji, T. Kubori, N. Kohara, T. Iizuka, J. Kimura, Muscle afferent block for the treatment of oromandibular dystonia. *Movement disorders : official journal of the Movement Disorder Society* **13**, 699-705 (1998).
135. C. W. McAleer, A. S. Smith, S. Najjar, K. Pirozzi, C. J. Long, J. J. Hickman, Mechanistic investigation of adult myotube response to exercise and drug treatment in vitro using a multiplexed functional assay system. *J Appl Physiol (1985)* **117**, 1398-1405 (2014).
136. L. C. Boyd-Clark, C. A. Briggs, M. P. Galea, Muscle spindle distribution, morphology, and density in longus colli and multifidus muscles of the cervical spine. *Spine* **27**, 694-701 (2002).
137. U. Proske, The distribution and abundance of muscle spindles. *Brain research bulletin* **75**, 502-503 (2008).
138. C. Osterlund, J. X. Liu, L. E. Thornell, P. O. Eriksson, Muscle spindle composition and distribution in human young masseter and biceps brachii muscles reveal early growth and maturation. *Anat Rec (Hoboken)* **294**, 683-693 (2011).
139. R. M. Brownstone, C. Lancelin, Escape from homeostasis: spinal microcircuits and progression of amyotrophic lateral sclerosis. *J Neurophysiol* **119**, 1782-1794 (2018).
140. H. K. Shorrock, T. H. Gillingwater, E. J. N. Groen, Molecular Mechanisms Underlying Sensory-Motor Circuit Dysfunction in SMA. *Frontiers in molecular neuroscience* **12**, 59 (2019).
141. S. P. Cohen, J. Mao, Neuropathic pain: mechanisms and their clinical implications. *BMJ (Clinical research ed.)* **348**, f7656 (2014).
142. M. K. Chung, J. Lee, J. Joseph, J. Saloman, J. Y. Ro, Peripheral group I metabotropic glutamate receptor activation leads to muscle mechanical hyperalgesia through TRPV1 phosphorylation in the rat. *The journal of pain : official journal of the American Pain Society* **16**, 67-76 (2015).
143. N. F. Capra, C. K. Hisley, R. M. Masri, The influence of pain on masseter spindle afferent discharge. *Archives of oral biology* **52**, 387-390 (2007).
144. M. S. Gold, G. F. Gebhart, Nociceptor sensitization in pain pathogenesis. *Nature medicine* **16**, 1248-1257 (2010).
145. A. B. M. a. K. R. Bley, Ed., *Turning up the Heat on Pain: TRPV1 Receptors in Pain and Inflammation*, (Burkhäuser, 2005), pp. 248.
146. K. A. Pollak, J. D. Swenson, T. A. Vanhaisma, R. W. Huguen, D. Jo, A. T. White, K. C. Light, P. Schweinhardt, M. Amann, A. R. Light, Exogenously applied muscle metabolites

- synergistically evoke sensations of muscle fatigue and pain in human subjects. *Experimental physiology* **99**, 368-380 (2014).
147. J. Y. Ro, J. S. Lee, Y. Zhang, Activation of TRPV1 and TRPA1 leads to muscle nociception and mechanical hyperalgesia. *Pain* **144**, 270-277 (2009).
 148. L. Colloca, T. Ludman, D. Bouhassira, R. Baron, A. H. Dickenson, D. Yarnitsky, R. Freeman, A. Truini, N. Attal, N. B. Finnerup, C. Eccleston, E. Kalso, D. L. Bennett, R. H. Dworkin, S. N. Raja, Neuropathic pain. *Nature reviews. Disease primers* **3**, 17002 (2017).
 149. M. J. Caterina, M. A. Schumacher, M. Tominaga, T. A. Rosen, J. D. Levine, D. Julius, The capsaicin receptor: a heat-activated ion channel in the pain pathway. *Nature* **389**, 816-824 (1997).
 150. K. Bolcskei, Z. Helyes, A. Szabo, K. Sandor, K. Elekes, J. Nemeth, R. Almasi, E. Pinter, G. Petho, J. Szolcsanyi, Investigation of the role of TRPV1 receptors in acute and chronic nociceptive processes using gene-deficient mice. *Pain* **117**, 368-376 (2005).
 151. P. Anand, K. Bley, Topical capsaicin for pain management: therapeutic potential and mechanisms of action of the new high-concentration capsaicin 8% patch. *British journal of anaesthesia* **107**, 490-502 (2011).
 152. P. Cavuoto, A. J. McAinch, G. Hatzinikolas, A. Janovska, P. Game, G. A. Wittert, The expression of receptors for endocannabinoids in human and rodent skeletal muscle. *Biochem Biophys Res Commun* **364**, 105-110 (2007).
 153. K. Wang, L. Arendt-Nielsen, P. Svensson, Capsaicin-induced muscle pain alters the excitability of the human jaw-stretch reflex. *Journal of dental research* **81**, 650-654 (2002).
 154. L. Vyklicky, K. Novakova-Tousova, J. Benedikt, A. Samad, F. Touska, V. Vlachova, Calcium-dependent desensitization of vanilloid receptor TRPV1: a mechanism possibly involved in analgesia induced by topical application of capsaicin. *Physiological research* **57 Suppl 3**, S59-68 (2008).
 155. S. Lotteau, S. Ducreux, C. Romestaing, C. Legrand, F. Van Coppenolle, Characterization of functional TRPV1 channels in the sarcoplasmic reticulum of mouse skeletal muscle. *PLoS one* **8**, e58673 (2013).
 156. X. Fang, L. Djouhri, S. McMullan, C. Berry, K. Okuse, S. G. Waxman, S. N. Lawson, trkA is expressed in nociceptive neurons and influences electrophysiological properties via Nav1.8 expression in rapidly conducting nociceptors. *The Journal of neuroscience : the official journal of the Society for Neuroscience* **25**, 4868-4878 (2005).
 157. J. Fritz, Cantilever biosensors. *Analyst* **133**, 855-863 (2008).
 158. C. Oleaga, C. Bernabini, A. S. T. Smith, B. Srinivasan, M. Jackson, W. McLamb, V. Platt, R. Bridges, Y. Cai, N. Santhanam, B. Berry, S. Najjar, N. Akanda, X. Guo, C. Martin, G. Ekman, M. B. Esch, J. Langer, G. Ouedraogo, J. Cotovio, L. Breton, M. L. Shuler, J. J. Hickman, Multi-Organ toxicity demonstration in a functional human in vitro system composed of four organs. *Scientific Reports* **6**, 20030 (2016).
 159. M. Stancescu, P. Molnar, C. W. McAleer, W. McLamb, C. J. Long, C. Oleaga, J.-M. Prot, J. J. Hickman, A phenotypic in vitro model for the main determinants of human whole heart function. *Biomaterials* **60**, 20-30 (2015).
 160. C. Oleaga, A. Riu, S. Rothmund, A. Lavado, C. W. McAleer, C. J. Long, K. Persaud, N. S. Narasimhan, M. Tran, J. Roles, Investigation of the effect of hepatic metabolism on off-

- target cardiotoxicity in a multi-organ human-on-a-chip system. *Biomaterials* **182**, 176-190 (2018).
161. J. Deng, Y. Qu, T. Liu, B. Jing, X. Zhang, Z. Chen, Y. Luo, W. Zhao, Y. Lu, B. Lin, Recent organ-on-a-chip advances toward drug toxicity testing. *Microphysiological Systems* **2**, (2018).
162. A. M. Ghaemmaghami, M. J. Hancock, H. Harrington, H. Kaji, A. Khademhosseini, Biomimetic tissues on a chip for drug discovery. *Drug Discovery Today* **17**, 173-181 (2012).
163. M. B. Esch, A. S. Smith, J.-M. Prot, C. Oleaga, J. J. Hickman, M. L. Shuler, How multi-organ microdevices can help foster drug development. *Advanced Drug Delivery Reviews* **69**, 158-169 (2014).
164. J. H. Sung, B. Srinivasan, M. B. Esch, W. T. McLamb, C. Bernabini, M. L. Shuler, J. J. Hickman, Using physiologically-based pharmacokinetic-guided “body-on-a-chip” systems to predict mammalian response to drug and chemical exposure. *Experimental biology and medicine* **239**, 1225-1239 (2014).
165. J. H. Lee, K. S. Hwang, J. Park, K. H. Yoon, D. S. Yoon, T. S. J. B. Kim, Bioelectronics, Immunoassay of prostate-specific antigen (PSA) using resonant frequency shift of piezoelectric nanomechanical microcantilever. **20**, 2157-2162 (2005).
166. D. Isarakorn, M. Linder, D. Briand, N. J. M. S. De Rooij, Technology, Evaluation of static measurement in piezoelectric cantilever sensors using a charge integration technique for chemical and biological detection. **21**, 075801 (2010).
167. V. Mohammadi, S. Mohammadi, F. Barghi, in *Piezoelectric Materials and Devices-Practice and Applications*. (IntechOpen, 2013).
168. J. Ali, J. Najeeb, M. A. Ali, M. F. Aslam, A. J. J. B. B. Raza, Biosensors: their fundamentals, designs, types and most recent impactful applications: a review. **8**, (2017).
169. P. Sangeetha, A. V. Juliet, MEMS Cantilever Based Immunosensors for Biomolecular Recognition. *International Journal of Computer Technology Electronics Engineering* **2**.
170. B. N. Johnson, R. Mutharasan, Biosensing using dynamic-mode cantilever sensors: a review. *Biosensors and Bioelectronics* **32**, 1-18 (2012).
171. S. Tadigadapa, K. Mateti, Piezoelectric MEMS sensors: state-of-the-art and perspectives. *Measurement Science Technology* **20**, 092001 (2009).
172. M. Das, C. A. Gregory, P. Molnar, L. M. Riedel, K. Wilson, J. J. Hickman, A defined system to allow skeletal muscle differentiation and subsequent integration with silicon microstructures. *Biomaterials* **27**, 4374-4380 (2006).
173. A. Colón, X. Guo, N. Akanda, Y. Cai, J. J. S. r. Hickman, Functional analysis of human intrafusal fiber innervation by human γ -motoneurons. **7**, 17202 (2017).
174. J. W. Rumsey, M. Das, A. Bhalkikar, M. Stancescu, J. J. Hickman, Tissue engineering the mechanosensory circuit of the stretch reflex arc: sensory neuron innervation of intrafusal muscle fibers. *Biomaterials* **31**, 8218-8227 (2010).
175. M. Das, K. Wilson, P. Molnar, J. J. Hickman, Differentiation of skeletal muscle and integration of myotubes with silicon microstructures using serum-free medium and a synthetic silane substrate. *Nature Protocols* **2**, 1795 (2007).

176. A. Natarajan, M. Stancescu, V. Dhir, C. Armstrong, F. Sommerhage, J. J. Hickman, P. Molnar, Patterned cardiomyocytes on microelectrode arrays as a functional, high information content drug screening platform. *Biomaterials* **32**, 4267-4274 (2011).
177. K. Wilson, M. Das, K. J. Wahl, R. J. Colton, J. J. Hickman, Measurement of contractile stress generated by cultured rat muscle on silicon cantilevers for toxin detection and muscle performance enhancement. *PloS one* **5**, e11042 (2010).
178. C. Oleaga, A. Lavado, A. Riu, S. Rothemund, C. A. Carmona-Moran, K. Persaud, A. Yurko, J. Lear, N. S. Narasimhan, C. J. Long, Long-Term Electrical and Mechanical Function Monitoring of a Human-on-a-Chip System. *Advanced Functional Materials* **29**, 1805792 (2019).
179. C. J. L. C.W. McAleer, D. Elbrecht, T. Sasserath, L.R. Bridges, J.W. Rumsey, C. Martin, M. Schnepfer, Y. Wang, F. Schuler, A.B. Roth, C. Funk, M.L. Shuler, J.J. Hickman, Reconfigurable Multi-Organ System for the Evaluation of Anti-Cancer Therapeutics on Efficacy and Off-Target Toxicity. *accepted to Sci. Trans. Med.*, (2019).
180. K. Pirozzi, C. Long, C. McAleer, A. Smith, J. Hickman, Correlation of embryonic skeletal muscle myotube physical characteristics with contractile force generation on an atomic force microscope-based bio-microelectromechanical systems device. *Applied Physics Letters* **103**, 083108 (2013).
181. A. Grosberg, P. W. Alford, M. L. McCain, K. K. Parker, Ensembles of engineered cardiac tissues for physiological and pharmacological study: heart on a chip. *Lab on a Chip* **11**, 4165-4173 (2011).
182. W. Liu, Z. Feng, R. Liu, J. Zhang, The influence of preamplifiers on the piezoelectric sensor's dynamic property. *Review of Scientific Instruments* **78**, 125107 (2007).
183. A. P. Haring, H. Sontheimer, B. N. Johnson, Microphysiological human brain and neural systems-on-a-chip: potential alternatives to small animal models and emerging platforms for drug discovery and personalized medicine. *Stem Cell Reviews and Reports* **13**, 381-406 (2017).
184. C. Luni, E. Serena, N. Elvassore, Human-on-chip for therapy development and fundamental science. *Current opinion in biotechnology* **25**, 45-50 (2014).
185. N. L. Strominger, R. J. Demarest, L. B. Laemle, in *Noback's Human Nervous System, Seventh Edition: Structure and Function*. (Humana Press, Totowa, NJ, 2012), pp. 143-154.